ABSTRACT

Title of dissertation: Computer Aided Design of Wide-Band Microwave Components

Mohamed Fahmi, Doctor of Philosophy, 2007

Dissertation directed by: Professor Kawthar A. Zaki
Department of Electrical and Computer Engineering

In recent years there was a notable developmental leap in communications systems operating at microwave frequencies. Such development was necessary to support a wide variety of emerging applications. Microwave communications systems can be found in many services such as satellite television and radar systems for civilian and military uses. Examples of such systems may include direct broadcast satellite (DBS) television, personal communications systems (PCSs), wireless local area networks (WLANs), global positioning systems (GPSs) as well as the 3G cellular services, which were designed for access to the Internet and to provide wide bandwidth applications.

In the dissertation, the goal is to demonstrate the challenges and to propose solutions that enable the successful design and realization of very wide band microwave components, in particular, microwave directional couplers and filters. Such components are essential for development of modern communications and radar system operating at microwave frequencies.

Directional couplers are an essential part in microwave systems. They are commonly used for dividing or combining signals. For example they are used in the generation of the desired power division in beam-forming networks for spacecraft antennas. In other applications, they are used for power monitoring.

In the dissertation, a comprehensive treatment of wide-band ridge waveguide directional couplers is included. Analysis and design of different configurations and arrangement of couplers realized in ridge waveguides are discussed. A new detailed systematic design procedure for ridge waveguide couplers in the two most used configurations "E-plane and H-plane" is proposed. The procedure is based on extracting equivalent circuit parameters of a building block from full electromagnetic wave simulation, and then assembling multiple units to realize higher order couplers.

Filters are also an integral part of any communication system. They separate communication channels operating at different frequencies thus eliminating interference between different channels. In the dissertation, design issues of wide-band ridge waveguide elliptic function filters realized in Low Temperature Co-fired Ceramics (LTCC) are discussed. Ridge waveguide filters have excellent characteristics such as wide stop-band and compact size. An excellent approach in manufacturing RF/microwave systems is the integration of components into multilayer substrates using LTCC which facilitates the design of microwave modules in the same package thus increasing reliability and reducing size. A new scheme to achieve the strong couplings, a crucial requirement for the realization of wide band elliptic filters is proposed in the dissertation. As an example, rigorous mode

matching method is successfully used in the analysis and design of a challenging wide-band ridge waveguide filter realized in LTCC technology.

Another interesting realization of couplers is the realization in strip-line transmission lines. In the dissertation, new proposed multi-section multi-layer LTCC stripline couplers are designed and analyzed. The proposed design enables the designer to achieve precise performance otherwise restricted by limitations posed by available technologies. The realization of wideband performance is made possible by such proposed design.

Computer Aided Design of Wide-Band Microwave Components

by

Mohamed M. Fahmi

Dissertation submitted to the Faculty of the Graduate School of the
University of Maryland, College Park in partial fulfillment
of the requirements for the degree of
Doctor of Philosophy
2007

Advisory Committee:

Professor Kawthar A. Zaki, Chair/Advisor
Professor Isaak D. Mayergoyz
Professor Thomas Antonsen
Professor Martin Peckerar
Professor Amr Baz

DEDICATION

To my mother and to Aya.

ACKNOWLEDGMENTS

I would like to express my deep and sincere gratitude to my advisor Prof. Kawthar A. Zaki for her invaluable guidance and enthusiastic support during the course of this work. I have benefitted greatly from her unparalleled knowledge,experience, and intuition. Her understanding, encouragement and trust were essential for the work in this dissertation. My unequivocal gratitude is due to Dr. Jorge A. Ruiz-Cruz, Universidad Autónoma de Madrid, Spain. He generously shared his codes with me. His friendliness allowed me to freely ask for help when I needed. My discussions with him were always fruitful due to his deep understanding and his valuable comments. I would like to thank Dr. Ali E. Atia for his innovative ideas and precious suggestions. I am very grateful to four other faculty members of the University of Maryland at College Park, Dr. Isaak D. Mayergoyz, Dr. Thomas Antonsen,Dr. Martin Peckerar, and Dr. Amr Baz, for serving in my Advisory Committee. I would also like to thank Dr. A. M. Saad, Scientific Microwave Corp.,Dorval, QC, Canada, for building the experimental prototype. My thanks go to Dr. Mahmoud Haddara and Mrs. Faiza Ennany for their kind support during some of my most difficult moments. I wish to acknowledge the limitless support from my family, especially the prayers of my mother and the smiles of my two sons. Finally I have to acknowledge the understanding, sharing of responsibilities, patience, encouragement, and love of my wife,Aya.

Contents

List of Tables

List of Figures

Chapter 1

Introduction

1.1 Motivation

Modern communication systems have seen a huge developmental leap in recent years to cope with an increasing demand from a variety of emerging applications. The applications are very diverse in nature, they include commercial applications such as direct broadcast satellite (DBS) television, personal communications systems (PCSs), wireless local area networks (WLANs), global positioning systems (GPSs), cellular phone and video systems, and local multipoint distribution systems (LMDS). The applications extend also to military applications such as radar systems. Radar systems are used militarily for detecting, locating and sensing remote targets These recent advances in modern communication systems serving both commercial and military applications have resulted in more stringent requirements for the microwave passive components used in these systems.

The traditional design methods of such passive components were mainly

based on equivalent circuit models of various components (These models were primarily developed by the MIT Radiation Laboratory during WWII and later published in the classical acclaimed multi-volume series) Although this design approach is still used today it suffers from some severe limitations, the most serious of them is that it considers only fundamental mode interactions. This results in discrepancies between theoretical and experimental results, that requires corrections in the form of post manufacturing tuning. Given the stringent requirements of economic constraints of today's communication systems such discrepancies and corrections can not be tolerated. The answer to this problem was the Computer Aided Design methods. Taking advantage of the huge leap in computational powers of modern computers, full wave design of microwave components was transferred to a whole new level of accuracy. By using full-wave electromagnetic models in the designs, higher order modes are taken into consideration thus reducing and almost eliminating the need of post manufacturing tuning of some classes of microwave components such as filters and couplers. The equivalent circuit approach still plays an important role as it provides initial designs that are further refined using CAD tools. At the core of any CAD tool is always the electromagnetic solver. whose function is to solve the electromagnetic problem of the structure under analysis, which is described by the Maxwell´s equations. The technology plays a key role as it determines the characteristics of the materials and the physical structure where the Maxwell´s equations have to be solved.

The main goal of the dissertation is to demonstrate the challenges and present solutions that enable the successful design and realization of very wide

band microwave components, namely microwave directional couplers and filters Such components are essential for the development of modern communication systems operating at microwave frequencies. Directional couplers are also an essential part of microwave systems. They are commonly used for dividing or combining signals. For example they are used in the generation of the desired power division in beam-forming networks for spacecraft antennas. In other applications, they are used for power monitoring. On the other hand microwave filters are an integral part of any communication system. They separate communication channels operating at different frequencies thus eliminating interference between different channels.

1.2 Dissertation Organization

The dissertation includes 6 chapters including the introduction. The second chapter provides a general overview of the numerical techniques used in the CAD of passive microwave components with special emphasis on the Mode Matching Techniques. The third chapter presents a comprehensive treatment of the subject of wide-band ridge waveguide directional couplers. Analysis and design of different configurations and arrangements of couplers realized in ridge waveguides are discussed. A new detailed systematic design procedure for ridge waveguide couplers in the two most used configurations "E-plane and H-plane" is presented. The procedure is based on extracting equivalent circuit parameters of a building block from full electromagnetic wave simulation, and then assembling multiple units to

realize higher order couplers. This part combines ideal circuit and electromagnetic modeling of the proposed structures to obtain very satisfactory initial results. It then utilizes the numerical efficiency of the modal analysis and the mode matching technique to quickly finalize the design, thus reducing the overall numerical simulation time and resources

The fourth Chapter provides an exhaustive discussion of the design of wide-band ridge waveguide elliptic function filters realized in Low Temperature Co-fired Ceramics (LTCC). This includes ideal circuit modeling, electromagnetic modeling of the three dimensional structures used to realize the filters, as well as discussion of practical aspects in LTCC realization. Ridge waveguide filters have excellent characteristics such as wide stop-band and compact size. An excellent approach in manufacturing RF/microwave systems is the integration of components into multilayer substrates using LTCC. This facilitates the design of microwave modules in the same package, thus increasing reliability and reducing size. A new scheme to achieve the strong couplings, a crucial requirement for the realization of wide band elliptic function filters, is presented. Also a novel approach to reduce unwanted spurious detrimental couplings is also presented. Rigorous modal analysis and mode matching technique are successfully used in the analysis and design of a challenging wide-band ridge waveguide filter realized in LTCC technology.

The fifth chapter focuses on another interesting realization of couplers, which is the realization in strip-line transmission lines. New proposed multi-section multi-layer LTCC stripline couplers are proposed, designed, and analyzed. The proposed design enables the achievement of precise performance otherwise re-

stricted by limitations posed by available technologies. The realization of ultra wideband performance is made possible by such proposed design. Limitations of the proposed couplers are also established. The last chapter presents the conclusions of the work presented in the dissertation.

1.3 Dissertation Contributions

The dissertation significance stems from the fact that it tackles design challenges and offers innovative solutions for some of the most important components in modern microwave communication systems which are essential in today's heavily interconnected communication-dependent world. The main contributions can be summarized as follows:

1-A complete design methodology for very wide band ridge waveguide branch-guide couplers. This includes designs for couplers in both E-plane and H-plane configurations The procedure presents an efficient equivalent circuit parameters extraction from full electromagnetic wave simulation. It provides a systematic procedure for realization of higher order couplers.

2- A new design of wide-band ridge waveguide elliptic function filters realized in Low Temperature Co-fired Ceramics (LTCC). A new scheme to achieve the strong couplings required for the realization of wide band elliptic function filters, is presented .In addition a novel approach to reduce unwanted spurious detrimental couplings is presented.

3-A new proposed multi-section multi-layer LTCC stripline couplers are de-

signed, and analyzed. The proposed couplers are capable of achieving very tight couplings over a huge fractional; bandwidth while occupying very small volume owing to the use of LTCC technology.

Chapter 2

Numerical Techniques for Electromagnetic Full-wave Simulation

The enormous advances in the field of computers ushered the beginning of a new stage in the design of microwave components. With the enormous computational power provided by modern computers full-wave modelling and design of passive components became possible. In full-wave design the higher order modes inside the structure under investigation are rigorously characterized, this results in designs whose simulation and experimental results are in close agreement. This is particularly of interest for the rapid large scale production of low-cost high performance passive components that do not require post production tuning.

2.1 General Purpose Numerical Techniques

The primary goal of all numerical techniques in electromagnetics is to find either exact or approximate solutions of Maxwell's equations that satisfy the given boundary and initial conditions. Numerous numerical techniques were developed.[1] They can be categorized based on three major distinctions [2]:

a) The approximated electromagnetic quantity (electric field, current distribution, and charge distributions, etc.).

b) The basis functions used to approximate the unknown solutions.

c) The algorithms used to calculate the expansion coefficients of the basis functions.

Some of the most widely used numerical techniques are summarized as follows:

a) Finite Element Method (FEM) [3, 4]. FEM is based on variational formulation of the electromagnetic problem. The recently proposed Boundary Element Method (BEM) [5] is a combination of the boundary integral equation and a discretization technique similar to the FEM is applied to the boundary. One of the most known software packages which uses the FEM technique is High Frequency Structure Simulator (HFSS) [6] This program offers great versatility regarding the possible physical geometries that can be handled. However, the accuracy and efficiency of the results depend

strongly on the analyzed problem and they are usually computational intensive in terms of memory and computation time. Optimization of designs in such technique is not a viable option at the current time.

b) Finite Difference Methods [7]. These methods include Finite Difference in Time Domain (FDTD) [8, 9] and Finite Difference in Frequency Domain (FDFD) [10]. The finite difference method is well known to be the least analytical. One of the commercially available software packages which uses the FDTD technique is EMPIRE [11]

c) The Method of Moments (MoM) [12]. This is by far the method of choice to analyze planar structures. It's based on either electric field or magnetic field integral equation Many software packages use the MoM technique in their core solvers. the list includes Sonnet Suites [13], and IE3D[14]

d) Transmission Line Matrix method (TLM) [15, 16]. The field problem is converted to a three dimensional equivalent network problem in this method. An available software package that utilizes this technique is MEFiSTo [17]

e) Spectral Domain Method (SDM) [18]. SDM is a Fourier-transformed version of the integral equation method applied to planar structures. SDM is very efficient but it's limited to well-shaped structures.

f) Mode Matching Method (MMM) [19, 20]. MMM is based on a field-matching algorithm. It's used to calculate the Generalized Scattering Matrices GSM's in the case of waveguide discontinuities or the Generalized admittance Matri-

ces GAMs in the case of waveguide junctions. The mode matching technique is very efficient but its applicability is limited to well behaved geometries and can not be used in a general purpose solver. Methods derived from mode matching techniques include Boundary Integral-Resonant Mode Expansion method (BIRME) [21, 22] and Boundary Contour Mode Matching method (BCMM) [23–26].

e) An emerging trend [27, 28] tries to harvest the potential of several techniques together by using a hybrid approach. The problem is segmented and each segment is solved by the best suitable numerical technique, then the total solution is obtained. Commercially available software packages [29, 30] use such hybrid approach .

Most of the analysis and design of microwave components presented in this dissertation uses mode matching techniques as the primary electromagnetic solver and verifies the results with a commercially available FEM solver [6] and by experiment where possible. Next we present a brief description to the mode matching technique.

2.2 Mode Matching Technique

MMM is used widely in formulating boundary value problems. It is one of the most efficient techniques used in solving a variety of waveguides problems. Such problems include the design of filters,couplers,power dividers, and many other passive waveguide components [31–38].The literature is rich in materials detailing

the analysis, using mode matching techniques, of various classes of microwave passive components [32, 39–42] Mode matching technique can be used for solving two types of problems:

a) Scattering Problems, where scattering parameters relating incident and reflected waves on and from the ports of the structure under consideration are calculated

b) Eigenvalue problems, where the resonant frequencies of a closed structure (cavity) , or the cut off frequencies and propagation constant of a certain waveguide are calculated

In general the mode matching technique is used in a modular fashion. Each structure to be studied using mode matching is first decomposed into regions of waveguides separated by discontinuities or junctions. The scattering parameters of each of these discontinuities are calculated using a field matching technique. The scattering parameters of the whole structure are then calculated by cascading the individual scattering matrices of the discontinuities [1]. If the problem under consideration is a scattering problem then the result is already obtained, if it is an eigen value problem then appropriate terminations are applied at the ports and an eigenvalue equation whose solution gives the required quantity. Fig. 2.1 shows a schematic diagram showing a general problem consisting of N regions of waveguides cascaded in the z direction along with the final goal which is the GSM of the whole structure under consideration.

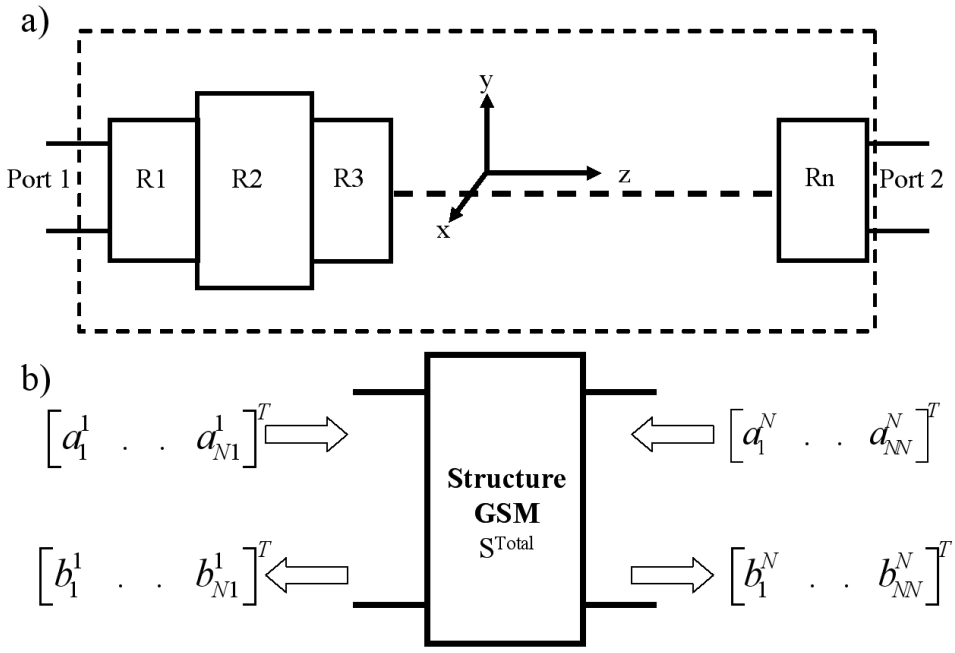

Figure 2.1: a)Schematic diagram of N regions of waveguides connected in cascade b) The total GSM characterization of the electromagnetic problem between incident waves a and reflected waves b at the ports, assuming $N1$ modes in region 1 and NN modes in region N

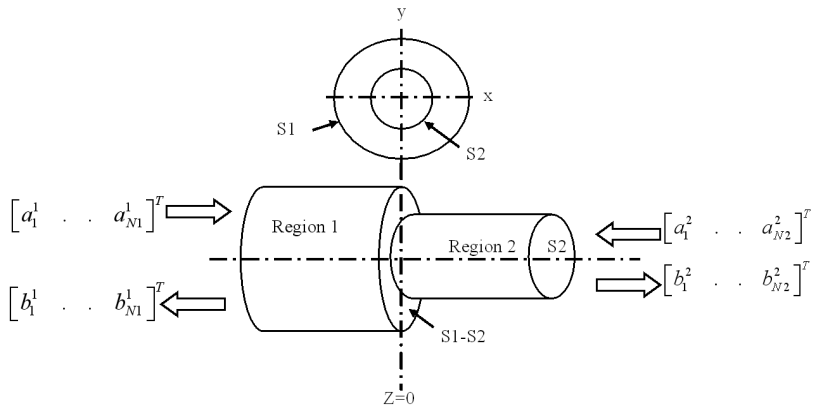

Figure 2.2: A basic waveguide discontinuity

2.2.1 Characterization of a waveguide discontinuity

The first step in the mode matching technique is to identify the regions of waveguides under consideration and calculating the eigen modes that are supported in those regions. In the case of waveguides whose cross sections coincide with a separable coordinate system such as rectangular or circular waveguides, the fields can be obtained analytically using the well know technique of separation of variables. In other cases of non-separable boundary cross sections such as striplines and ridge waveguides eigen modes have to be found numerically either by Generalized Transverse Resonance Technique (GTR) [1, 39, 41–44], or by Boundary Contour Mode Matching (BCMM) [23–26]. In this dissertation the modes were calculated using the GTR technique so a discussion of that technique is presented in the last section of this chapter.

Once the eigen modes of each region of waveguides is known, the next step becomes characterizing discontinuities between different waveguides. Since the

eigen modes of the waveguide represents a complete set , they can be considered basis function whose weighted sum can represent the fields inside the waveguide. Fig. 2.2 shows two waveguides (one totally inclosing the other) connected to each other representing a general waveguide discontinuity. In order to apply the mode matching technique to calculate the scattering matrix relating the amplitudes of incident and reflected waves from the discontinuity the following steps are followed

1. The transversal electromagnetic fields E_T and H_T of the waves in regions 1 and 2 shown in Fig. 2.2 are expressed as a truncated weighted sum of the basis functions of the transverse electromagnetic fields $E_i and\ H_i$. The basis functions can be either Transverse Electric TE, ,Transverse Magnetic TM or Transverse Electromagnetic TEM depending on the supported modes in every waveguide region. The weights represent the amplitudes of the waves of each mode i travelling either in the positive or negative z directions with propagation constant $\gamma_i^{(1,2)}$ The superscript denotes the region where the wave is propagating. This is expressed in the following set of equations:

$$E_T^1 = \sum_{i=1}^{N1}(a_i^1 e^{-\gamma_i^1 z} + b_i^1 e^{\gamma_i^1 z})E_i^1;\text{on } S1 \tag{2.1}$$

$$H_T^1 = \sum_{i=1}^{N1}(a_i^1 e^{-\gamma_i^1 z} - b_i^1 e^{\gamma_i^1 z})H_i^1;\text{on } S1 \tag{2.2}$$

$$E_T^2 = \sum_{j=1}^{N2}(a_j^2 e^{\gamma_j^2 z} + b_j^2 e^{-\gamma_j^2 z})E_j^2;\text{on } S2 \tag{2.3}$$

$$H_T^2 = \sum_{j=1}^{N2}(a_j^2 e^{\gamma_j^2 z} - b_j^2 e^{-\gamma_j^2 z})H_j^2;\text{on } S2 \tag{2.4}$$

2. At the plane of the discontinuity $z = 0$,the continuity of the tangential electric and magnetic fields across the discontinuity is imposed on the smaller

cross sectional area ($S2$)inclosed in the larger one ($S1$).(there are no currents flowing on the surface area $S2$ while there are currents flowing on the area $S1 - S2$ with a surface current density $\overrightarrow{J}_s$)

$$\sum_{i=1}^{N1}(a_i^1 + b_i^1)E_i^1 = \begin{cases} \sum_{j=1}^{N2}(a_j^2 + b_j^2)E_j^2;\text{on } S2 \\ 0;\text{on } S1 - S2 \end{cases} \tag{2.5}$$

$$\sum_{j=1}^{N2}(a_j^2 - b_j^2)H_j^2 = \begin{cases} \sum_{i=1}^{N1}(a_i^1 - b_i^1)H_i^1;\text{on } S2 \\ \overrightarrow{J}_s \times \widehat{n};\text{on } S1 - S2 \end{cases} \tag{2.6}$$

3. The orthogonality properties of the electromagnetic eigen modes is utilized to reduce the sums into a linear system of equations by taking the self inner product with one mode in the summation in a certain region so that its amplitude can be expressed as a truncated sum of the amplitudes of the field in the other region multiplied by the mutual inner product with the respective modes of the second region as shown in the following set of equations:

$$(a_i^1 + b_i^1)\psi_{1i} = \sum_{j=1}^{N2}(a_j^2 + b_j^2)m_{ij} \tag{2.7}$$

$$(a_j^2 - b_j^2)\psi_{2i} = \sum_{i=1}^{N1}(a_i^1 - b_i^1)m_{ji} \tag{2.8}$$

$$\psi_{1i} = \iint_{S2} \overrightarrow{E_i^1} \times \overrightarrow{H_i^1} \cdot \widehat{n} dS \tag{2.9}$$

$$\psi_{2j} = \iint_{S2} \overrightarrow{E_j^2} \times \overrightarrow{H_j^2} \cdot \widehat{n} dS \tag{2.10}$$

$$m_{ij} = \iint_{S2} \overrightarrow{E_j^2} \times \overrightarrow{H_i^1} \cdot \widehat{n} dS \tag{2.11}$$

4. The resulting system of equations can be formulated in matrix format as

follows:

$$\Psi_1[A_1 + B_1] = M[A_2 + B_2] \tag{2.12}$$

$$\Psi_2[A_2 - B_2] = M^T[A_1 - B_1] \tag{2.13}$$

where

$$A_1 = [\ a_1^1 \ . \ . \ a_{N1}^1\ ]^T \tag{2.14}$$

$$B_1 = [\ b_1^1 \ . \ . \ b_{N1}^1\ ]^T \tag{2.15}$$

$$A_2 = [\ a_1^2 \ . \ . \ a_{N2}^2\ ]^T \tag{2.16}$$

$$B_2 = [\ b_1^2 \ . \ . \ b_{N2}^2\ ]^T \tag{2.17}$$

$$\Psi_1(i,j) = \begin{cases} \psi_{1i}; i = j \\ 0; otherwise \end{cases} \tag{2.18}$$

$$\Psi_2(j,i) = \begin{cases} \psi_{2j}; j = i \\ 0; otherwise \end{cases} \tag{2.19}$$

$$M(i,j) = m_{ij}$$

With simple algebra we can get the relation between the amplitudes of the incident and reflected waves at each port as follows:

$$B_1 = S_{11}A_1 + S_{12}A_2 \tag{2.20}$$

$$B_2 = S_{21}A_1 + S_{22}A_2 \tag{2.21}$$

We have

$$[A_1 + B_1] = \Psi_1^{-1} M [A_2 + B_2] = \Phi_1 [A_2 + B_2] \quad (2.22)$$

$$[A_2 - B_2] = \Psi_2^{-1} M^T [A_1 - B_1] = \Phi_2 [A_1 - B_1] \quad (2.23)$$

$$S_{11} = -(I - \Phi_1\Phi_2)^{-1}(I + \Phi_1\Phi_2) \quad (2.24)$$

$$S_{12} = 2(I - \Phi_1\Phi_2)^{-1}\Phi_1 \quad (2.25)$$

$$S_{21} = \Phi_2(S_{11} - I) \quad (2.26)$$

$$S_{21} = (I + \Phi_2 S_{12}) \quad (2.27)$$

Where I is the identity matrix.

2.2.2 Cascading discontinuities

Once each discontinuity in the structure is fully characterized , they are cascaded in order to obtain the scattering matrix of the whole structure. As shown in Fig. 2.3 , the process of cascading discontinuities is a process of reducing two steps (the first step is the step from cross-section $c1$ to cross-section $c2$ characterized by S^{c1-c2} and the second step is the step from cross-section $c2$ to cross-section $c3$ characterized by S^{c2-c3}) to an equivalent S-parameters black box characterized by $S^{eq(1-3)}$, This equivalent black box has a behavior identical to the whole structure. According to Fig. 2.3 the incident and reflected waves at the ports are of the two discontinuity structure is given by

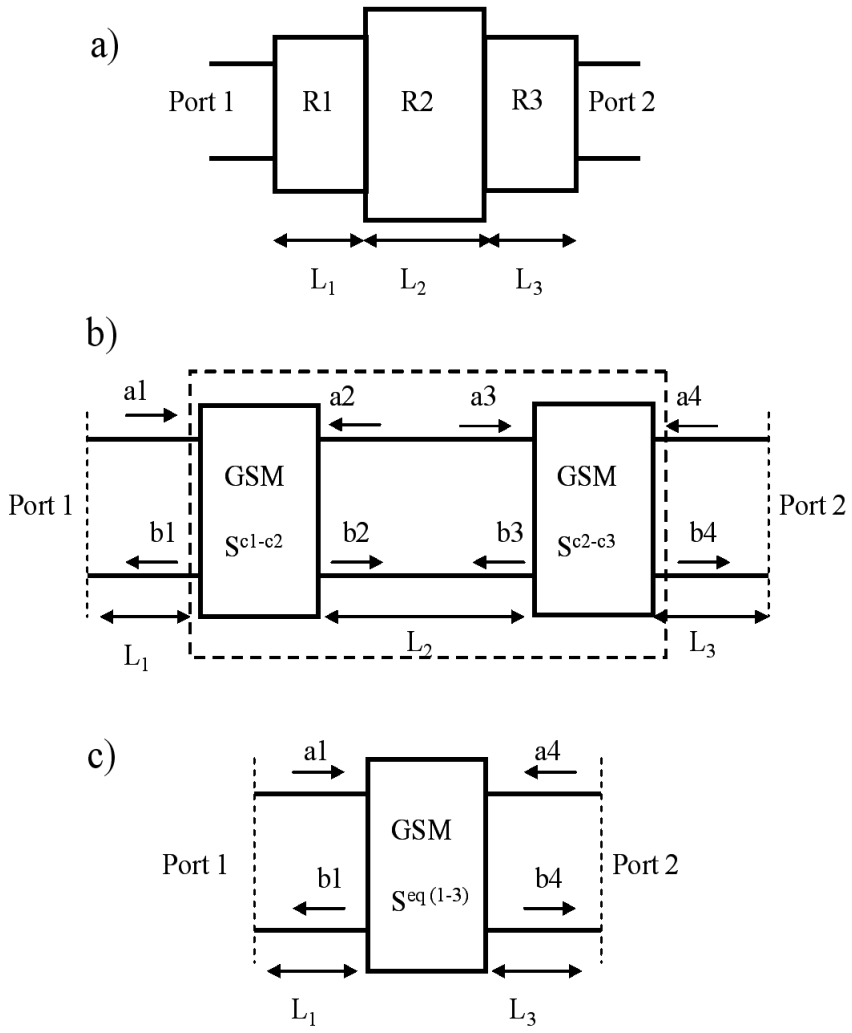

Figure 2.3: a) Schematic of a general two discontinuity problem b) GSM representation of the problem c) The reduced GSM of the two discontinuities

$$\begin{pmatrix} b_1 \\ b_2 \end{pmatrix} = \begin{pmatrix} S_{11}^{c1-c2} & S_{12}^{c1-c2} \\ S_{21}^{c1-c2} & S_{22}^{c1-c2} \end{pmatrix} \begin{pmatrix} a_1 \\ a_2 \end{pmatrix} \tag{2.28}$$

$$\begin{pmatrix} b_3 \\ b_4 \end{pmatrix} = \begin{pmatrix} S_{11}^{c2-c3} & S_{12}^{c2-c3} \\ S_{21}^{c2-c3} & S_{22}^{c2-c3} \end{pmatrix} \begin{pmatrix} a_3 \\ a_4 \end{pmatrix} \tag{2.29}$$

Since the waves a_2, a_3, b_2, and b_3 are propagating in the same region (R2) they are simply related by the following relation

$$a_3 = Db_2 \tag{2.30}$$

$$a_2 = Db_3 \tag{2.31}$$

$$D(i,j) = \begin{cases} e^{-\gamma_i^2 L_2}; i = j \\ 0; otherwise \end{cases} \tag{2.32}$$

where γ_i^2 is the propagation constant of mode i in region 2 (R2) and L_2 is the length of region 2 By means of algebraic manipulations the previous system of equations can be used to obtain an equivalent S-matrix which relates the mode amplitudes in region 1 directly to those in region three, such relation is given by the following set of equations:

$$\begin{pmatrix} b_1 \\ b_4 \end{pmatrix} = \begin{pmatrix} S_{11}^{eq(1-3)} & S_{12}^{eq(1-3)} \\ S_{21}^{eq(1-3)} & S_{22}^{eq(1-3)} \end{pmatrix} \begin{pmatrix} a_1 \\ a_4 \end{pmatrix} \tag{2.33}$$

$$\begin{aligned} S_{11}^{eq(1-3)} &= [S_{11}^{c1-c2} + S_{12}^{c1-c2} D(I - S_{11}^{c2-c3} D S_{22}^{c1-c2} D)^{-1} S_{11}^{c2-c3} D S_{21}^{c1-c2}] \\ S_{12}^{eq(1-3)} &= [S_{12}^{c1-c2} D(I - S_{11}^{c2-c3} D S_{22}^{c1-c2} D)^{-1} S_{12}^{c2-c3}] \\ S_{21}^{eq(1-3)} &= [S_{21}^{c2-c3} (I - D S_{22}^{c1-c2} D S_{11}^{c2-c1})^{-1} D S_{21}^{c1-c2}] \\ S_{22}^{eq(1-3)} &= [S_{22}^{c2-c3} + S_{21}^{c2-c3} (I - D S_{22}^{c1-c2} D S_{11}^{c2-c3})^{-1} D S_{22}^{c1-c2} D S_{12}^{c2-c3}] \end{aligned} \tag{2.34}$$

So to calculate the frequency response of a structure consisting of several discontinuities as shown in Fig. 2.4, one has to first calculate the scattering matrix of each discontinuity and then cascade progressively till the whole structure is characterized by a single S-matrix that relates the mode amplitudes in the first region directly to those in the last region. To account for the lengths of the first and last regions when calculating the frequency response (adjusting the reference planes for phase calculations) the following equations were utilized

$$S_{11}^{Final} = D_1 S_{11}^{Total} D_1 \tag{2.35}$$

$$S_{12}^{Final} = D_1 S_{12}^{Total} D_N \tag{2.36}$$

$$S_{21}^{Final} = D_N S_{21}^{Total} D_1 \tag{2.37}$$

$$S_{22}^{Final} = D_N S_{22}^{Total} D_N \tag{2.38}$$

$$D_1(i,j) = \begin{cases} e^{-\gamma_i^1 L_1}; i = j \\ 0; otherwise \end{cases} \tag{2.39}$$

$$D_N(i,j) = \begin{cases} e^{-\gamma_i^N L_N}; i = j \\ 0; otherwise \end{cases} \tag{2.40}$$

where γ_i^1, γ_i^N are the propagation constant of mode i in region 1 and N respectively and L_1 and L_n are the lengths of regions 1 and N respectively. This constitutes the full solution to the scattering problem using mode matching technique.

2.2.3 Formulation of the Eigenvalue problem

In the case of a finite closed 3D structure the eigenvalue problem is used to calculate resonant frequencies of the structure subject to certain termination conditions

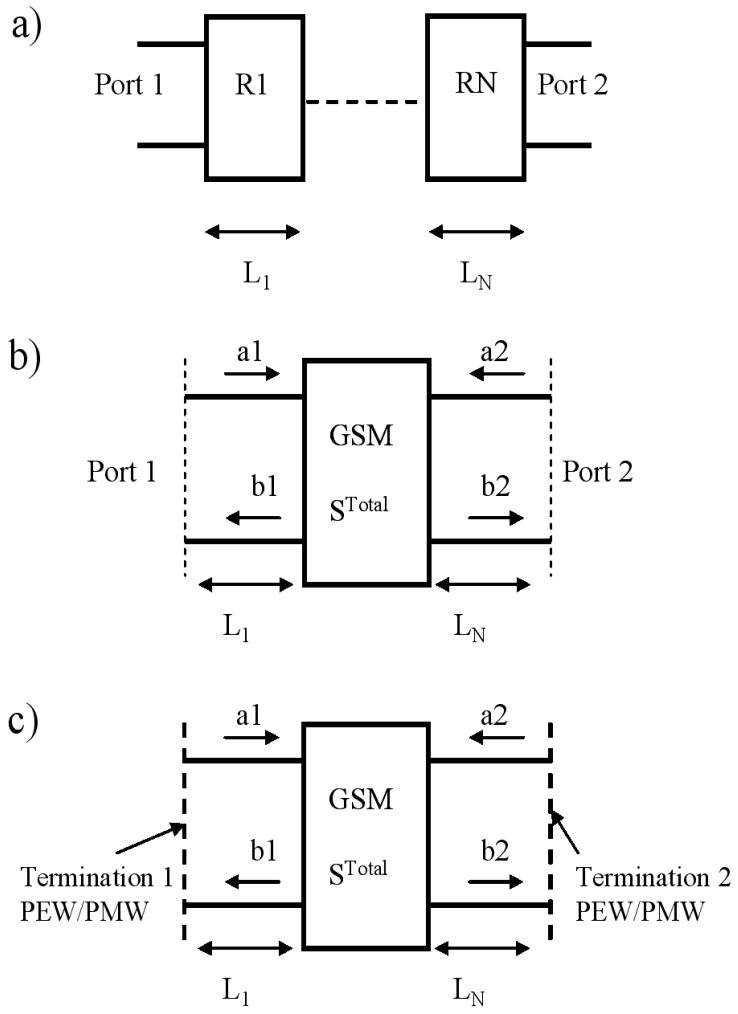

Figure 2.4: a) Schematic diagram of a structure of a cascade of N regions of waveguides b)Scattering problem formulation c) Eigenvalue problem formulation

at the ports. The structure will have resonances at certain frequencies depending on the port termination conditions, whether the termination type is Perfect Electric Wall (PEW) on which tangential electric fields must vanish, or Perfect Magnetic wall on which tangential magnetic fields must vanish. To calculate the resonant frequencies of the structure a simple analysis was followed, starting with the cascaded S-matrix of structure and enforcing the terminations at the ports the situations depicted in Fig. 2.4-c. A null-system of equations is obtained,note that there are four possibilities for the combinations of the termination conditions but two of them are redundant and can be obtained by simply interchanging the port notations. The system can be described algebraically by the following set of equations where D_1 and D_N are the diagonal matrices defined in equation 2.39 and equation 2.40 respectively:

$$\begin{pmatrix} 0 \\ 0 \end{pmatrix} = \begin{pmatrix} Q_{11} & Q_{12} \\ Q_{21} & Q_{22} \end{pmatrix} \begin{pmatrix} b_2 \\ b_3 \end{pmatrix} \tag{2.41}$$

For the case of PEW at port 1 and PEW at port 2 we have:

$$Q = \begin{pmatrix} I + S_{11}^{Total} D_1 D_1 & S_{12}^{Total} D_N D_N \\ S_{21}^{Total} D_1 D_1 & I + S_{22}^{Total} D_N D_N \end{pmatrix} \tag{2.42}$$

For the case of PEW at port 1 and PMW at port 2 we have:

$$Q = \begin{pmatrix} I + S_{11}^{Total} D_1 D_1 & -S_{12}^{Total} D_N D_N \\ S_{21}^{Total} D_1 D_1 & I - S_{22}^{Total} D_N D_N \end{pmatrix} \tag{2.43}$$

The null condition obtained in equation 2.41 indicate that to have a non zero solution to the null system of equation the determinant of the matrix Q

must vanish. The frequencies for which this condition is satisfied are the resonant frequencies of the structure. So by searching for the zeros of the determinant of the matrix Q one should be able to find the resonant frequencies of the whole structure. This constitutes the full solution to the eigenvalue problem using mode matching technique.

2.3 Generalized Transverse Resonance Method

The Generalized Transverse Resonance method (GTR) is a well-known technique used to analyze waveguide cross-sections that can be segmented into rectangular regions. The literature about GTR is very extensive, and its theory and applications can be found in many references [1, 39, 41–44]. A comprehensive formulation for a general case scenario where GTR was used to characterize the TEM, TE and TM modes for a generalized cross section was presented in [39] A brief discussion of the technique is given here for completeness.

In essence GTR is a special case of the eigenvalue problem solved by mode matching technique which was presented in the previous section. It's a two dimensional case where any non separable cross section is segmented into interlacing regions of parallel plate waveguides as shown in Fig.2.5 Since all the eigen modes of parallel plate waveguides are known analytically and they represent a complete set. The electromagnetic field inside each parallel plate region is expressed as a weighted sum of the basis functions. The same mode matching procedure discussed earlier is then applied with the only difference that the matching is done

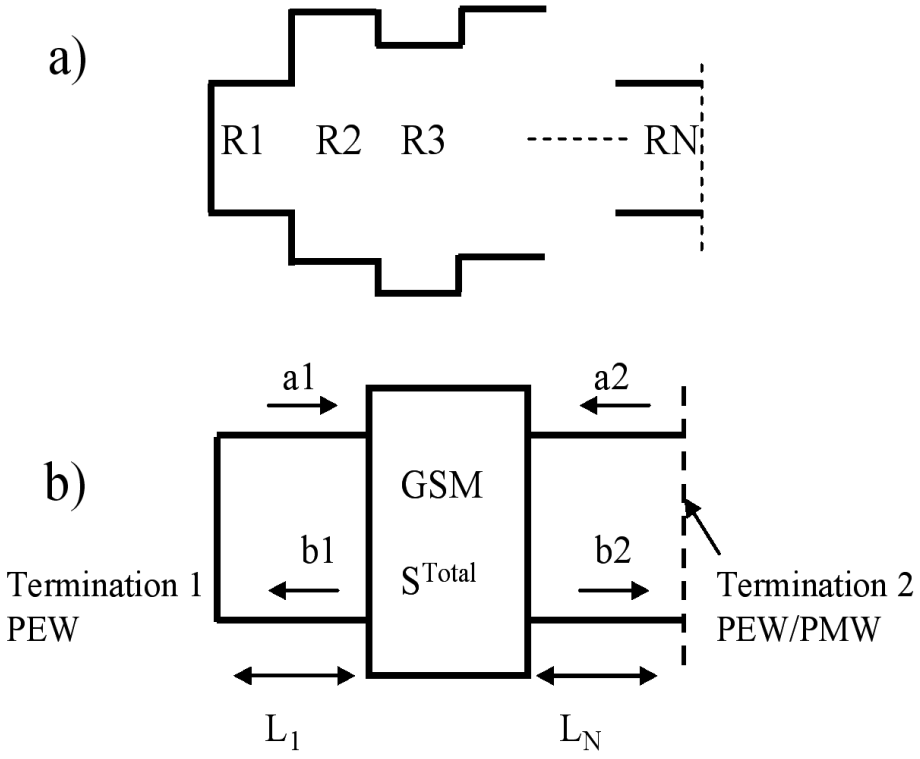

Figure 2.5: a) Generalized cross-section segmented into parallel plate regions b) GSM characterization of the cross-section

on the line of intersection of the two parallel plate regions rather than on the surface area of intersection in the three dimensional mode matching case. At the final step appropriate termination conditions are enforced, the eigen values here will be the cut off frequencies of the modes which is the two dimensional counterpart of the resonant frequencies in the three dimensional case. As an example , a non-separable cross section of a ridge waveguide is shown in Fig.2.6. Taking the symmetry into consideration, it can be segmented into two parallel plate regions R1 and R2. Using the technique outlined earlier the cut off frequencies and subsequently complete field descriptions of the cross sections can be found. Even symmetry modes can be obtained by imposing PMW at the symmetry line while odd modes can be obtained by imposing PEW at the symmetry line.

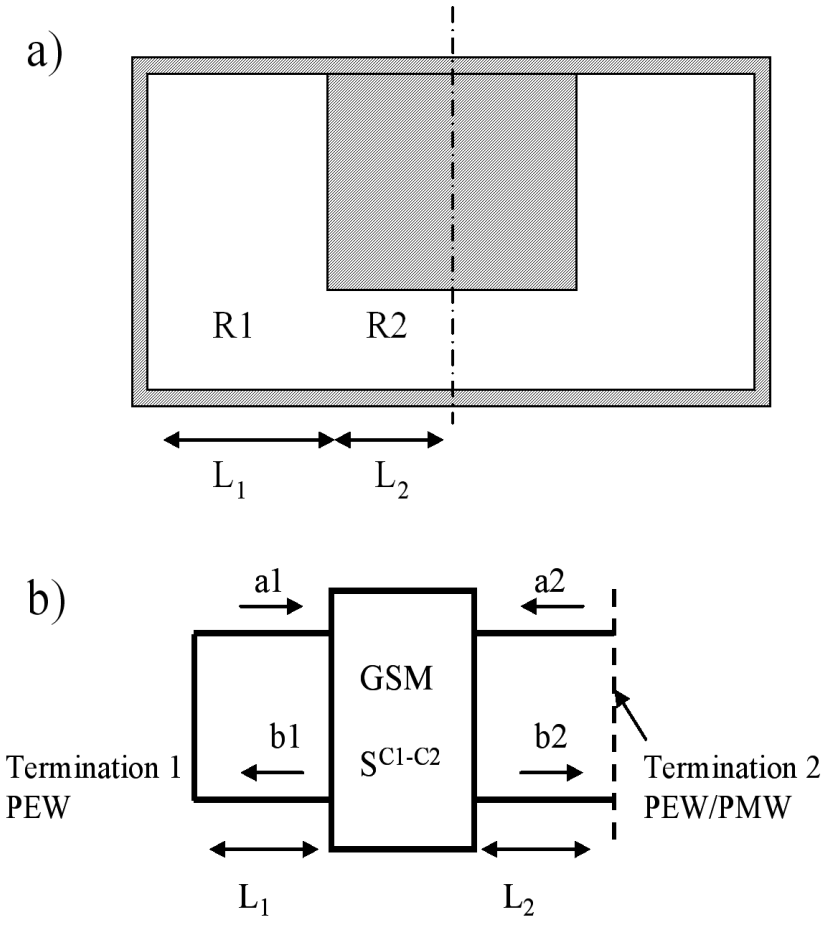

Figure 2.6: a) Ridge waveguide cross-section segmented into parallel plate regions b) GSM characterization of the ridge waveguide cross-section

Chapter 3

Wide-Band Ridge Waveguide Branch-guide Directional Couplers

3.1 Introduction

Directional couplers are key components in modern microwave systems. They find applications in power monitoring, in antenna beam forming networks, several test assemblies and variable power dividers [20, 45–47]. They can also be utilized to construct directional filters and multiplexers [47].

In waveguide technology directional couplers are usually realized by coupling two main waveguides by some sort of coupling mechanism located in the joint wall between the main guides. Waveguide directional couplers can be categorized based on the type of the coupling mechanism used to realize the coupler.

The categories include multi-aperture couplers [45, 46, 48–51], and branchguide couplers. [52–59] The design of multi-aperture couplers was originally based on Bethe's small aperture theory [60] Extensions to the theory addressed the large apertures and the effects of aperture resonances and interactions between apertures[49, 61, 62] The design of branchguide couplers is based on the theory of quarter-wave transformer prototype.[63, 64] Rectangular waveguide branchguide couplers can be implemented in E-plane configuration where the two main lines are stacked vertically with coupling provided by branches realized in the broad wall of the waveguide.[57, 59] Another implementation is the H-plane configuration where the two main lines are placed side by side and a coupling mechanism is introduced in the narrow intermediate walls.[58] These couplers are easy to manufacture but provide limited bandwidth.

In ridge waveguide technology cross couplers were proposed by Getsinger [65]but that configuration does not satisfy tight (>6dB)coupling performance. Recently ridge waveguide couplers in E-plane configuration were proposed by Ruiz-Cruz [66] ; however the work did not provide a systematic design procedure for such couplers.

In this chapter a detailed systematic dimensional synthesis procedure for ridge waveguide couplers in both E-plane and H-plane configurations is presented. The procedure is modular and is based on an equivalent circuit representation of a building block comprised of a single branch unit section. By extracting equivalent circuit parameters from full-wave simulation of the unit section, suitable physical dimensions of the unit section can be synthesized. Using this modular design

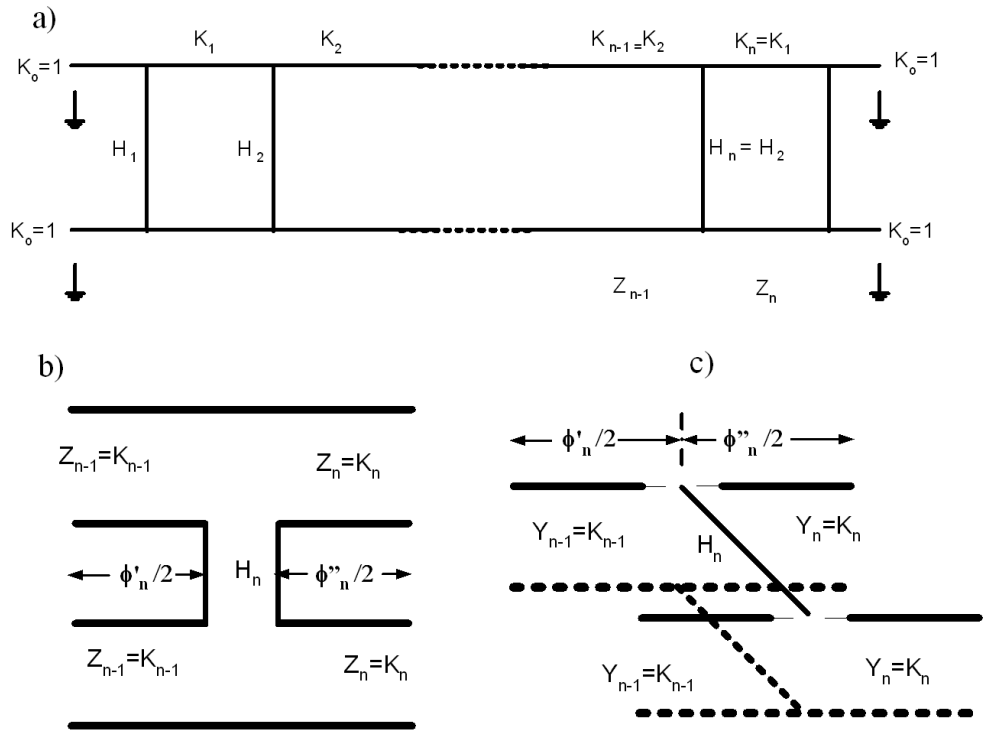

Figure 3.1: a) Ideal Circuit of a branch line coupler using immitance notation b) Ideal circuit of n^{th} branch in the case of series branches c) Ideal circuit of n^{th} branch in the case of parallel branches

scheme enables the assembly of N unit sections each representing a branch and a piece of main line. By such assembly an N^{th}-order coupler can be readily realized. The ideal circuit synthesis is discussed in details in the next section

3.2 Ideal Circuit Branch-line Coupler Synthesis

Branch-line couplers are composed of pieces of transmission lines connected to each other in a certain arrangement, as shown in Fig. 3.1-a There are two dual ideal circuits that describe branch-line couplers one describes the case where the branches connecting the main lines are series connected between the main

lines as shown in Fig. 3.1-b while the dual case describes the circuit where the branches are parallel connected as shown in Fig. 3.1-c. In the case of the series representation the purpose of Ideal circuit synthesis is to calculate the impedance ratios of the main lines and of the branches with respect to the impedance of the terminating ports. In the case of the parallel representation the admittance ratios are calculated. In the literature the expression immitance was used to describe the ratios independently of the realization with the understanding that the ratio is between impedances in series case and admittances in the parallel case The expression K_i represents the ratios of the immitance of the main line w.r.t. the terminating port impedance and H_i represents the ratios of the immitance of the branches w.r.t. the same terminating port impedance.

Ideal circuit synthesis of equal-ripple branch-line couplers was originally presented in [67, 68] where the ratios K_i were fixed to unity then a better synthesis was proposed in by Young [52]where the ratios K_i were allowed to be varied to achieve optimal performance. Alternative approach to the synthesis by Young was presented by Levy in [53] .

3.2.1 Quarter-Wave Transformer prototype design

Since the design of branchguide couplers is based on the theory of optimum equal ripple Chebyshev quarter-wave transformer prototype[69] We will start by reviewing the synthesis of the quarter wave transformer this treatment follows the work presented in [20, 47] which are in turn following the original work by [63, 64]. An

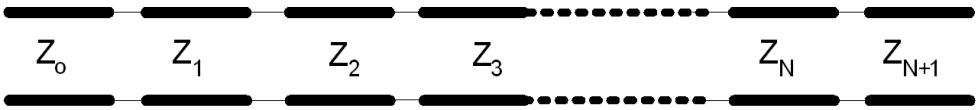

Figure 3.2: Ideal circuit representation of an N^{th} order Transformer

N section quarter wave transformer is a cascade connection of N quarter wavelength sections of transmission lines with different characteristic impedances. The frequency at which the sections are quarter wavelength is the center frequency of the transformer.

Problem Statement.

Given a frequency range $f_1 \rightarrow f_2$ and a ratio between source and load impedance of $S = \frac{Z_{N+1}}{Z_o}$ find the number of sections N and the impedance of each section Z_i such that the Voltage Standing Wave Ratio VSWR at the input port does not exceed a prescribed quantity $S_{\max}$ over the whole frequency band $f_1 \rightarrow f_2$

Step1: Find the Order of the Transformer

start by $N = 1$ and see if the following relation is satisfied:

$$S_{\max} > 1 + \frac{\ln(S)}{T_N(\frac{1}{\cos\varphi})} \tag{3.1}$$

with

$$\begin{aligned} T_n(x) &= 2xT_{n-1}(x) - T_{n-2}(x) \\ T_2(x) &= 2x^2 - 1 \\ T_1(x) &= x \\ T_0(x) &= 1 \end{aligned} \tag{3.2}$$

and the angle φ defines the electric length at the lower frequency f_1, it's related to the relative bandwidth w_q of the transformer by the following relation:

$$\begin{aligned} \varphi &= (2 - w_q)\frac{\pi}{4} \\ w_q &= \frac{f_2 - f_1}{f_o}; \\ f_o &= \frac{f_2 + f_1}{2} \end{aligned} \tag{3.3}$$

if relation 3.1 is not satisfied increase N by 1 and retry till the correct order is reached

Step2: Find the Junctions Impedance Ratios

After finding the order of the transformer the task now is to find the characteristic impedances Z_1 to Z_n The procedure involves finding the impedance ratios at each junction between the transformer sections . The impedance ratio $\rho_i = \frac{Z_{i+1}}{Z_i}$ at the junctions can be calculated using the following relation

$$\ln(\rho_i) = \frac{a_i \ln(S)}{\sum_{j=1}^{N} a_j} \tag{3.4}$$

The parameter a_n can be calculated based on a tabular recursive relation originally presented in [63]:First start by populating an initially zero-filled matrix x of dimension n x n using the following relations:

$$\begin{aligned} x(1,1) &= 2 \\ x(2,2) &= \frac{1}{\cos((2-w_q)\frac{\pi}{4})} \\ x(i,1) &= 2x(2,2)x(i-1,2) - x(i-2,1); i = 3,4,,.. \\ x(i,j) &= x(2,2)(x(i-1,j-1) + x(i-1,j+1)) - x(i-2,j); i,j = 3,4,,.. \end{aligned} \tag{3.5}$$

The first non-zero entry of the n^{th} row of the matrix x represents the impedance ratio at the middle section(s) of the transformer , the next element represents the next impedance ratios at the two adjacent junctions and so forth. Explicit recursive expressions for a_i is given by:

$$a_{(i)} = a_{(n+1-i)} = x(n, n+2-2i); i = 1,2,...,\frac{n+1}{2} \tag{3.6}$$

Once the junction impedance ratios are known the section impedances can be calculated readily according to the following relation:

$$Z_{i+1} = Z_i \rho_i \tag{3.7}$$

3.2.2 Synthesis of Ideal Banch-line Couplers

An ideal branch line coupler shown schematically in Fig. 3.3 is a symmetrical four port lossless network. The ideal coupler is characterized by a scattering matrix

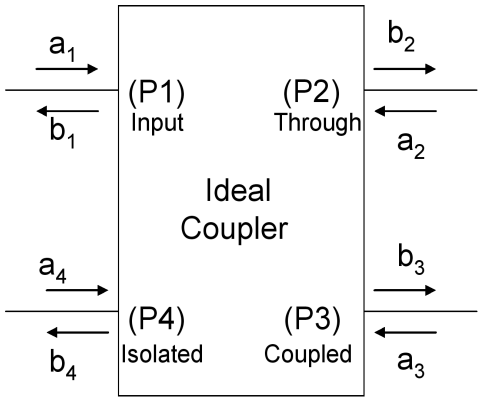

Figure 3.3: A schematic diagram of a general coupler circuit with port designations and incident waves $a_i$and reflected waves b_i

relating the incident and reflected waves at its four ports as given by 3.8. Special relations hold for the ideal coupler:

1. The four ports are all matched , $S_{ii} = 0;\ i = 1, 2, 3, 4$

2. The four ports are isolated in a special way $S_{14} = S_{23} = S_{32} = S_{41} = 0$.

3. There is a quadrature between the phases of certain ports $< S_{13} - < S_{13} = 90°$

$$\begin{bmatrix} b_1 \\ b_2 \\ b_3 \\ b_4 \end{bmatrix} = \begin{bmatrix} S_{11} & S_{12} & S_{13} & S_{14} \\ S_{12} & S_{11} & S_{14} & S_{13} \\ S_{13} & S_{14} & S_{11} & S_{12} \\ S_{14} & S_{13} & S_{12} & S_{11} \end{bmatrix} \begin{bmatrix} a_1 \\ a_2 \\ a_3 \\ a_4 \end{bmatrix} \tag{3.8}$$

A coupler is usually characterized mainly by an important quantity which is the coupling C. The coupling indicates how much energy is coupled from an input port to the corresponding coupled port, this is given by S_{13}.This is a design parameter, i.e. the coupling is specified before starting the design. Next we will

present the ideal circuit synthesis of branch line couplers.

Problem Statement.

Given a frequency range $f_1 \rightarrow f_2$ and a required coupling factor C find the number of sections N and the immitance ratios of each section such that the input reflection coefficient at the four ports does not exceed a prescribed quantity r

Step1: Relate the Coupler to a Corresponding Transformer

To be able to synthesize the branch line coupler imittance ratios one has to relate the parameters of the coupler, i.e. the coupling C, the return loss r and the bandwidth.w_c to a set of parameters of the prototype transformer i.e. an impedance ratio S, a return loss S_{max} and a bandwidth w_q that will be used in the synthesis procedure. This is done as follows:

The coupler bandwidth is related to the transformer bandwidth by a contraction factor β . That factor can be estimated either graphically in [47] or through approximate expressions in [20] In addition all other parameters required for the synthesis of the prototype transformer are given by:

$$S = \frac{1+C}{1-C} \tag{3.9}$$

$$S_{\max} = 1 + C(S_{c\max} - 1) \tag{3.10}$$

$$S_{c\max} = \frac{1+r}{1-r} \tag{3.11}$$

$$w_q = \frac{w_c}{\beta} \tag{3.12}$$

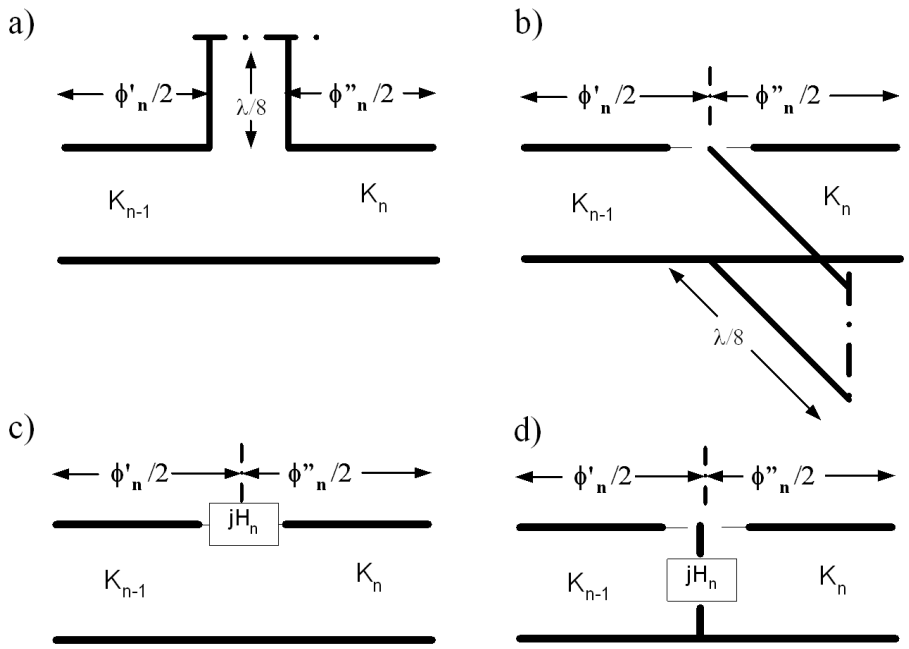

Figure 3.4: Equivalent circuit at the n^{th} junction of the coupler a,c series representation b,d parralel representation

Once the parameters of the transformer are known it can be readily synthesized as explained before in 3.2.1 from the synthesis one will be able to calculate the order N and the junction impedance ratios. The order of the coupler is $N+1$

Step2: Calculate the Immitance Ratios

A single section of the coupler is depicted in Fig.3.4 The dual cases of series and parallel representations are depicted with symmetry planes at the middle of the branches. In the series case the reactance jH_n represents the impedance looking into branch n when it's terminated at it's symmetry plane while in the parallel case it represents the susceptance looking into branch n when it's terminated at it's symmetry plane. Both values are numerically equal to the immitance value

of the branch since this would be the input impedance/susceptance looking into a terminated transmission line of electrical length of $\frac{\pi}{4}$

Noting that the branches are separated by a $\frac{\pi}{2}$ pieces of transmission lines, we can conclude that:

$$\phi"_n + \phi'_{n+1} = \frac{\pi}{2} \tag{3.13}$$

Now define the ratios

$$u_n = \frac{H_n}{K_{n-1}} \tag{3.14}$$

$$w_n = \frac{K_n}{K_{n-1}} \tag{3.15}$$

After obtaining the VSWR's of the transformer 3.4 a new quantity is defined

$$\Gamma_n = \frac{\rho_n - 1}{\rho_n + 1} \tag{3.16}$$

The solution for the ratios un and wn is a numerical calculation that was presented in [20] and which follows a graphical; procedure originally presented in [52], it starts as follows:

for odd N

1-Set $n = \frac{N+1}{2}$ and $\phi"_n = \frac{\pi}{4}$

2-Solve the two equations 3.17 and 3.18 simultaneously subject to the condition that $w_n > 1$

$$u_n^2 + w_n^2 - 2w_n\frac{1+\Gamma_n^2}{1-\Gamma_n^2} + 1 = 0 \tag{3.17}$$

$$u_n^2 - w_n^2 - 2\frac{w_n u_n}{\tan(2\phi"_n)} + 1 = 0 \tag{3.18}$$

3-Calculate

$$\phi'_n = \frac{1}{2}\tan^{-1}\left(\frac{2u_n}{u_n^2 + w_n^2 - 1}\right) \tag{3.19}$$

$$\phi"_{n-1} = \frac{\pi}{2} - \phi'_n \tag{3.20}$$

4-Decrease n by 1 and recurs till $n = 0$

for even N

1-Set $n = \frac{N+2}{2}$ and w_n=1

2-Calculate

$$u_n = \sqrt{\rho_n} - \frac{1}{\sqrt{\rho_n}} \tag{3.21}$$

$$\phi'_n = \phi''_n = \frac{1}{2}\tan^{-1}\left(\frac{2}{u_n}\right) \tag{3.22}$$

$$\phi"_{n-1} = \frac{\pi}{2} - \phi'_n \tag{3.23}$$

3-Decrease n by 1 and use recursion relations given in equations 3.17-3.20 until $n = 0$

By calculating the ratios u_n and w_n successive denormalization can be used to calculate all the immitance values given that K_0 is equal to one as shown in Fig. 3.1.

3.3 Modular Design of Ridge waveguide branch-guide coupler

3.3.1 Representation of the Unit Section using Equivalent Circuits

In this section we will present a modular approach to the design of ridge waveguide branch-guide couplers. Central to this approach is the basic building block, which will be called the unit section. The unit section is a four port network representing a branch connected between two main lines. The four port equivalent circuit representation of the unit section is shown in Fig. 3.5-a where the branch is realized by a transmission line of admittance Y_{branch} connected in parallel between the two main lines of unity admittance; this is used to represent the unit section in the H-plane configuration. Its dual circuit has the branch realized by a transmission line of impedance Z_{branch} connected in series between the two main lines of unity impedance; this is used to represent the unit section in the E-plane configuration. Since the unit section is fully symmetric the analysis of the four port problem can be reduced to calculation of two decoupled two port circuits by placing appropriate boundary conditions at the symmetry planes. In ideal circuit terms the odd mode circuit would be obtained if a short circuit is placed at the symmetry plane. In the electromagnetic problem this corresponds to a Perfect Electric Wall (PEW) being placed at the plane of symmetry forcing all tangential electric field components to vanish. The even mode case is where in ideal circuits an open

circuit is placed at the plane of symmetry. In the corresponding electromagnetic problem a Perfect Magnetic Wall (PMW) being placed at the plane of symmetry forcing all tangential magnetic field components to vanish . The unit sections realization for ridge waveguide H-plane unit section is shown in Fig. 3.5-b, while the E-plane counter part is shown in Fig. 3.5-c Their split halves can also be seen in Fig. 3.5-e and f.

The goal is to extract the equivalent circuit parameters of the unit sections at a fixed frequency, namely Φ, θ_{branch} and Y_{branch} or Z_{branch}. Consider the equivalent circuits for the series case shown in Fig. 3.5-d. The circuit is comprised of a unity impedance transmission line of length $\Phi/2$ cascaded by a series stub of impedance Z_{branch} and length $\Theta/2$ then cascaded by another unity impedance transmission line of length $\Phi/2$. By multiplying the three individual $ABCD$ matrices, it can be readily shown that the $ABCD$ matrix of the odd (PEW) circuit is:

$$\begin{pmatrix} A & jB \\ jC & D \end{pmatrix}_{odd} = \begin{pmatrix} \cos\Phi - \frac{x_o \sin\Phi}{2} & j(\sin\Phi + \frac{x_o(1+\cos\Phi)}{2}) \\ j(\sin\Phi - \frac{x_o(1-\cos\Phi)}{2}) & \cos\Phi - \frac{x_o \sin\Phi}{2} \end{pmatrix} \quad (3.24)$$

$$jx_o = jZ_{branch}\tan(\theta_{branch}/2)$$

While the $ABCD$ matrix of the even (PMW) circuits is:

$$\begin{pmatrix} A & jB \\ jC & D \end{pmatrix}_{even} = \begin{pmatrix} \cos\Phi - \frac{x_e \sin\Phi}{2} & j(\sin\Phi + \frac{x_e(1+\cos\Phi)}{2}) \\ j(\sin\Phi - \frac{x_e(1-\cos\Phi)}{2}) & \cos\Phi - \frac{x_e \sin\Phi}{2} \end{pmatrix} \quad (3.25)$$

$$jx_e = -jZ_{branch}\cot(\theta_{branch}/2)$$

Upon inspection of the two $ABCD$ matrices, one can identify the possibility of obtaining the required parameters by simple algebraic operations. The

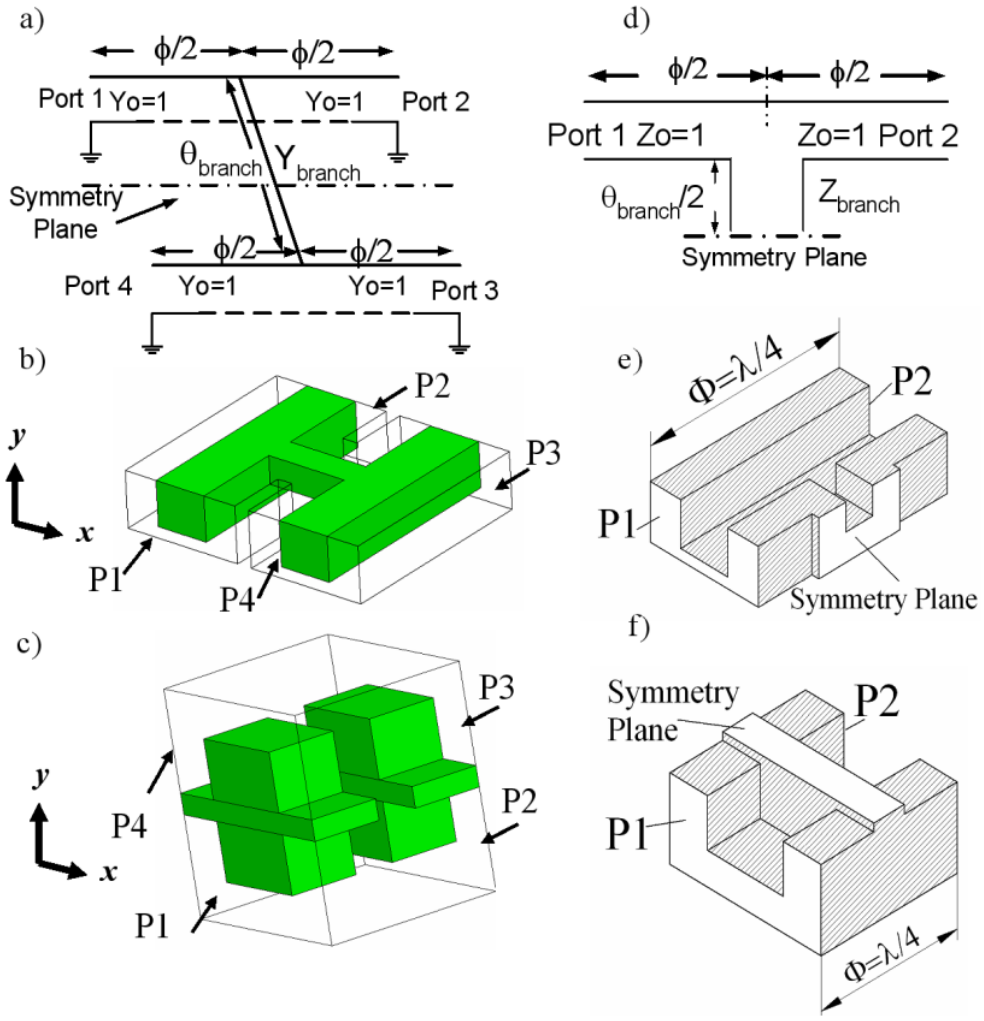

Figure 3.5: a) Equivalent circuit for a unit section "Parallel representation" b) Unit section in H-plane configuration c) Unit section in E-plane configuration d) Equivalent circuit of half unit section "Series representation". e) H-plane half unit section cut along symmetry plane f) E-plane half unit section cut along symmetry plane

parameters Φ, θ_{branch} and Z_{branch} can be obtained as explained in the following equation:

$$\begin{aligned} Z_{branch} &= \sqrt{(B-C)_{odd}(B-C)_{even}} \\ \theta_{branch} &= 2\tan^{-1}\left(\left|\frac{Z_{branch}}{(B-C)_{even}}\right|\right) \\ \Phi &= \sin^{-1}\left(\frac{B+C+(C-B)A}{2+\frac{(B-C)^2}{2}}\right)_{even/odd} \end{aligned} \tag{3.26}$$

Similarly for the parallel representation case:

$$\begin{aligned} Y_{branch} &= \sqrt{(B-C)_{odd}(B-C)_{even}} \\ \theta_{branch} &= 2\tan^{-1}\left(\left|\frac{Y_{branch}}{(B-C)_{odd}}\right|\right) \\ \Phi &= \sin^{-1}\left(\frac{B+C+(B-C)A}{2+\frac{(B-C)^2}{2}}\right)_{even/odd} \end{aligned} \tag{3.27}$$

To obtain the equivalent circuit parameters of the unit section, rigorous Mode Matching Method is used to compute the scattering parameters of half the unit section at the chosen fixed frequency with both PEW and PMW boundary conditions at the appropriate symmetry planes. Then the $ABCD$ parameters are computed by S to $ABCD$ transformation. Finally, from the $ABCD$ parameters of both the odd and even sub-sections the equivalent circuit parameters are obtained, using equation 3.26 or equation 3.27.

3.3.2 Analysis of the unit section using mode matching

The full-wave analysis of this unit section is carried out by a rigorous mode-matching method in two stages. First, the eigen modes in all the waveguides constituting the unit section are calculated. Then the electromagnetic field in each

point of the structure is represented as a modal series. In the second stage, the field representations on each side of the discontinuity between two waveguides are matched. The complete 2 port scattering parameters of the unit section is obtained by cascading the generalized scattering matrix (GSM) of each basic discontinuity. Detailed treatment of the characterization of waveguides and the discontinuities can be found in [39, 70]

Mode Matching Analysis of the E-plane Unit Section

Fig. 3.6. shows the different cross-sections involved in the full-wave analysis of the E-plane unit section. There are two cross sections involved. The first is a single ridge waveguide and the second is a rectangular waveguide. A single GSM with each boundary condition imposed at the symmetry plane of the second cross-section to characterize the discontinuity between the ridge waveguide and the rectangular waveguide. A schematic diagram of the building blocks of the mode matching analysis of the E-plane unit section is shown in Fig.3.7

Mode Matching Analysis of the H-plane Unit Section

Fig. 3.8 . shows the different cross-sections involved in the full-wave analysis of the H-plane unit section. Here there are three cross-sections. The first one is that of a single ridge waveguide and the second is a double ridge waveguide while the third cross section is a triple ridge waveguide. Two GSM 's are calculated with each boundary condition imposed at the symmetry planes of cross sections 2 and 3 to characterize the discontinuities between the different waveguides of

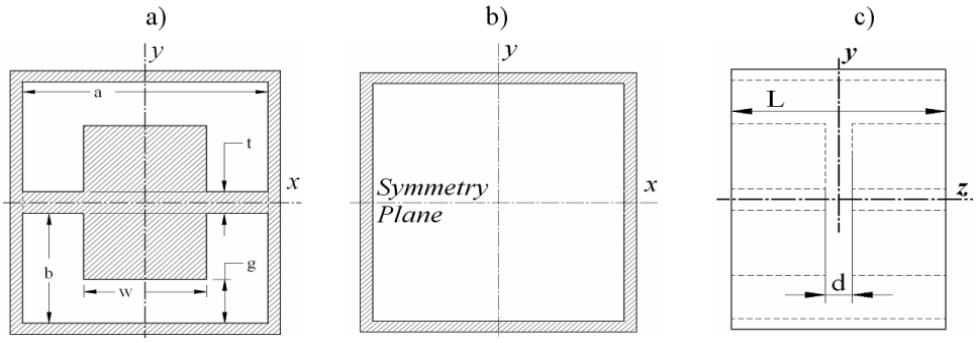

Figure 3.6: a) First Cross-section: Two separate single ridge waveguides b) Second cross-section simple rectangular waveguide of dimensions a times (2b+t) c) Dimensions of the E-plane unit section along the Z-direction

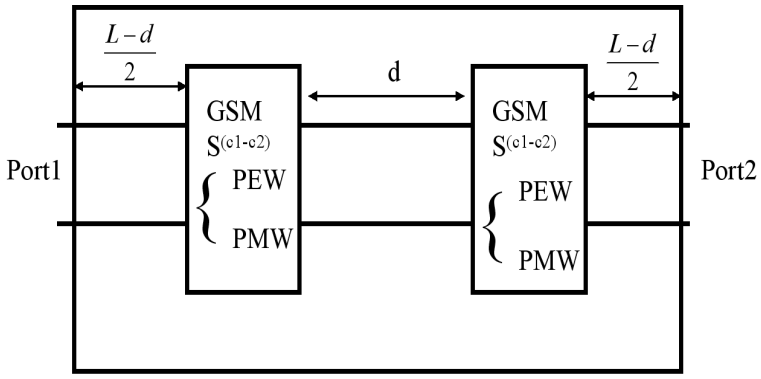

Figure 3.7: Schematic representation of the calculation of the generalized scattering matrix for a unit section in teh E-plane configuration dimensions are according to Fig. 3.6

the structure. A schematic diagram of the building blocks of the mode matching analysis of the H-plane unit section is shown in Fig.3.9

It is important to note that the procedure for extracting the equivalent circuit parameters described in the previous section includes the effects of the discontinuities at the junctions of all the ridge waveguides involved. Although the equivalent circuit does not explicitly include the discontinuities, the parameter values obtained include these effects, since the mode matching method accounts for the exact fields and hence all the discontinuities involved. However the extracted parameters are valid at a single frequency and therefore the equivalent circuit will be frequency dependent.

3.3.3 Choosing Initial Dimensions

Choice of the cross-sectional dimensions of the ridge waveguide, for the main line, depends mainly on the frequency band of the coupler operation. They are usually chosen such that the fundamental mode in the main ridge waveguide has a cut-off frequency adequately below the lower band edge and the first higher order mode has its cut-off frequency as far as possible from the higher band edge. As for the longitudinal dimensions of the lines and branches, the equivalent circuit approach discussed earlier is used to obtain their initial values. To design a unit section, the longitudinal dimensions have to be chosen in such a way to satisfy, as close as possible, the conditions required for best performance; namely $\Phi \approx \theta_{branch} \approx 90^{\circ}$ and Y_{branch} or $Z_{branch} \approx$ the immitance value obtained from ideal

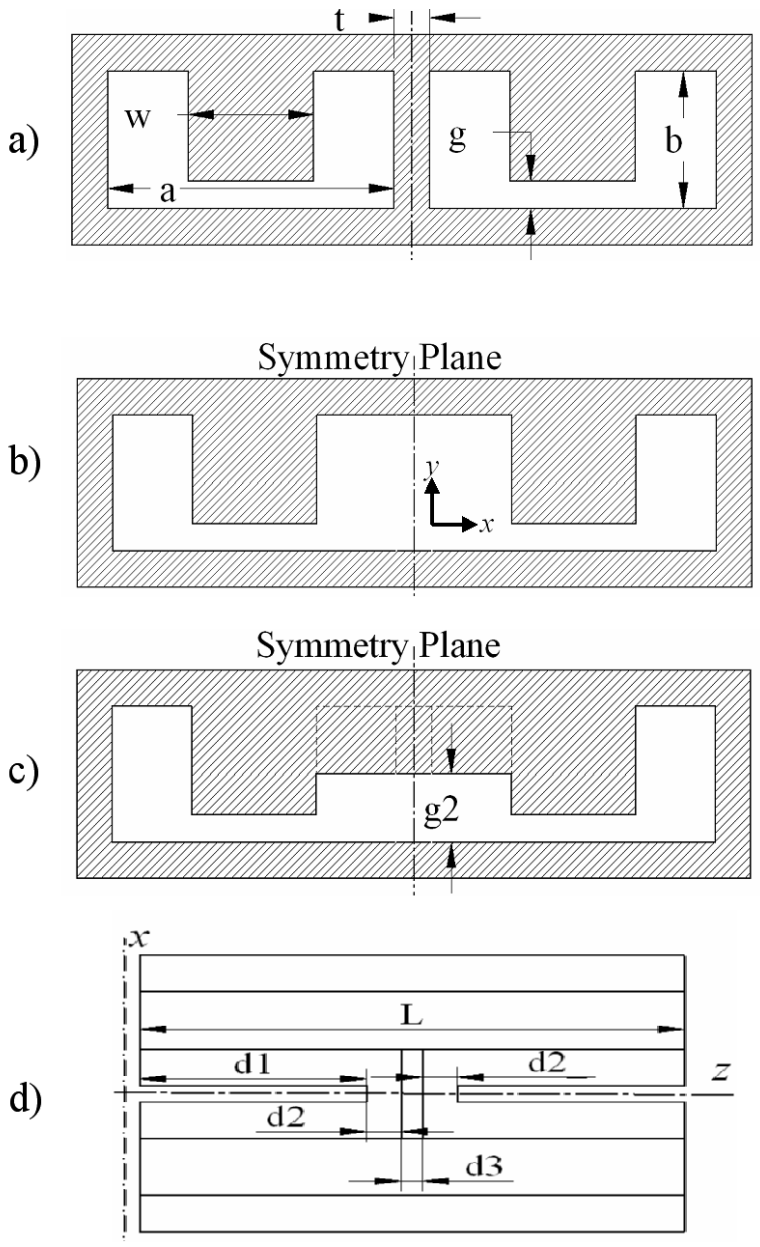

Figure 3.8: a) First Cross-section: Two separate single ridge waveguides b) Second cross-section: double ridge waveguide c) Third cross-section: multiple ridge waveguide d) Dimensions of the H-plane unit section along the Z-direction.

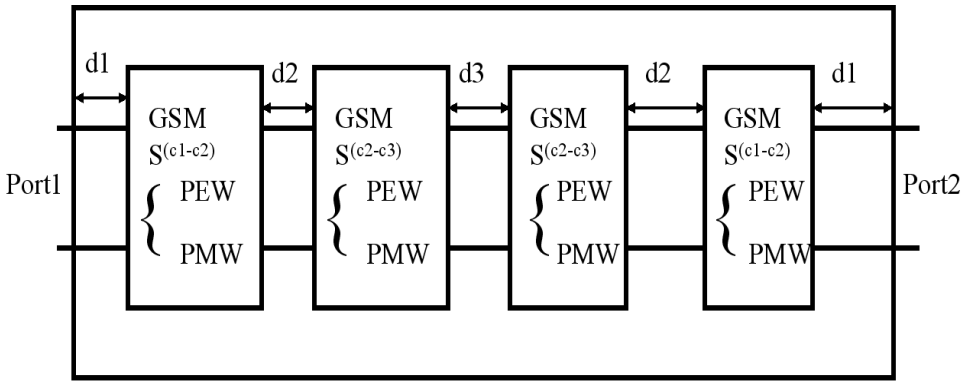

Figure 3.9: Schematic representation of the calculation of the generalized scattering matrix for a unit section in the H-plane configuration dimensions are according to Fig. 3.8

circuit synthesis. To be able to realize different immitance values for the branches of the coupler suitable combinations of the longitudinal dimensions have to be found. To demonstrate the systematic steps of the synthesis procedure two design examples, one H-plane coupler realized in LTCC technology and one E-plane coupler realized in empty metallic ridge waveguide technology, are presented.

3.4 H-planeCoupler Design Example

A coupler is required to have a return loss and isolation of better than 25dB over the frequency band (4.5-7.5) GHz the coupling is specified as3±0.5 dB over the whole frequency band. The coupler will be designed assuming LTCC technology.

3.4.1 Ideal Circuit Design.

Initial design is based on ideal circuit model of the branch line coupler. This is used to reduce the amount of full-wave optimization. Given the specifications of the coupler a synthesis procedure [52, 53] is used to get the admittance ratios needed to realize the coupler.

For tight coupling and wider bandwidths the admittance ratios of the branches to the main line tend to get extremely low and sometimes the synthesis procedure fails to produce immitance ratios that satisfy the synthesis goals. In our case with the wide bandwidth and in order to avoid such extremities tandem realization is used to get reasonable admittance ratios. The tandem connection method is based on cascading two or more identical loose couplers to realize an overall tight coupling performance. Fig. 3.10 shows a schematic view of a such arrangement.

Writing down the scattering parameters equations of the whole system according to equation 3.8. We will assume that each of the two couplers is perfectly matched $S_{11} = 0$ and perfectly isolated $S_{14} = 0.$; i.e. ideal. We can write:

$$b'_2 = S_{12}a'_1 + S_{13}a'_4 \tag{3.28}$$

$$b'_3 = S_{13}a'_1 + S_{12}a'_4 \tag{3.29}$$

$$a'_1 = b_2 = S_{12}a_1 + S_{13}a_4 \tag{3.30}$$

$$a'_4 = b_3 = S_{13}a_1 + S_{12}a_4 \tag{3.31}$$

$$b'_2 = (S_{12}^2 + S_{13}^2)a_1 + 2S_{12}S_{13}a_4 \tag{3.32}$$

$$b'_3 = 2S_{12}S_{13}a_1 + (S_{12}^2 + S_{13}^2)a_4 \tag{3.33}$$

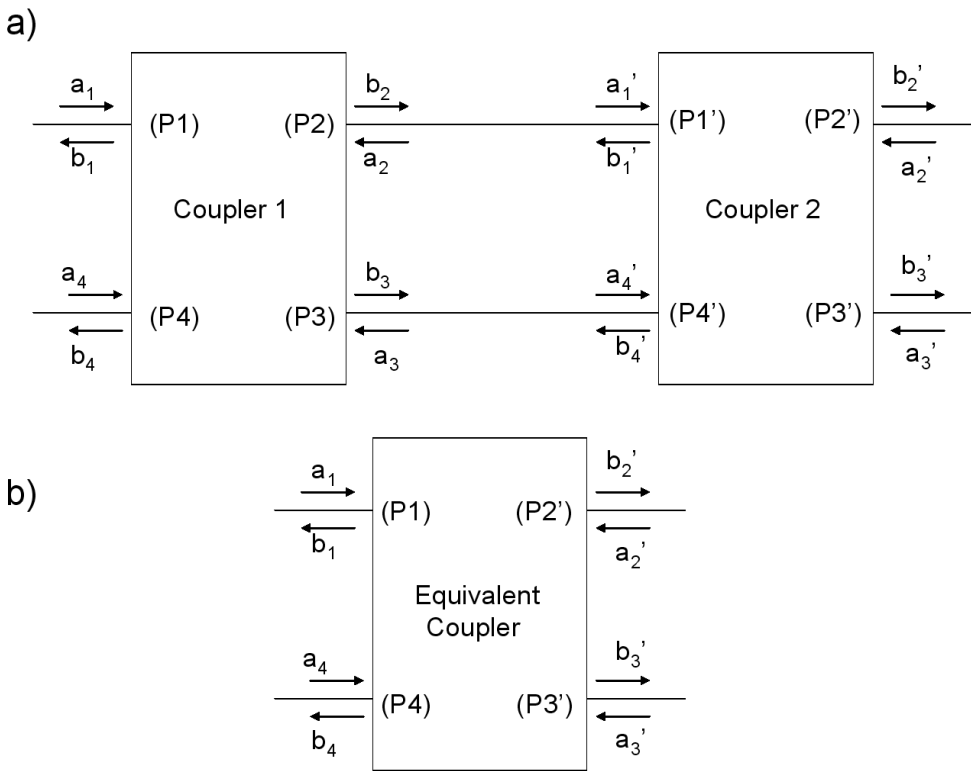

Figure 3.10: a)Connection of two identical Couplers b) Equivalent overall coupler

So the magnitude of the coupling of the two cascaded couplers is given by $\|2S_{12}S_{13}\|$ while the lossless condition dictates that :

$$\|S_{12}\|^2 + \|S_{13}\|^2 = 1 \tag{3.34}$$

Then we can relate the coupling of the single section S_{13} to the overall coupling given by $\|2S_{12}S_{13}\|$ as follows:

$$\|S_{13overall}\| = 2\|S_{13}\|\sqrt{1-\|S_{13}\|^2} \tag{3.35}$$

$$\|S_{13}\| = \sqrt{\frac{1-\sqrt{1-\|S_{13overall}\|^2}}{2}} \tag{3.36}$$

For the case of equal power split or $3dB$ coupler $\|S_{13overall}\| = \sqrt{\frac{1}{2}}$ which results in a required tandem connection of two couplers with $\|S_{13}\| = 0.3827$ or 8.3432 dB

In our case, to achieve the required coupling over the required bandwidth, a tandem connection of two $8.9dB$ rather than 8.3432 dB couplers is used. Fig.3.11 shows a comparison of the two cases. Each cascaded coupler is an 8^{th} order coupler with admittance ratios given by equation3.37.

$$Y_{line} = \begin{bmatrix} 1.025 & 1.046 & 1.062 & 1.068 & 1.062 & 1.046 & 1.025 \end{bmatrix} \tag{3.37}$$

$$Y_{branch} = \begin{bmatrix} 0.076 & 0.081 & 0.105 & 0.115 & 0.115 & 0.105 & 0.081 & 0.076 \end{bmatrix}$$

It can be seen that the line admittances are very close to unity so for simplicity all line admittances are fixed to unity without much effect on the performance of the coupler (see Fig. 3.12).

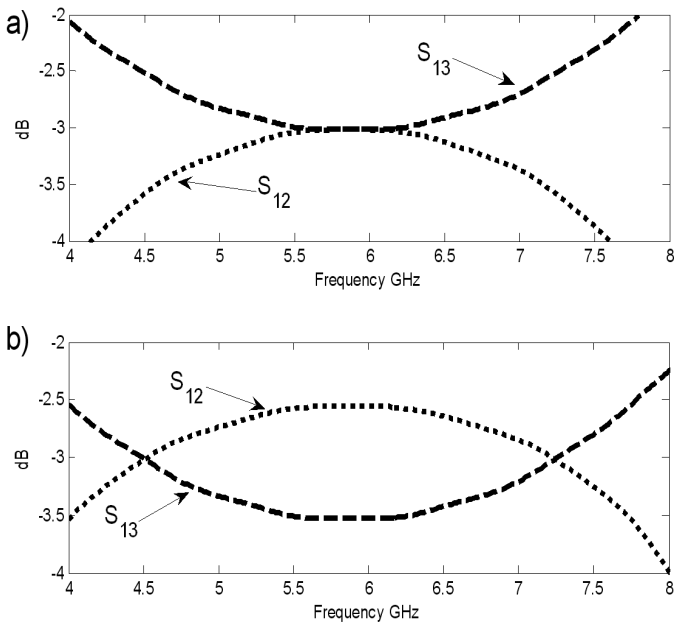

Figure 3.11: a) Response of two cascaded 8.32 dB couplers b) Response of two cascaded 8.9 dB couplers

3.4.2 Dimensional synthesis

The first step in the dimensional synthesis is the choice of the cross section. The choice of the cross section is subject to certain considerations. These considerations include frequency band at which the component operates, and the required power handling capabilities of the component. In the case of ridge waveguides some criteria have been established as to the ratios of the dimensions of the cross section namely the width of the enclosure a, its height b the width of the ridge w an the gap g. as shown in Fig. 3.6-c. These criteria can be summarized as follows:For best mode separation (the frequency separation between the fundamental mode cut off frequency and the first higher order mode) the following relation should hold $\frac{b}{a} \approx \frac{w}{a} \approx 0.45$ [71]. That leaves two main quantities to choose

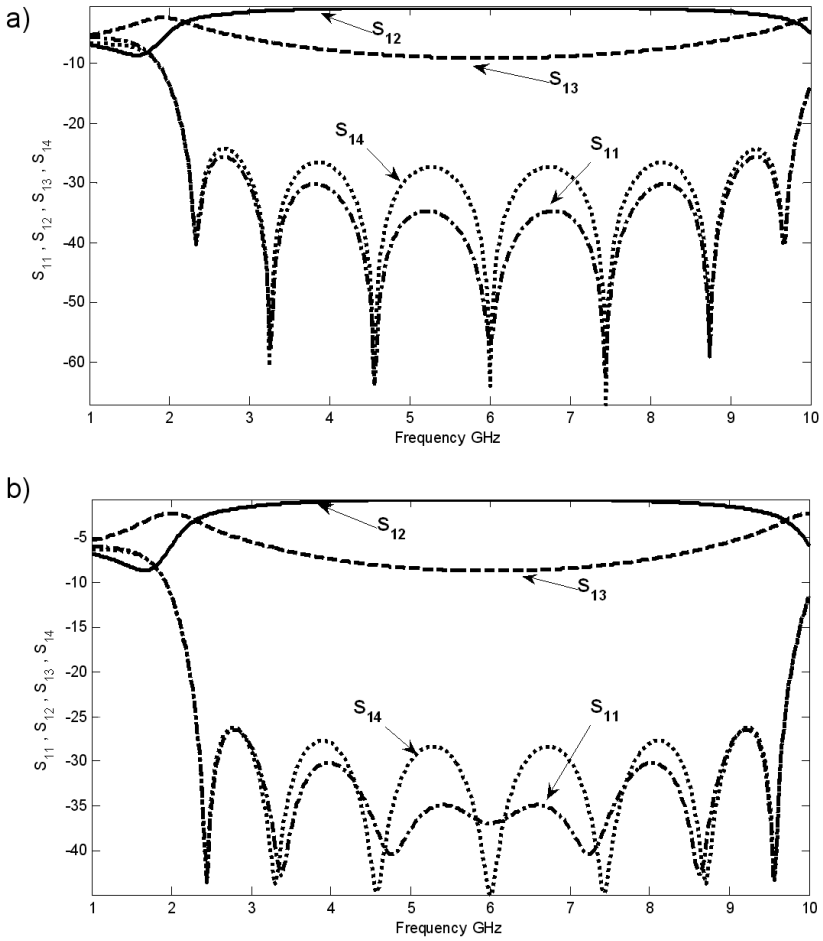

Figure 3.12: a) Ideal circuit response of an 8^{th} order $8.9dB$ coupler with admittance ratios according to 3.37 b) Ideal circuit response of an 8^{th} order $8.9dB$ coupler with admittance ratios according to 3.37 but with with all $Y_{line} = 1$.

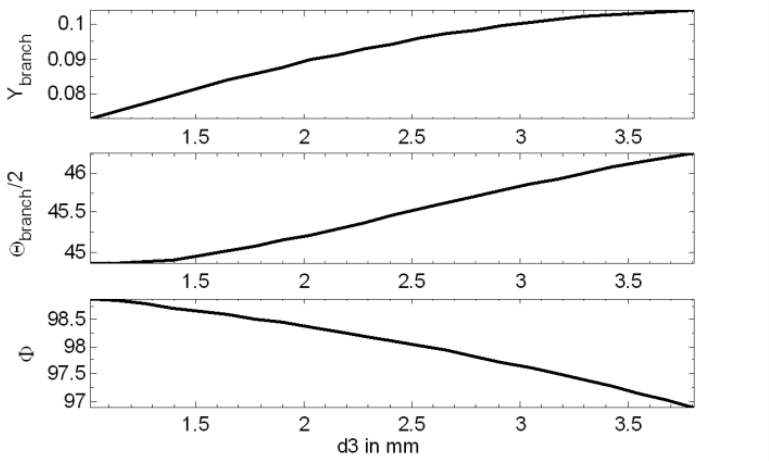

Figure 3.13: Variation of equivalent circuit parameters with dimension d3 according to Fig..3.8 -d, L=6.6 mm, d1=0.64 mm at f=5.5 GHz.

the a dimension and the gap g. These should be chosen in such a way that the cut off frequency of the fundamental mode is adequately below the frequency band of interest so that the models that assume ideal transmission line behavior of the waveguide hold. In addition the first higher order mode should be pushed as far away as possible from the frequency band of interest. Table 3.1 shows the variation of the cut off frequencies of the fundamental and first higher order modes of a ridge waveguide. The first entry (g = 4 LTCC layers)was chosen because it offered the best mode separation as well as an appropriate location of the cut off frequency of the fundamental mode.

In order to realize the different values of Y_{branch} obtained by the ideal circuit synthesis, suitable dimensions have to be found. Fig. 3.13 shows the variation of the equivalent circuit parameters while sweeping the longitudinal dimension $d3$. Required values of Y_{branch} from 0.076 to 0.115 can be synthesized by choosing the

Table 3.1: Variation of fundamental mode cut off frequency and first higher order mode cut off frequency vs. the gap of the ridge waveguide according to Fig.. 3.6-a with a=10.16 mm, b=4.75 mm (50 LTCC layers), w=4.445 mm, and LTCC layer thickness=0.095mm.

g	$f_{c1}(GHz)$	$f_{c2}(GHz)$
4 LTTC Layers	1.94279	10.44128
6 LTTC Layers	2.30939	10.01987
8 LTTC Layers	2.60909	9.77073
10 LTTC Layers	2.86963	9.62728

appropriate values for the dimension $d3$ from 1 mm to 3.5 mm while maintaining the total length of the unit section $L \simeq \lambda_g/4$ at the center frequency of the coupler. It's also noted that $\Phi \approx \theta_{branch}$ are close to their optimum values. After choosing the dimensions for all sections of the coupler they are assembled together to form the whole coupler. Figure 3.14 shows the interconnection of two sections i and $i+1$.

Rigorous mode matching is used to analyze the complete structure. It's worth noting that the structure is symmetric with respect to the yz and xz planes so this reduces the task to calculating one quarter of the structure with appropriate boundary conditions imposed at the symmetry planes. Fig. 3.15-a shows the initial response obtained by the dimensional synthesis procedure without any optimization.

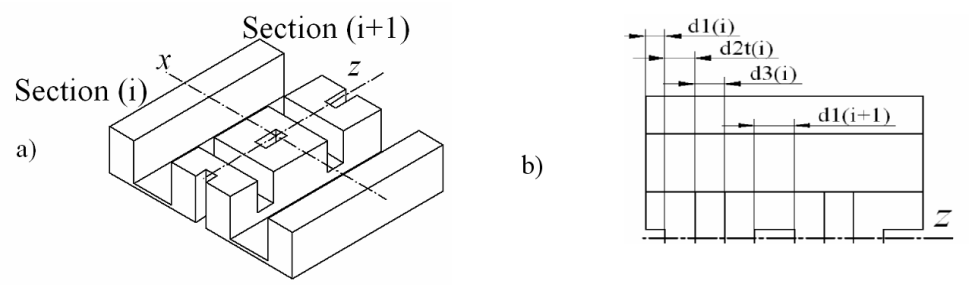

Figure 3.14: Two connected unit sections a) 3D view b) top view of half the structure with dimension convention

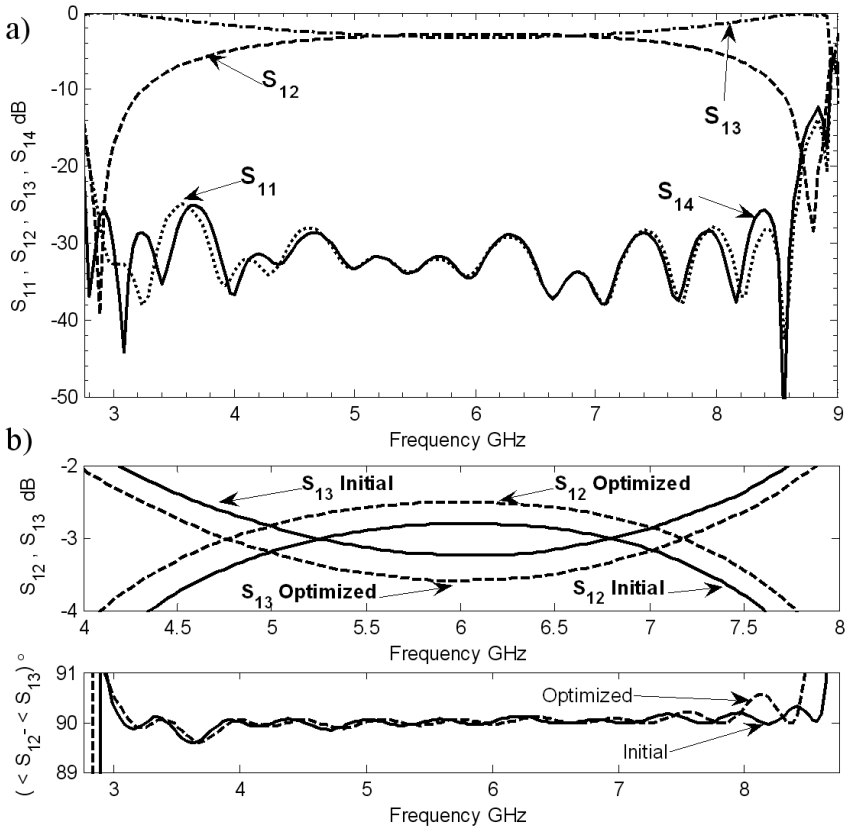

Figure 3.15: a) Initial response b) Initial and optimized response.

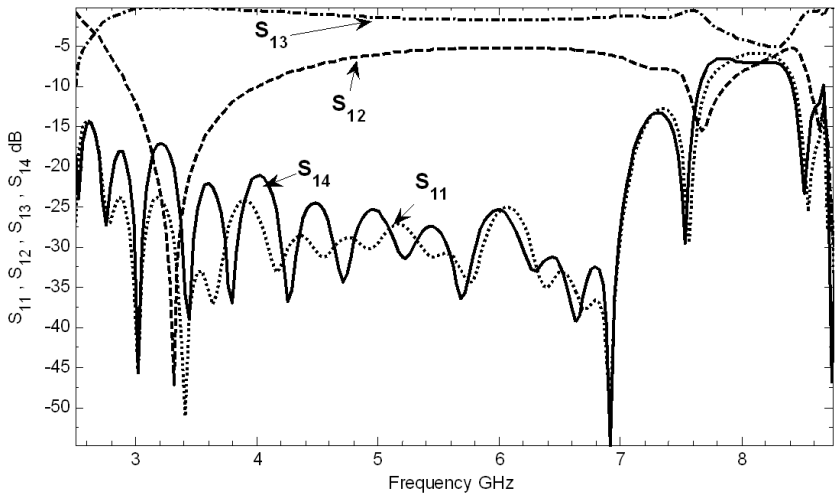

Figure 3.16: Initial response for the classical design approach.

The powerfulness of the proposed approach is evident by how close the initial response to the requirement is. Considering the symmetry of the branches in the 8.9 dB coupler, and optimizing only four branch dimensions $d3$ and the interconnecting length between the two 8.9 dB couplers; the optimized response shown in Fig. 3.15-b was obtained through 48 iterations taking 2.8 minutes. Efficient mode matching method enables simulating the whole 16 branch coupler structure in only 0.14 seconds per frequency, on a 3 GHz P4 processor with 2GB of memory.

For comparison purposes, a more classical approach was used to design the same coupler. The approach includes using closed form expressions for stand alone ridge waveguides [72]to calculate the Y_{branch} and λ_g of the wave guide. A second design with the same number of branches with the objective of satisfying the same specifications is attempted. Poor initial response (see Fig. 3.16) is obtained given

that the huge discontinuities were not taken into account in the synthesis. The same optimization was terminated after 1000 iterations after failing converge to the desired response.

3.4.3 Transition Design

A transition from the input LTCC ridge waveguide to a standard 50Ω strip line is needed to enable the interconnection of the coupler with other components in any microwave system, or simply for measurement purposes. Design procedures for such transition can be seen in.[73] The design starts by taking advantage of the similarity of field distribution of a single ridge waveguide and the field distribution of a single stripline aligned vertically with the bottom of the ridge waveguide near the gap as shown in Fig. 3.17 A connection between the ridge waveguide and an aligned stripline will facilitate a subsequent design of a stripine to a 50Ω stripline transition

The transition is basically a quarter wave transformer composed of striplines of different characteristic impedances that should be used to match the impedance of the first stripline to the 50Ω stripline. The synthesis procedure outlined in 3.2.1 will be employed here. The impedance of the first stripline is calculated to be 10.2498Ω to match that to 50Ω the impedances obtained using 3.2.1 are given by3.38 and its ideal circuit response is shown in Fig.3.18.

$$\begin{bmatrix} 10.2498 & 11.4336 & 15.0261 & 22.6382 & 34.1067 & 44.8233 & 50 \end{bmatrix} \Omega \qquad (3.38)$$

The given transition is realized in striplines whose width along with the width of

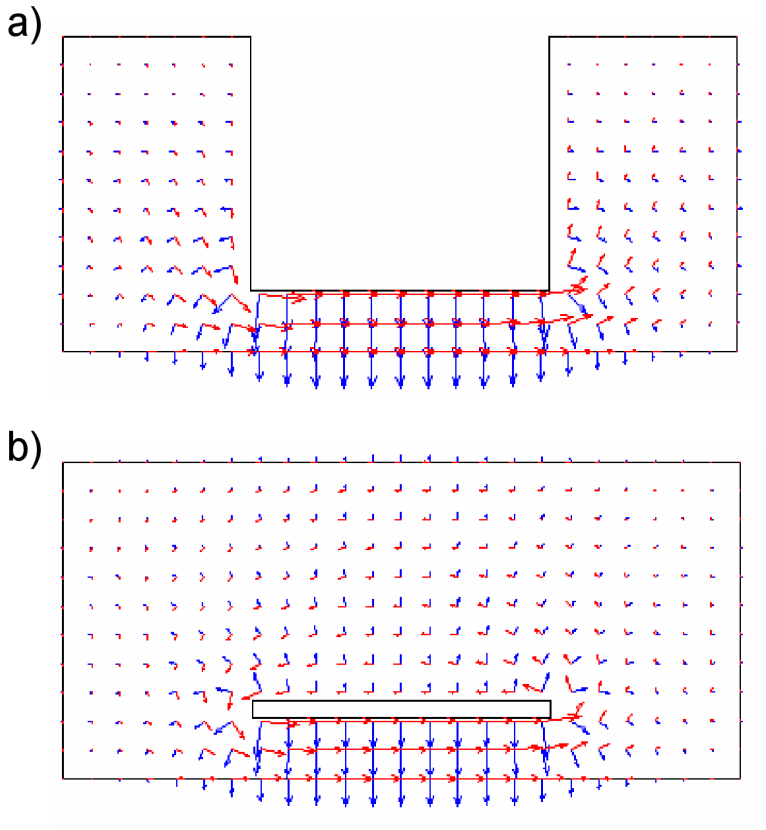

Figure 3.17: a)Field distribution of a single ridge waveguide b)Field distribution of a stripline aligned with the single ridge waveguide in (a)

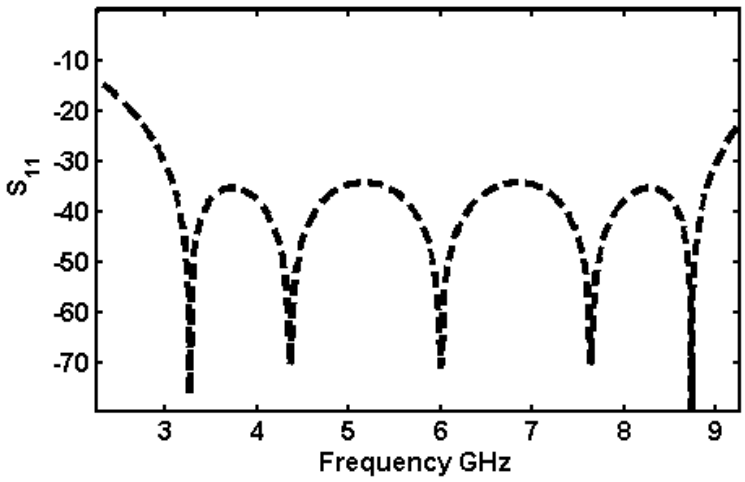

Figure 3.18: Ideal circuit response of the transition whose impedances are given by3.38

Table 3.2: Transition Cross Sectional Dimensions in mm and Impedances in Ohms

$a(i)$	[10.16 7.62 7.62 5.08 5.08 5.08 5.08 5.08 5.08 5.08]
$w(i)$	[4.45 4.45 3.94 3.94 3.05 2.03 1.22 0.71 0.48 0.41]
$Z(i)$	[10.24 10.17 11.28 10.76 13.61 18.81 26.99 37.49 45.98 50]

the enclosure control the characteristic impedance of the line. The a dimension of the rectangular enclosure of the transition is gradually reduced to prevent the propagation of higher order modes of the stripline sections that may be detrimental to the overall performance. The realized impedances are given in TABLE 3.2. The transition is simulated and optimized using rigorous mode matching technique and the results are verified by HFSS.

A transition with a return loss of better than 25 dB from 2.75 GHz to 9 GHz was designed. The response of the optimized transition is shown in Fig. 3.19 along

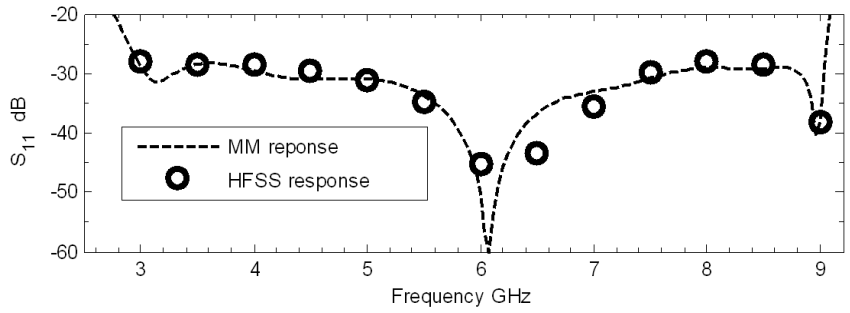

Figure 3.19: Optimized response of a transition from single ridge to 50 Ohm stripline

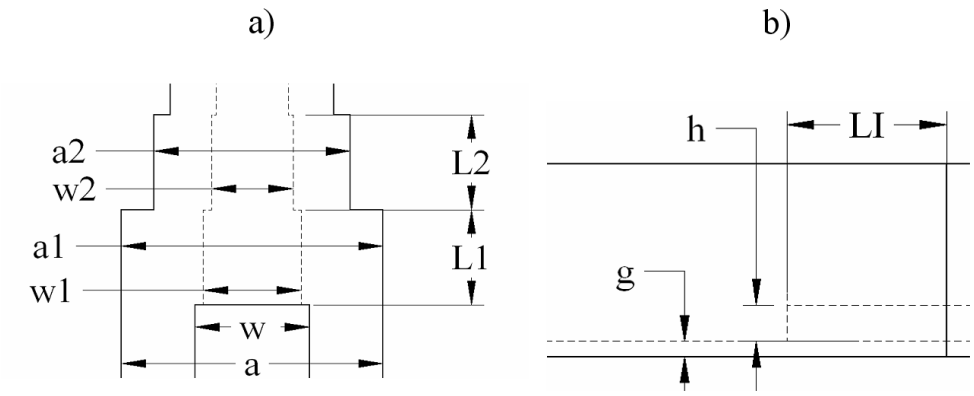

Figure 3.20: a) Top view of the first two sections of the transition b) side view showing the connection of the first section to the ridge waveguide

with HFSS simulation results to verify the mode matching results. A schematic drawing of the first two sections of the transition is shown in Fig. 3.20Detailed dimensions are given in Table 3.3.

3.4.4 Final full-wave Optimization

When the optimized coupler is connected with the optimized transition, slight deterioration of the response is observed. Final full-wave optimization is used to optimize the whole component. For the full-wave optimization an error function

to be minimized was constructed as follows:

$$
\begin{aligned}
F(X) \;=\; & W_{11} \sum_{i=N1}^{N2} \Psi(S_{11}(X, f_i), Goal_{S11}) + \\
& W_{14} \sum_{i=N1}^{N2} \Psi(S_{14}(X, f_i), Goal_{S14}) + \\
& W_{12} \sum_{j=M1}^{M2} \Delta(S_{12}(X, f_j), Goal_{S12up}, Goal_{S12down}) + \\
& W_{13} \sum_{j=M1}^{M2} \Delta(S_{13}(X, f_j), Goal_{S13up}, Goal_{S13down})
\end{aligned}
\tag{3.39}
$$

with

$$
\Psi(x, y) = \begin{cases} (x-y)^2 & if(x > y) \\ 0 & otherwise \end{cases} \tag{3.40}
$$

$$
\Delta(x, y, z) = \begin{cases} (x - average(y, z))^2 & if(x \notin [y, z]) \\ 0 & otherwise \end{cases} \tag{3.41}
$$

where X represents the set of variables to be used in the optimization, $f_{N1} - f_{N2}$ are the frequency set of points on which certain requirements on the isolation $Goal_{S14}$ and return loss $Goal_{S11}$for the coupler are specified and $f_{M1} - f_{M2}$ are the frequency set of points on which certain requirements on the through $Goal_{S12up}, Goal_{S12down}$and coupling $Goal_{S13up}, Goal_{S13down}$for the coupler are specified. The wights $W_{11}, W_{12}, W_{13}, W_{14}$ are used to balance the contribution of each of their corresponding terms to the total error function , their choice depends on how much deviation from the goal is tolerable in each term . In order to speed up the optimization only longitudinal dimensions are used in the optimization, this way the time-consuming part of calculating the modes is carried out once at the

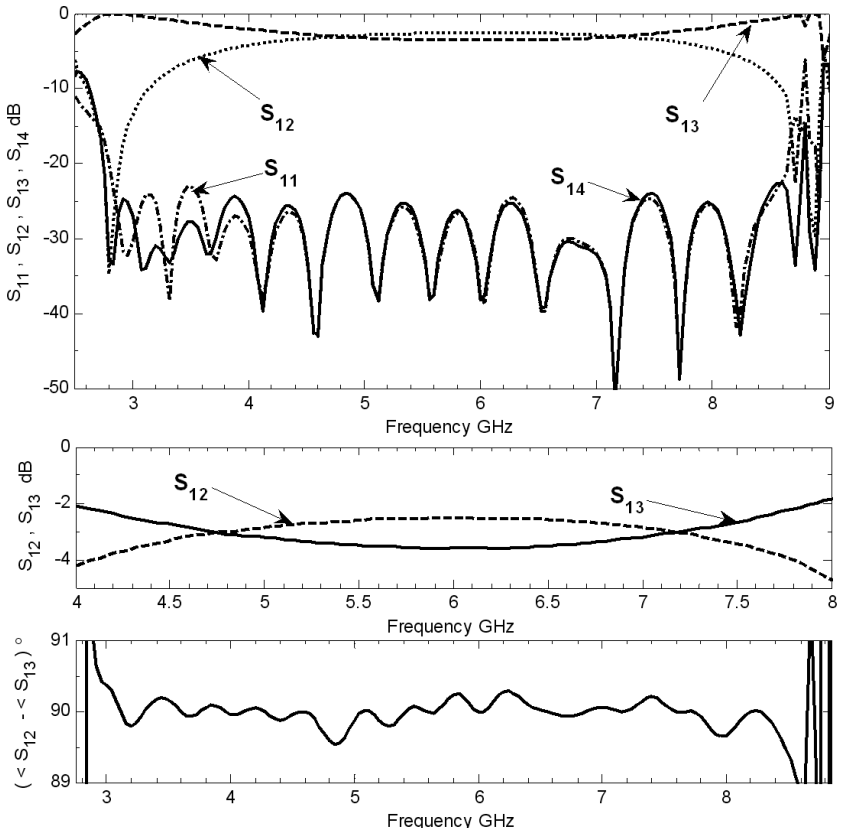

Figure 3.21: Final optimized response of the coupler and transition.

beginning rather than at each iteration of the optimization. Fig. 3.21. shows the final response of the optimized component. All dimensions are given in Table 3.3.

The LTCC technology has layer thickness of 0.095 mm and dielectric constant of 5.9. All vertical dimensions are multiple integers of layer thickness. The metallization used has a thickness h =0.0127mm, the interconnecting length between the two 8.9 dB couplers is the last entry in $d1$.

The transition is composed of 10 sections each with a housing width $a(i)$ and all share the same housing height b each section has a strip of width $w(i)$ and length $L(i)$ the first two sections of the transition are shown in Fig. 3.20.

Table 3.3: Dimensions of the Final optimized Coupler according to Fig. 3.8 and Fig. 3.14 and Transition according to Fig. 3.20.

Coupler Dimensions in mm					
a	10.16	b	4.75 (50 layers)	$g2$	1.52(16 layers)
w	4.445	g	0.38 (4 layers)	t	1.27
$d1(i)$	[2.54	0.66	0.67	0.67	0.71	0.67	0.67	0.66	0.69]
$d2(i)$	[2.02	2.06	1.37	1.11	1.10	1.43	2.05	2.03]	
$d3(i)$	[1.29	1.17	2.34	3.00	2.94	2.34	1.12	1.29]	

Transition Dimensions in mm										
$a(i)$	[10.16	4.62	7.62	5.08	5.08	5.08	5.08	5.08	5.08	5.08]
$w(i)$	[4.45	4.45	3.94	3.94	3.05	2.03	1.22	0.71	0.48	0.41]
$L(i)$	[2.7	0.89	12.53	0.29	4.70	4.55	4.29	4.43	4.87	6.35]

3.5 E-plane Coupler Design Example

A coupler that has a return loss and isolation of better than 25dB over the frequency band (3.1-4.9) GHz. The coupling is specified as3±0.5 dB over the whole frequency band. The coupler will be designed assuming air filled metallic ridge waveguide technology.

3.5.1 Ideal Circuit Design and dimensional synthesis

Given the specifications of the coupler a synthesis procedure [52, 53] is used to get the impedance ratios needed to realize the coupler. Since the bandwidth here is moderate compared to the design example of the H-plane coupler;the requirement can be met with a single 5^{th} order coupler without the need for tandem realization. The coupler has the following impedance ratios:

$$\begin{aligned} Z_{line} &= \begin{bmatrix} 1.088 & 1.119 & 1.119 & 1.088 \end{bmatrix} \\ Z_{branch} &= \begin{bmatrix} 0.206 & 0.400 & 0.512 & 0.400 & 0.206 \end{bmatrix} \end{aligned} \tag{3.42}$$

The considerations for choosing the cross sections of the ridge waveguide were discussed earlier (pp. 51). Table 3.4 shows the variation of the cut off frequencies of the fundamental and first higher order modes of a ridge waveguide. The first entry ($g = 3$ mm)was chosen because it offered the best mode separation as well as an appropriate location of the cut off frequency of the fundamental mode

In this design the line impedances are not as close to unity as the wider bandwidth coupler in the H-plane design example, so cross-sections of the lines

Table 3.4: Variation of fundamental mode cut off frequency and first higher order mode cut off frequency vs. the gap of the ridge waveguide according to Fig.. 3.6-a with a=55.52 mm, b=10.92 mm, and w=27.76 mm.

g	$f_{c1}(GHz)$	$f_{c2}(GHz)$
3	1.58127	8.57930
3.81	1.75513	8.46884
5.08	1.98718	8.36784

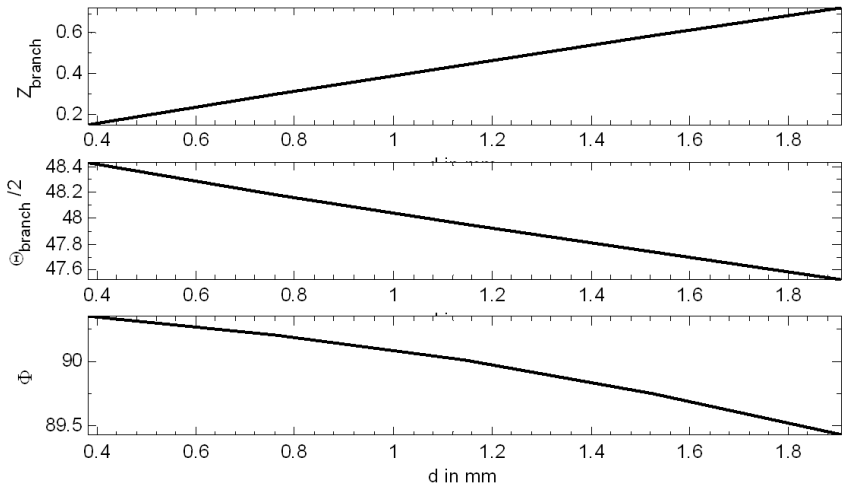

Figure 3.22: Variation of equivalent circuit parameters with longitudinal dimension d according to Fig. 3.6-c L=20.32 mm at f=4 GHz.

have to be chosen to have those line impedances.

It was shown in [66] that the gap of the ridge waveguide relates directly to the impedance of the line. In order to synthesize the branches, the same procedure introduced before will be followed here Fig. 3.22 shows the variation the equivalent

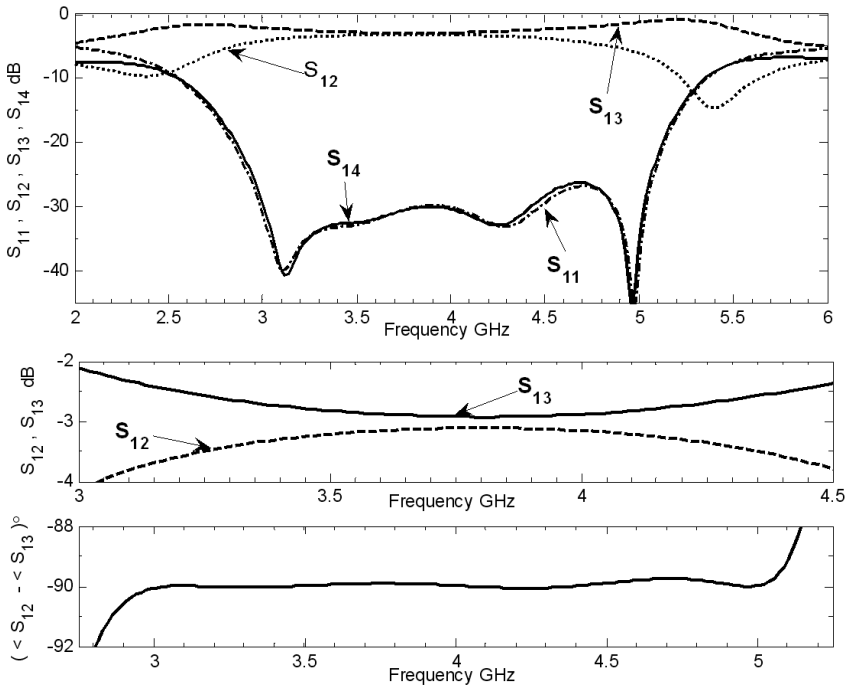

Figure 3.23: Initial Response of the 5 branch E-Plane Coupler

circuit parameters while sweeping the longitudinal dimension d.

Initial dimensions of the coupler can be obtained using the equivalent circuit information provided by Fig. 3.22 Given the symmetry of Z_{branch}, three unit sections with appropriate longitudinal dimensions were synthesized. The initial response of the synthesized coupler is shown in 3.23.

3.5.2 Transition to standard SMA connector

A transition from the input ridge waveguide to a standard 50Ω SMA connector is designed to enable measurement of the designed coupler. The transition is comprised of sections of strip lines which are connected to the edge of the input ridge waveguide near its gap benefiting from the similarity of the field distribution of

the strip line and that of the ridge waveguide in the gap region. The design procedures for such transition can be seen in [74]. The transition is basically a quarter wave transformer composed of striplines of different characteristic impedances that should be used to match the impedance of the first stripline to the last stripline which has a characteristic impedance of 50Ω The last stripline is then tapped in by the inner conductor of a standard 50Ω SMA connector. A transition with a return loss of better than 30 dB from $2GHz$ to $6GHz$ was designed. Schematic view of the transition along with dimension convention is shown in Fig. 3.24. The response, obtained by mode matching method, of the optimized transition is shown in Fig. 3.25. All dimensions are given in Table 3.5.

3.5.3 Final Full-wave optimization

The optimized coupler is connected with the optimized transition, and final full-wave optimization is used to optimize the whole component. Only longitudinal dimensions are used as optimization variables to speed up the optimization. The error function used in the optimization is based on a mask on the return loss, isolation, through and coupling. Figure 3.27. shows the final HFSS response of the optimized coupler with the transition to SMA. All dimensions are given in Table 3.5. while Figure 3.26 shows a schematic diagram of the coupler, with the dimensions convention used. Again in the E-plane structure, it's worthy to note that the structure is symmetric with respect to the yz and xz planes so this reduces the task to calculating one quarter of the structure with appropriate boundary

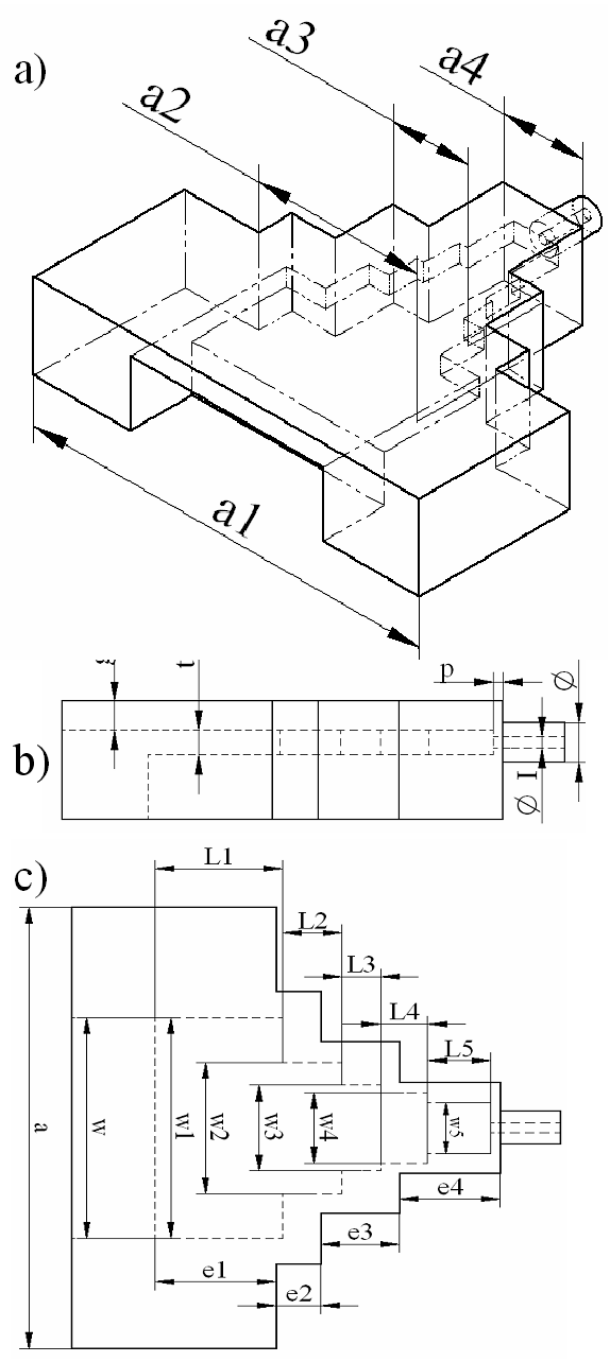

Figure 3.24: A transition from single ridge waveguide to a 50 Ohm SMA connector a)3D view b) side view c) top view

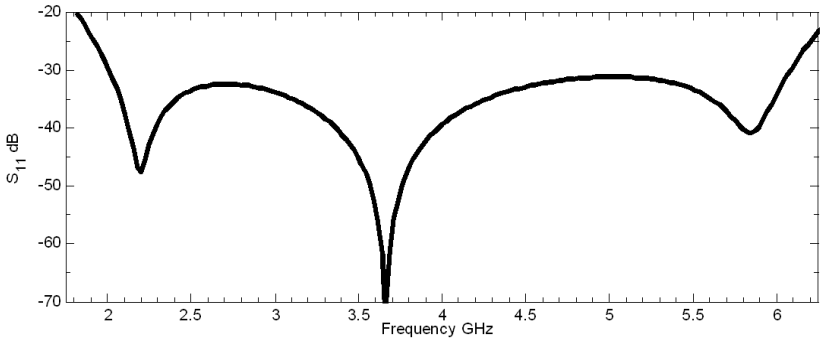

Figure 3.25: Full-wave response of a transition from ridge waveguide to a 50 Ohm SMA connector

conditions imposed at the symmetry planes.

3.5.4 Results of the Experimental Coupler

The optimized coupler was machined without any tuning screws. A photograph of the manufactured component is shown in Figure 3.29. The response of the component is shown in Figure.3.28 . Slight deterioration is observed and is believed to be due to the tolerances of the machining process. The machining tolerance was ± 1 mil. The coupler was assembled from several separate mechanical pieces and the contact of the SMA inner conductor with the stripline transition was difficult to align perfectly which contributed to worsen the observed return loss. Mode Matching was used to perform a random tolerance analysis of the coupler. In computation, a margin tolerance of ± 1 mil in the longitudinal dimensions of the coupler was used. Fig. 3.30 shows the results for the random tolerance analysis.

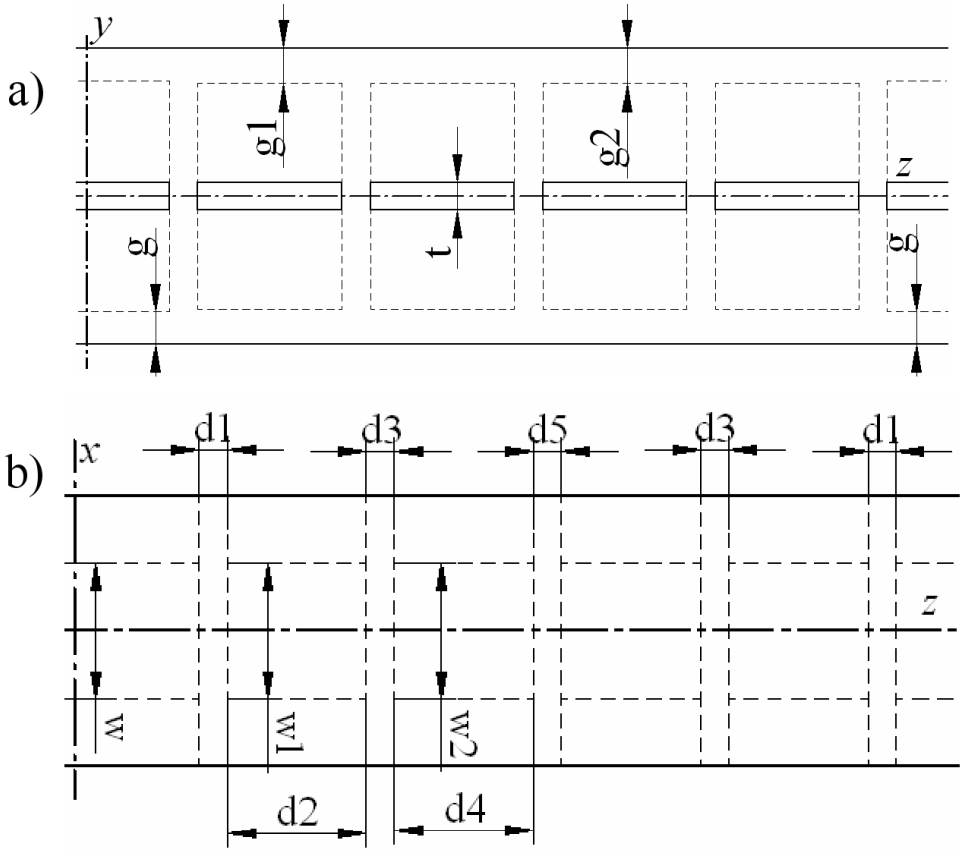

Figure 3.26: Schematic diagram of the 5 branch E-Plane Coupler a) Top view b) Side view

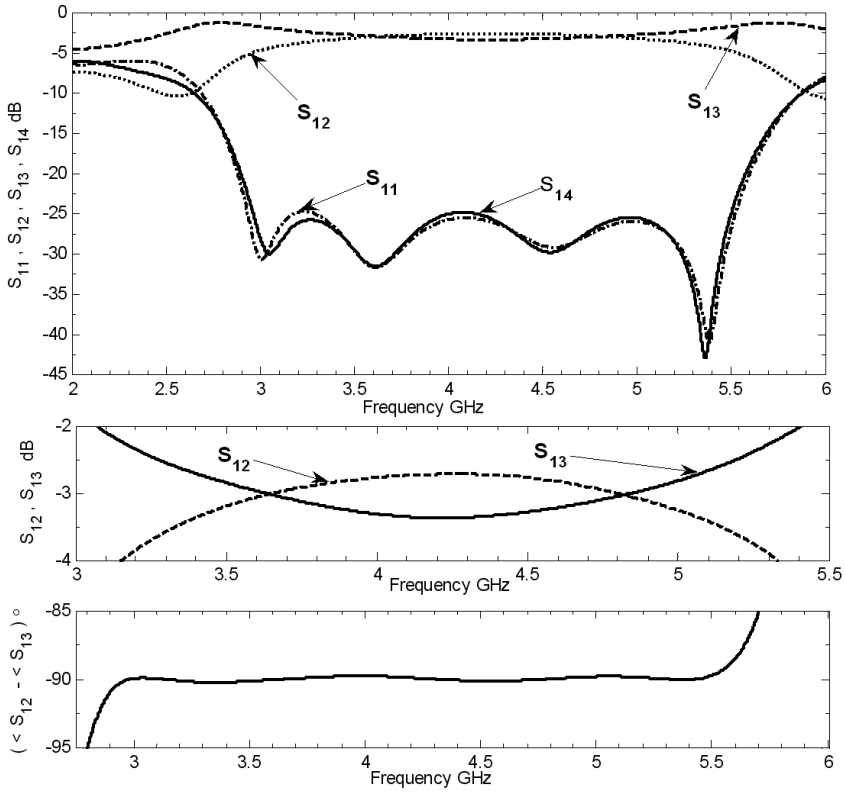

Figure 3.27: Final optimized response of coupler with transition

Table 3.5: Dimensions of the final optimized coupler according to Fig. 3.6 and Fig. 3.25. and transition according to Fig. 3.24.

Coupler Dimensions in mm							
a	55.52	b	10.92	g	3	w	27.76
$w1$	29.98	$g1$	3.23	$w2$	25.67	$g2$	3.23
$d1$	0.6	$d2$	18.79	$d3$	0.87	$d4$	19.67
$d5$	1.11	t	2.54				
Transition Dimensions in mm							
Φ_{II}	4.11	Φ_I	1.27	p	0.97	t	2.54
$w(i)$	[27.76 16.51 10.80 8.89 6.35]						
$L(i)$	[13.76 2.86 4.27 6.18 20.22]						
$a(i)$	[55.52 34.29 21.59 11.43]						
$e(i)$	[13.76 2.48 6.56 25.79]						

3.6 Conclusions

In this chapter a modular procedure for the synthesis, design and optimization of ridge waveguide couplers, in both H-Plane and E-plane configurations, has been presented. This approach was shown to enable the design of wideband couplers utilizing the characteristics of the ridge waveguide (compact size, wide mono-mode range). The modular approach consists of modeling a unit section that corresponds to a single branch, using an equivalent ideal transmission line circuit and utilizing rigorous mode matching method to obtain initial dimensions for the branches. By virtue of the very good initial response obtained by the synthesis procedure; the proposed approach of the design process greatly reduces the amount of full-wave optimizations needed to finalize the design process. Two design examples are given; a prototype was built and measured to validate the design process. Limitations to the proposed design methodology stems from inherent limitations in the ideal circuit synthesis. For the synthesis of the prototype quarter wave transformer the maximum fractional bandwidth allowed by theory is 200% taking the contraction factor between allowed coupler bandwidth and corresponding transformer bandwidth this limits achievable coupler bandwidth to around 125% . Another limitation was evident in the design of the E-plane couplers. Generally the wider the coupler transform the smaller the immitance ratios of the branches. In the E-plane case,this leads impractically small values of the width of the gap between main lines. This poses a technological limitation on achieving wider bandwidth in the E-plane case. Fortunately this limitation

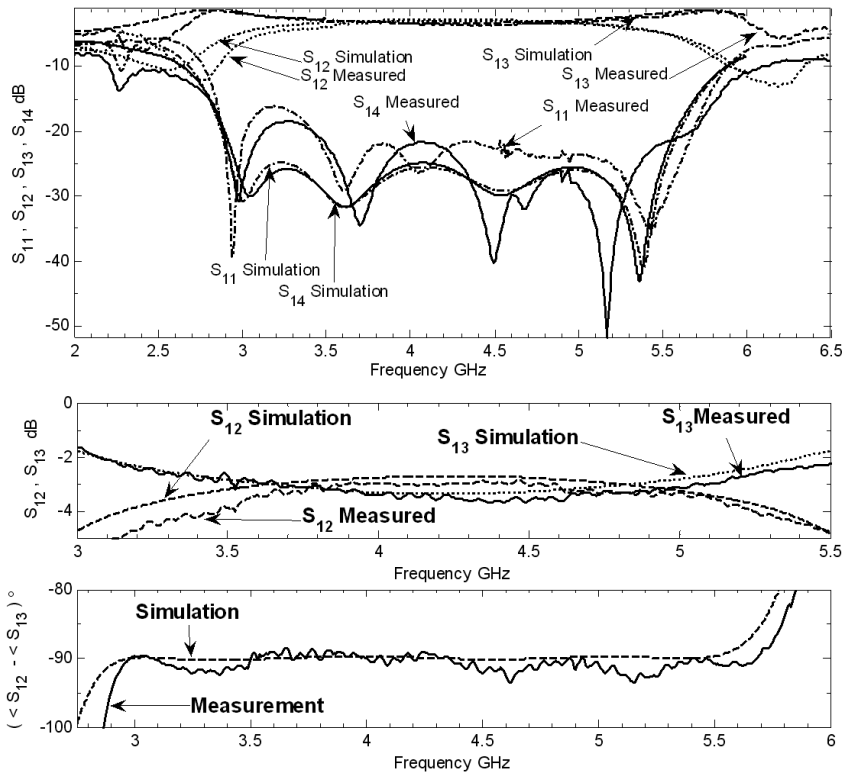

Figure 3.28: Measured Response vs. HFSS response

is overcome in the H-plane case, where the gap of the narrow ridge representing the branch controls to a great extent the immitance of the branch and the larger the gap the smaller the immitance which completely overcome the mentioned limitation. Finally the proposed structures offer good sensitivity with respect to manufacturing tolerances,as shown in Fig.3.30

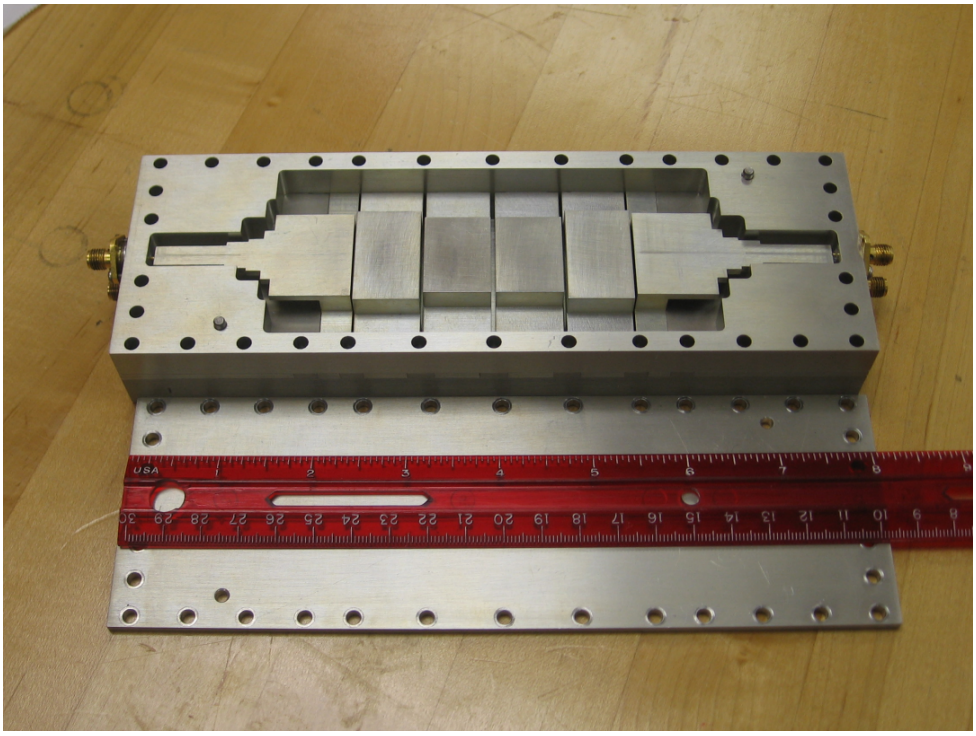

Figure 3.29: The manufactured coupler

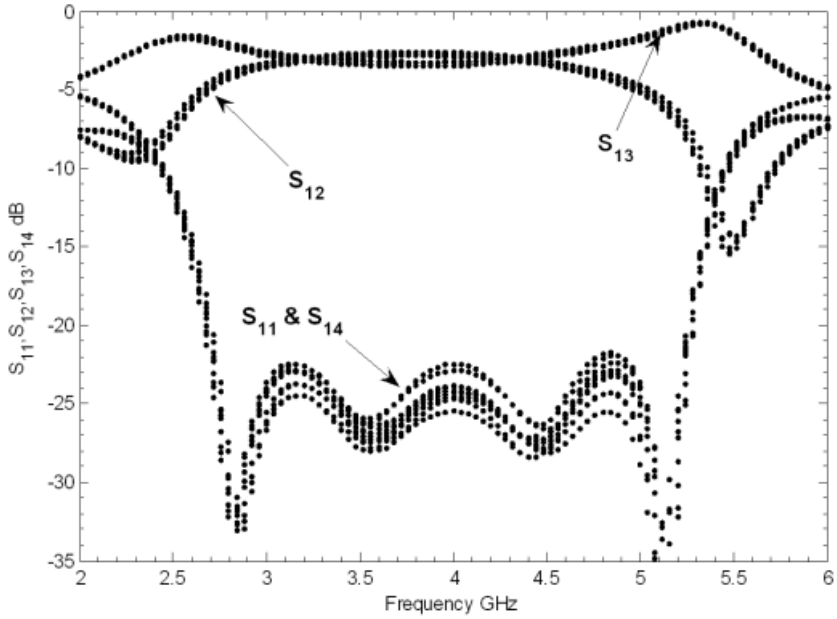

Figure 3.30: Random tolerance analysis of the 5 branch E-plane coupler

Chapter 4

Wide-Band Canonical Ridge waveguide Filters

4.1 Introduction

Microwave filters are widely used in many microwave systems. They are usually composed of resonators and coupling structures that exhibit pass and stop band characteristics in different frequency regions. The design challenge is how to find the set of dimension in a certain technology to realize a set of electrical, mechanical and environmental specifications. The subject of microwave filters has been under investigation for well over half a century with enormous body of literature available. Some very good historical review articles can be found in [75–79]

Although the subject of microwave filter design is well-established; the emerging modern communication systems greatly stimulate the need of more compact microwave filters with more stringent requirements. The predominant technology

historically employed for low-loss microwave filters is empty waveguide technology, where either rectangular or circular waveguides are used to realize the filters. Although ridge waveguides were known for quite long time [80–82],inadequate design methodologies hampered the utilization of their full potential. With advances in numerical techniques and the rapidly growing computational capabilities of modern computers ridge waveguide came to be considered a very good candidate to be utilized in realizing filters.[32, 40–42, 70, 83–88] Ridge waveguide offer excellent characteristics such as wide mono-mode band where the frequency separation between the cut off frequency of the fundamental and the first higher order mode is large compared to the corresponding mode separation of a rectangular waveguide with the same cut off frequency. This particular characteristic results in a better stop-band performance of the filters. Another advantageous characteristic is that for the same outer cross-section ridge waveguides operate at a much lower frequency compared to rectangular waveguides,this results in a more compact size of the filter On the other hand power handling capability of ridge waveguides are limited in comparison to rectangular waveguides.

In recent years an excellent approach to reduce size, cost,and increase reliability of RF/microwave systems is the integration of components into multilayer substrates using Low Temperature Co-fired Ceramics (LTCC) [89]. This technology employs a multilayer substrate manufactured by deposition, layer by layer, of dielectric and metallic patterns. Three-dimensional structures such as rectangular and ridge waveguides can be implemented in LTCC by the via technology [90–93].

Another key aspect in filter design is the selectivity of the filter, which

can be provided by an introducing finite transmissions zeros or elliptic function response. Elliptic function filters realized in waveguides have been extensively researched. Dual mode filters in circular [94–96] and elliptic [97] cavities were designed. Canonical filters using rectangular [98, 99] and ridge waveguide [9] were also proposed. However, all these designs were meant for narrow bandwidths (relative bandwidths $< 6\%$). More challenging requirements in modern communication and radar systems call for wider bandwidths.(relative bandwidths $> 10\%$) Wider bandwidths filters are more challenging to design. In this chapter we will discuss the challenges encountered in the design of such filters and explain possible solutions to successfully design wide-band canonical ridge waveguide filters realized in LTCC technology.

4.2 Ideal Circuit Representation of the filter

The generalized ideal lossless circuit used to model the network characteristics of the folded canonical elliptic function filter is shown in Fig.4.1, It consists of n (where n is an even number) LC resonators arranged in two identical rows. Each resonator in a row is coupled through a mutual inductance/capacitance M to adjacent resonators in the same row as well as to the corresponding resonator in the other row across the plane of symmetry. Each resonator (i) has total loop inductance L_i and capacitance C_i. The natural resonant frequency of the loop $f_{oi} = \frac{1}{2\pi}\sqrt{\frac{1}{L_i C_i}}$. In the case of synchronously tuned filters all resonators have the same resonant frequency and thus the assumption will be made that $L_i = L$ and

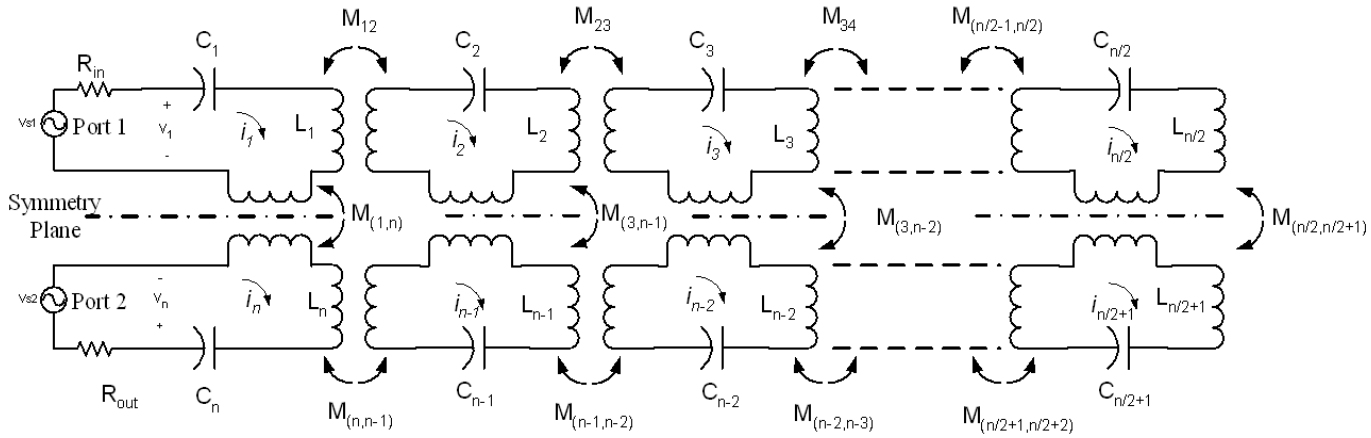

Figure 4.1: Ideal Circuit of a Canonical Folded Band Pass Filter

$C_i = C$

Writing the loop equations of the folded network shown assuming all loop currents are in the clock-wise direction one can easily construct the following impedance matrix representation of the loop equations:

$$[V] = [Z][J] \tag{4.1}$$

$$[V] = [\ v_1 \quad 0 \quad 0 \quad 0 \quad v_n\ ]^T \tag{4.2}$$

$$[J] = [\ i_1 \quad i_2 \quad ... \quad i_{n-1} \quad i_n\ ]^T \tag{4.3}$$

$$[Z] = j(diag(\lambda) - \omega[M]) \tag{4.4}$$

$$\lambda = Z_o(\frac{f}{f_o} - \frac{f_o}{f}); Z_o = \sqrt{\frac{L}{C}} \tag{4.5}$$

$$f_o = \frac{1}{2\pi}\sqrt{\frac{1}{LC}} \tag{4.6}$$

$$[M] = \begin{bmatrix} 0 & M_{1,2} & . & . & . & M_{1,n} \\ M_{1,2} & 0 & M_{2,3} & ... & M_{2,n-1} & 0 \\ . & . & . & . & . & . \\ . & . & . & . & . & . \\ . & M_{2,n-1} & . & . & 0 & M_{1,2} \\ M_{1,n} & . & . & . & . & 0 \end{bmatrix} \tag{4.7}$$

Now define the absolute coupling coefficient $k_{ij} = M_{ij}/L$ near the center frequency of the filter $\omega \approx \omega_o = \sqrt{\frac{1}{LC}} = \sqrt{\frac{L}{C}}\frac{1}{L} = \frac{Z_o}{L}$ we can write

$$[Z] = j(\lambda I - \frac{Z_o}{L}[M]) \tag{4.8}$$

$$[Z] = j(\lambda I - Z_o[K]) \tag{4.9}$$

$$[Z] = j(\lambda I - [m]) \tag{4.10}$$

Where $[m]$ is called the normalized coupling matrix, whose elements are $m_{ij} = Z_o k_{ij}$

From simple circuit theory, for a filter of bandwidth BW and center frequency f_o the following frequency transformation is very well-known

$$\lambda = \frac{f_o}{BW}(\frac{f}{f_o} - \frac{f_o}{f}) \tag{4.11}$$

The following correspondence between filter specifications i.e. center frequency and bandwidth and the ideal circuit model parameters can be easily established

$$Z_o = \frac{f_o}{BW} \tag{4.12}$$

From 4.12 and 4.9 it can be readily shown that the absolute coupling coefficient $k_{ij} = m_{ij}/Z_o = m_{ij}(\frac{BW}{f_o})$; thus for filters with wider bandwidths the required absolute coupling coefficient is directly proportional to the required bandwidth for a given center frequency.

4.3 Realization of Canonical Filters Using Ridge Waveguide and LTCC Technology

To obtain the electrical response given by the ideal circuit shown in Fig. 4.1 All elements of the ideal circuits should be mapped into a physical realization. the physical realization of choice in this design is ridge waveguide. The task is to realize all elements of the ideal circuit i.e. resonators, input coupling resistance and all other couplings including adjacent couplings and cross couplings

4.3.1 Realization of Resonators

The resonators are usually realized using a single ridge waveguide with its cross section chosen such that the cutoff frequency of the fundamental mode is approximately 30% below the lower frequency edge of the pass band. This choice enables the rejection characteristics of the filter at the lower frequency rejection band to be satisfied while maximizing the benefits of the wide mono-mode band of the ridge waveguide.

To realize ridge waveguide resonators in LTCC technology solid walls are approximated by interlaced vertical rows of vias while solid blocks like ridges are realized using both vertical vias and horizontal strips metallization to approximate the characteristics of a solid block of metal. Fig. 4.2 shows an idealized ridge waveguide resonator along with its LTCC realization.

4.3.2 Realization of Input/Output Coupling R_{in}/R_{out}

The input coupling resistance R_{in} is the termination resistance of the voltage source connected to the first LC lossless resonator of the circuit. Fig. 4.3 shows the equivalent circuit of the input coupling resistance connected to a single LC resonator along with a typical ideal circuit response. The input impedance looking into the LC resonator can be easily derived [69, 100]:

$$Z_{in} = j\sqrt{\frac{L}{C}}\left(\frac{f}{f_o} - \frac{f_o}{f}\right) \tag{4.13}$$

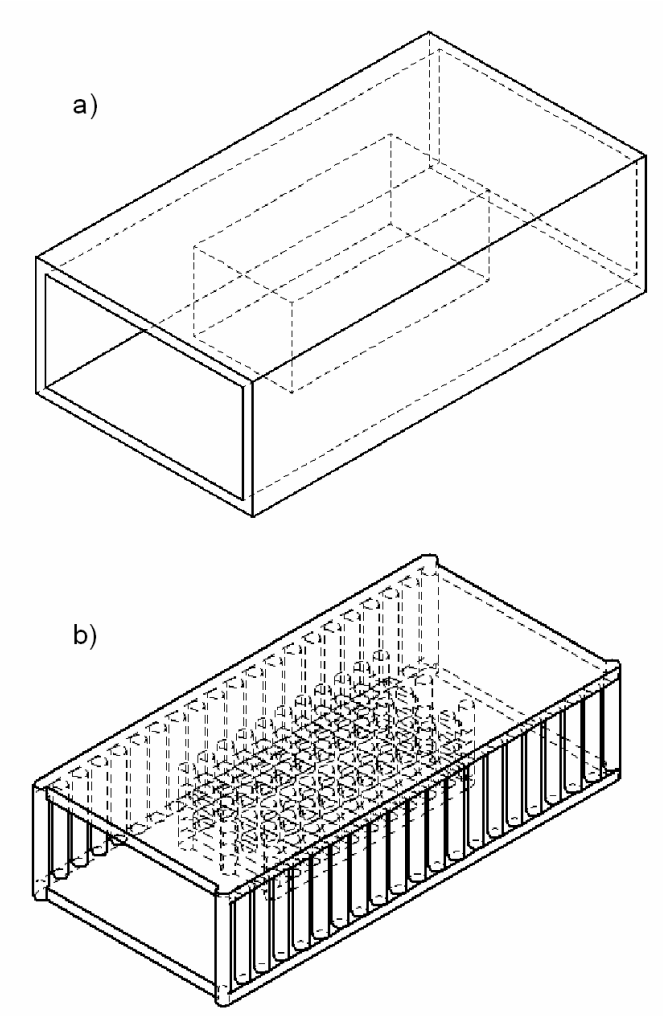

Figure 4.2: a) Idealized ridge waveguide resonator b) LTCC realization of ridge waveguide resonator

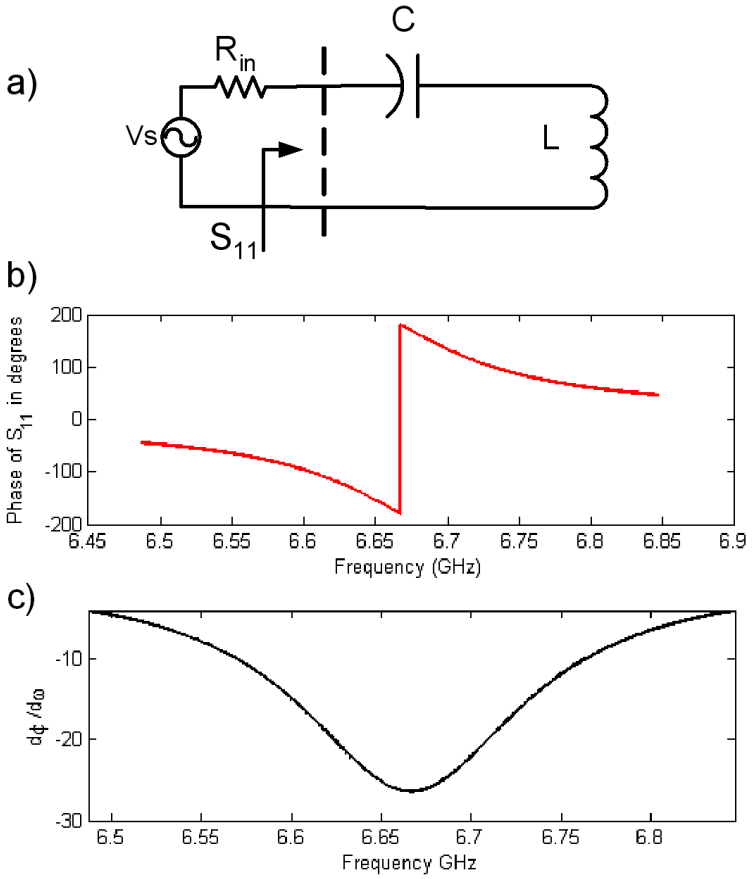

Figure 4.3: a) Single resonator with input coupling b)Phase of S_{11} c) Derivative of phase w.r.t. angular frequency ω

Taking $L = C = 1/(2\pi f_o)$ this expression reduces to

$$Z_{in} = j(\frac{f}{f_o} - \frac{f_o}{f}) \approx j\frac{2}{f_o}(f - f_o) = j\lambda \tag{4.14}$$

Calculating the reflection coefficient $S_{11}$and its phase ϕ we get

$$S_{11} = \frac{Z_{in} - R_{in}}{Z_{in} + R_{in}} = \frac{j\lambda - R_{in}}{j\lambda + R_{in}} = \frac{\lambda^2 - R_{in}^2 + j2R_{in}\lambda}{\lambda^2 + R_{in}^2} \tag{4.15}$$

and

$$< S_{11} = \phi = \tan^{-1}(\frac{2R_{in}\lambda}{\lambda^2 - R_{in}^2}) \tag{4.16}$$

The derivative of the phase w.r.t. frequency can be easily calculated to be

$$\frac{d\phi}{df} = \frac{-4R_{in}}{f_o}\frac{1}{R_{in}^2 + \frac{4}{f_o^2}(f - f_o)^2} \tag{4.17}$$

From equation 4.17 it can be seen that the minimum of the quantity $\frac{d\phi}{df}$ (which is negative) will be at the resonant frequency of the LC resonator. and at that specific frequency $\frac{d\phi}{df} = \frac{-4}{R_{in}f_o}$ or in other words

$$R_{in} = \frac{4}{\left|\frac{d\phi}{df}\right| f_o} \tag{4.18}$$

To calculate the resulting input coupling R_{in} corresponding to the chosen dimensions , the S parameters of the physical input/output structure is calculated numerically using full-wave simulation and through the use of equation 4.18

4.3.3 Realization of Inter-Cavity Couplings

Couplings between two lossless LC resonators can be represented by a mutual inductance/capacitance .[101]. The ideal circuit describing two identical LC resonators coupled by a mutual inductance M that corresponds to an absolute coupling coefficient k such that $k = \frac{M}{\sqrt{LL}} = \frac{M}{L}$, as shown in Fig. 4.4-a. Utilizing

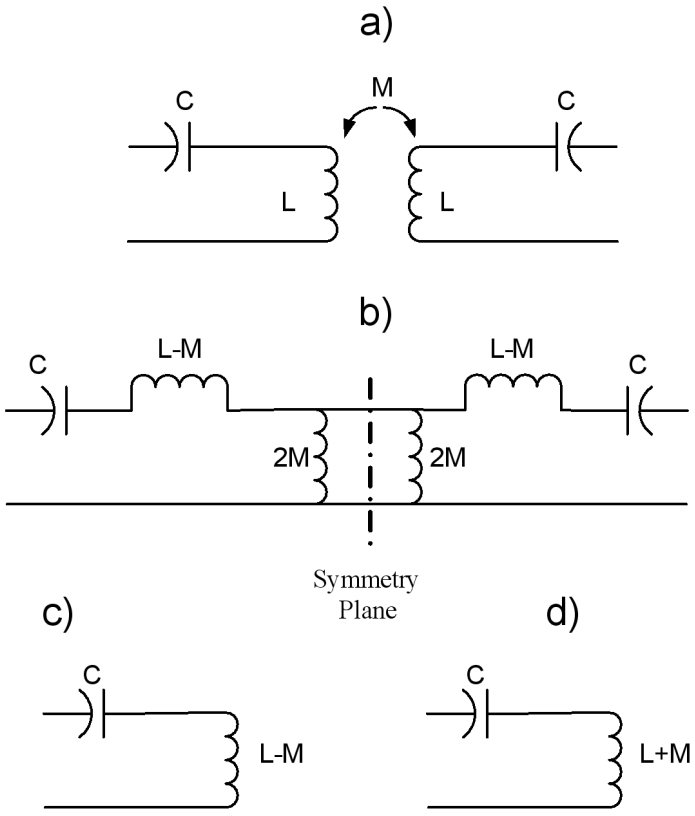

Figure 4.4: a) Two Coupled Resonators b)Alternative equivalent circuit for two coupled resonators c)Sub-circuit with short circuit imposed at plane of symmetry d)Sub-circuit with open circuit imposed at plane of symmetry

simple circuit transformations one can get the circuit shown in Fig. 4.4-b At the symmetry plane two conditions can be applied either a short circuit condition or an open circuit condition. In the case of short circuit termination at the plane of symmetry Fig. 4.4-c we will have a resonator that will resonate at a frequency $f_e = 1/2\pi\sqrt{C(L-M)}$ while in the case of open circuit termination Fig. 4.4-d the corresponding resonator will resonate at $f_m = 1/2\pi\sqrt{C(L+M)}$. Simple mathematics can be used to show that

$$k = \frac{f_e^2 - f_m^2}{f_e^2 + f_m^2} \tag{4.19}$$

$$f_o = \frac{f_e f_m}{\sqrt{(f_e^2 + f_m^2)/2}} \tag{4.20}$$

In the case of physical realization we can use the shown analysis conversely .We start by two identical coupled resonators and apply the two boundary conditions at the plane of symmetry in the following manner : for a short circuit the corresponding physical boundary condition is a Perfect Electric Wall (PEW) at which tangential electric field components vanish. In the case of open circuit the corresponding physical boundary condition is a Perfect Magnetic Wall (PMW) at which tangential magnetic field components vanish. By calculating the resonant frequencies for the physical structure under the two boundary conditions and using equations 4.19 and 4.20 we can calculate the inter-cavity coupling coefficient k and the synchronous resonant frequency f_o and the coupling in frequency units is given by $M = kf_o$.The sign of the coupling k has a physical meaning , if k has a positive sign this indicate that the coupling is dominated by magnetic field couplings while if the sign is negative this indicates that the coupling is dominated

by electric field coupling.

a) Adjacent Couplings

Adjacent couplings can be represented by a mutual inductance/capacitance between two lossless LC resonators. To map this into a physical realization a reactance between two resonators must be realized. That can be achieved by using a section of waveguide working under cutoff frequency so it can be represented by a reactance over the band of the filter Two possible realizations will be presented, in the first case shown in Fig. 4.5 the adjacent couplings are realized by sections of evanescent rectangular waveguide. In the second design shown in Fig. 4.6 the adjacent couplings are realized by sections of evanescent ridge waveguide with the same housing of the resonator sections but with narrower ridges (lower cutoff frequency for the evanescent mode). It will be shown that the second design is more advantageous for wide-band filters. The reasons for that will be discussed in details in later sections.

b) Cross Couplings

Cross couplings are those couplings that couple resonators in different rows in the folded configuration. They are required to have either negative or positive signs. Given the field distribution of a resonant ridge waveguide cavity, the best way to achieve electric (negative) coupling is to use an iris centered below the ridge waveguide resonator where the electric field is concentrated and provides the strongest coupling. On the other hand magnetic (positive) coupling is best

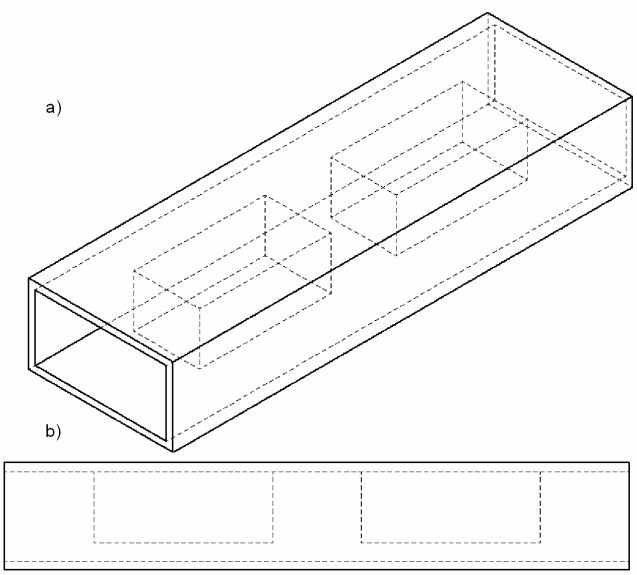

Figure 4.5: Two ridge waveguide resonators coupled by evenescent rectangular waveguide section a) 3-D view b) Side view

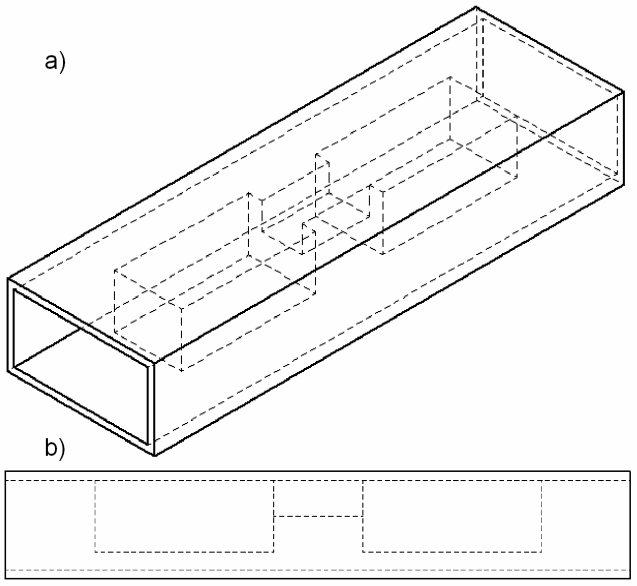

Figure 4.6: Two ridge waveguide resonators coupled by evenescent narrow ridge waveguide section a) 3-D view b) Side view

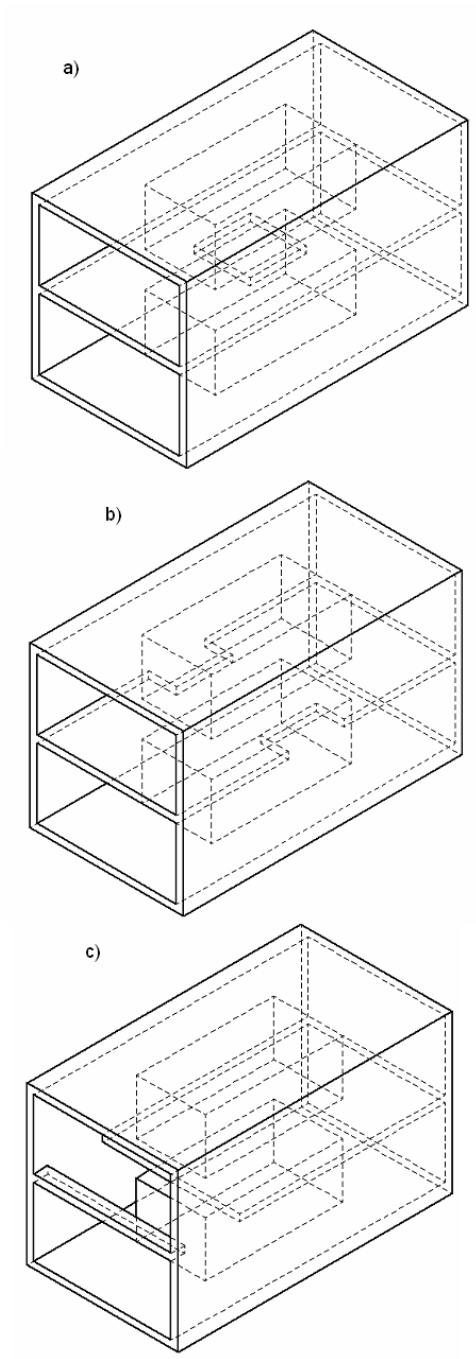

Figure 4.7: b) Two ridge waveguide reonators coupled by two magnetic type side irises

3) Two ridge waveguide reonators coupled by a magnetic type strip iris

achieved by using irises on the periphery around the ridge waveguide resonator. Traditionally that was achieved in [98, 99] by side irises adjacent to the lateral walls of the waveguide. This approach will be proven not suitable for filters with larger bandwidths.

4.4 Design Examples

To show the complete design process of a canonical folded quasi-elliptic filter realized in ridge waveguide. We will design, a sixth order filter with center frequency of 6.665 GHz and bandwidth of 720 MHz The minimum required stop-band rejection is 40 dB, and the maximum in-band return loss should be better than 26.4 dB. To realize the response in LTCC ridge waveguide the following steps are followed.

4.4.1 Ideal Circuit Design

An ideal lumped element circuit satisfying the specifications is obtained according to ideal network synthesis [102, 103]. The ideal circuit has normalized input/output resistance $R_{in} = R_{out} = 1.262$ and a normalized coupling matrix given by 4.21 The ideal circuit response corresponding to the given coupling matrix is

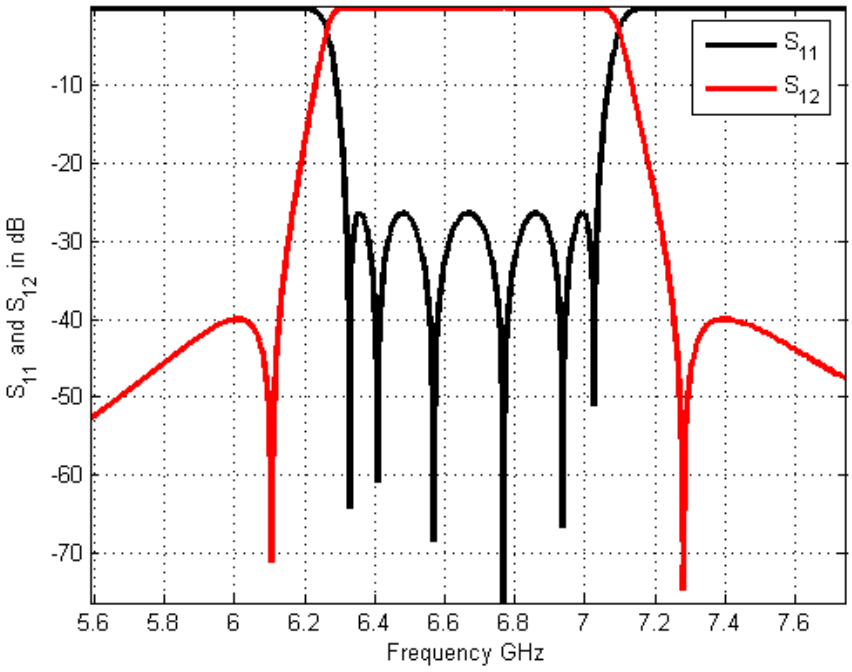

Figure 4.8: Ideal circuit response corresponding to 4.21

shown in Fig. 4.8.

$$M_n = \begin{bmatrix} 0 & 0.9547 & 0 & 0 & 0 & 0 \\ 0.9547 & 0 & 0.6312 & 0 & -0.1327 & 0 \\ 0 & 0.6312 & 0 & 0.7168 & 0 & 0 \\ 0 & 0 & 0.7168 & 0 & 0.6312 & 0 \\ 0 & -0.1327 & 0 & 0.6312 & 0 & 0.9547 \\ 0 & 0 & 0 & 0 & 0.9547 & 0 \end{bmatrix} \tag{4.21}$$

The filter is implemented by a ridge waveguide configuration first proposed in [88], with cavities arranged in two layers. The adjacent cavities are coupled by sections of evanescent waveguides, while the non-adjacent resonators employ irises opened at the intermediate wall. Fig. 4.9 shows a visualization of the physical

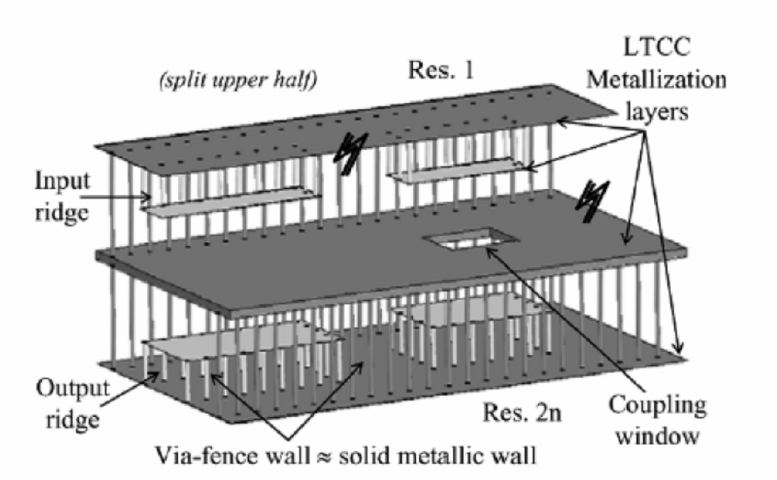

Figure 4.9: Physical realization of a part of canonical LTCC ridge waveguide filters [70]

realization in LTCC technology.

4.4.2 Dimensional Synthesis of Resonators and Coupling Structures

The considerations for choosing the cross sections of the ridge waveguide were discussed earlier (PP. 51). For Filter applications choosing the cut off frequency of the fundamental frequency is of great importance. A good rule is to have the cut off frequency of the fundamental mode such thet $f_{c1} \approx 0.7 f_1$ where f_1 is the frequency of the lower edge of passband of the filter[104]. Table 4.1 shows the variation of the cut off frequencies of the fundamental and first higher order modes of a ridge waveguide. The first entry ($g = 6$ LTCC layers) was chosen because it offered the best mode separation as well as an appropriate location of the cut off frequency of the fundamental mode

Table 4.1: Variation of fundamental mode cut off frequency and first higher order mode cut off frequency vs. the gap of the ridge waveguide according to Fig.. 4.10-b with arec=250 mil, brec=115.94 mil (31 LTCC layers), w=110 mil, and LTCC layer thickness=3.74 mil.

$hrid$	$f_{c1}(GHz)$	$f_{c2}(GHz)$
6 LTTC Layers	4.53263	21.11472
8 LTTC Layers	5.13341	21.16784
10 LTTC Layers	5.66934	21.23902

In order to realize the filter function using ridge waveguide transmission lines a set of dimensions of the resonators and coupling structures must be found such that the electromagnetic response of the structure comprised of those resonators and coupling structures gives the ideal circuit response shown in Fig. 4.8. A good starting point may be obtained by examining individual sections of the filter separately with the aim of synthesizing good initial dimensions of the whole filter. This can be done by considering the following segments of the filter:

1. Input/Output
2. Longitudinal Coupling
3. Electric Cross-Coupling
4. Magnetic Cross-Coupling

Throughout this section all electromagnetic full wave calculations will utilize

a rigorous mode-matching method consisting of two stages. In the first stage the modes of all the waveguide cross-sections involved in the problem are calculated. With the information obtained from the modal analysis of the waveguides;the electromagnetic fields at each point of the structure is represented as a modal series. In the second stage, the modal series in each discontinuity between two waveguides of the problem are matched. The complete response of the structure is obtained by cascading the generalized scattering matrix (GSM) of each basic discontinuity.

Input/Output Sections

Fig. 4.10 shows the structure used to realize R_{in}. It consists of a cascade of an infinite ridge waveguide representing the input then an evanescent section of rectangular waveguide to represent the input coupling section , then another section of ridge waveguide to represent the first resonator. then another evanescent section which is then terminated by a short circuit or in electromagnetic terms in a Perfect Electric Wall "PEW". Analyzing the one-port circuit represented by the structure and using equation 4.18 R_{in} and corresponding resonant frequency can be calculated. By sweeping the dimensions of the coupling section and the resonator a set of design curves can be obtained. The goal is to achieve the right amount of coupling at the right resonant frequency. A parametric design curve is generated and is shown in Fig. 4.11.

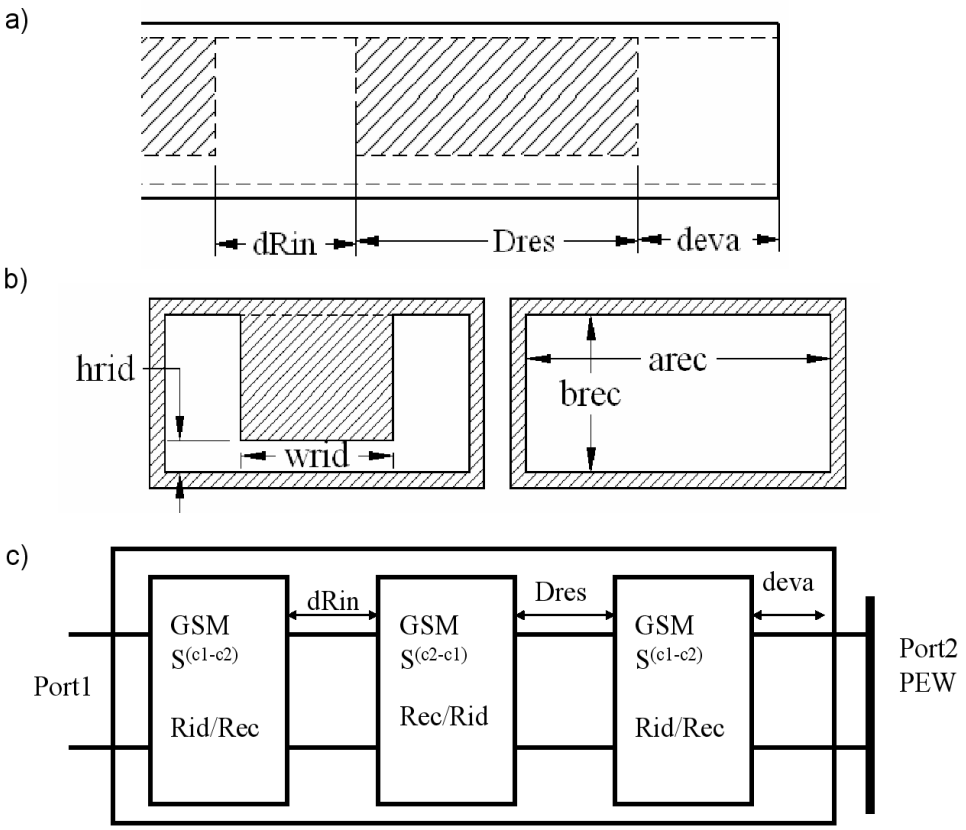

Figure 4.10: a) Side view of the structure used to realize R_{in} b) Cross sections involved in the mode matching analysis of the structure c) Schematic representation of the calculation of the generalized scattering matrix of the structure

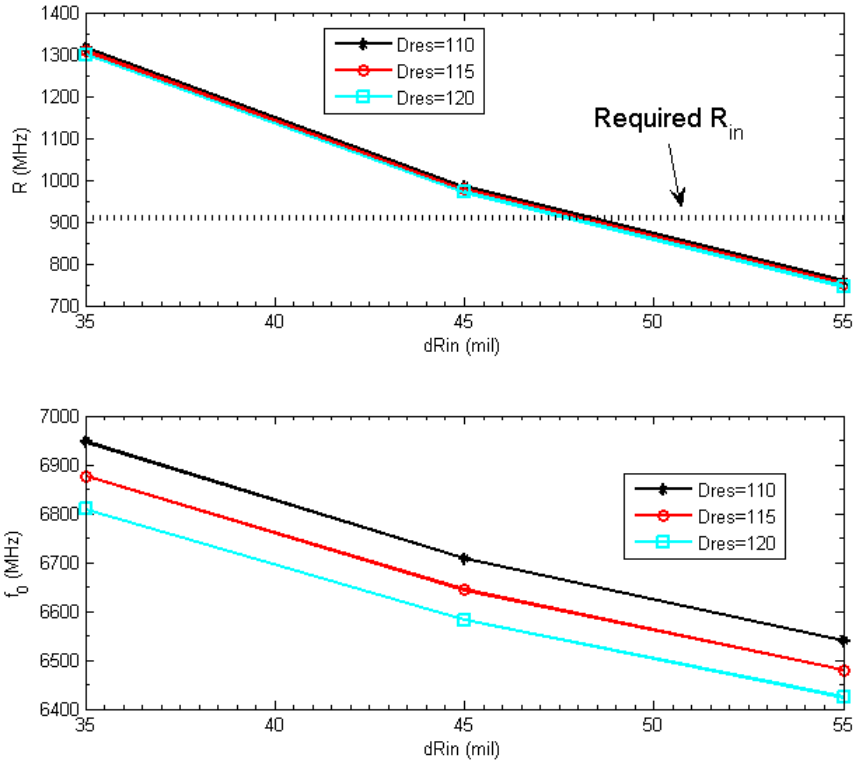

Figure 4.11: Coupling in MHz $=R_{in} \times BW$ and resonant frequency according to Fig. 4.10 $arec = 250$ mil, $brec = 115.94$ mil, $wrid = 110$ mil, $hrid = 22.44$ mil and $deva = 200$ mil

Longitudinal Coupling Sections

Fig. 4.12 shows the structure used to realize longitudinal. couplings m_{12n} and m_{23n} It consists of two ridge waveguide resonators coupled by an evanescent section of rectangular waveguide. By using PEW and PMW terminations at the plane of symmetry and calculating the corresponding resonant frequencies one can calculate both the synchronous resonant frequency of the two resonators and the inter-cavity coupling using equations 4.19 and 4.20. Again by sweeping the dimensions of the coupling section and the resonator a set of design curves can be obtained. The goal is to achieve the right amount of coupling at the right resonant frequency. A parametric design curve is generated and is shown in Fig. 4.13.

Electric Cross Coupling Sections

Since the electric field distributions in a resonant ridge waveguide cavity is mainly concentrated beneath the ridge section[70], it's convenient to use an iris centered beneath the ridge section to achieve electrical coupling between resonators in different rows,Fig. 4.14 shows the structure used to realize electric cross-couplings m_{25n} It consists of two ridge waveguide resonators coupled by an iris centered in the intermediate wall between the ridge waveguide sections of the cavities. By using PEW and PMW boundary conditions at the plane of symmetry and calculating the corresponding resonant frequencies of a single cavity one can calculate both the synchronous resonant frequency of the two resonators and the inter-cavity coupling using equations 4.19 and 4.20. Again by sweeping the dimensions of

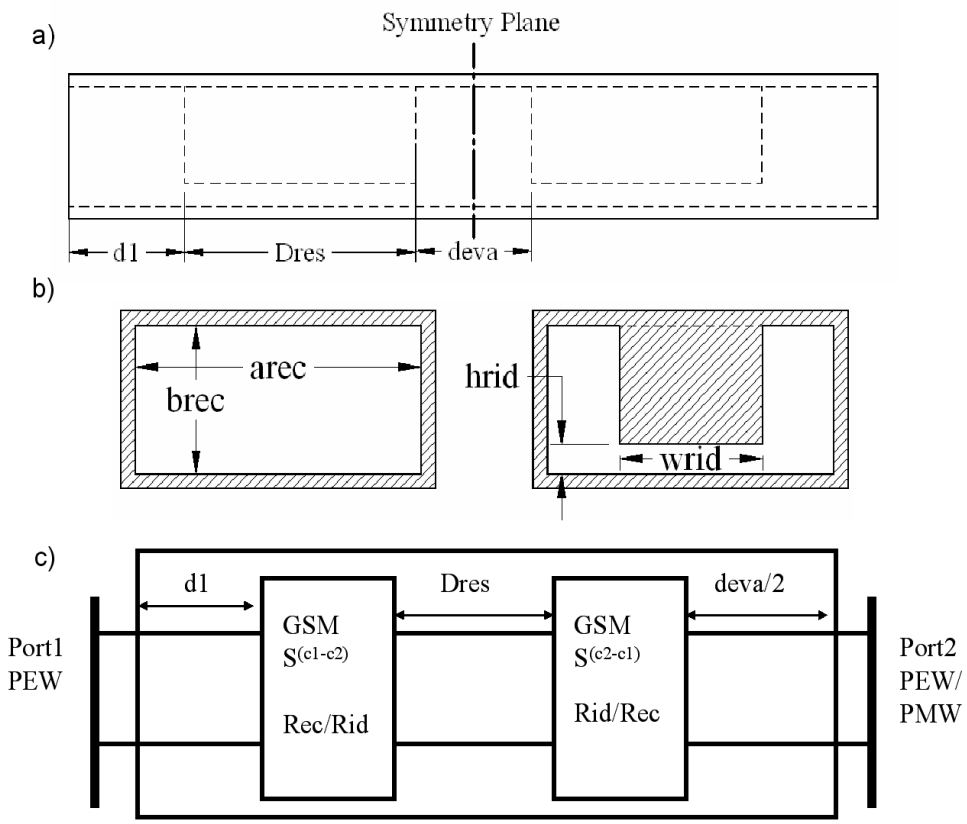

Figure 4.12: a) Side view of the structure used to realize m_{12n} and m_{23n} b) Cross sections involved in the mode matching analysis of the structure c) Schematic representation of the calculation of the generalized scattering matrix of the structure

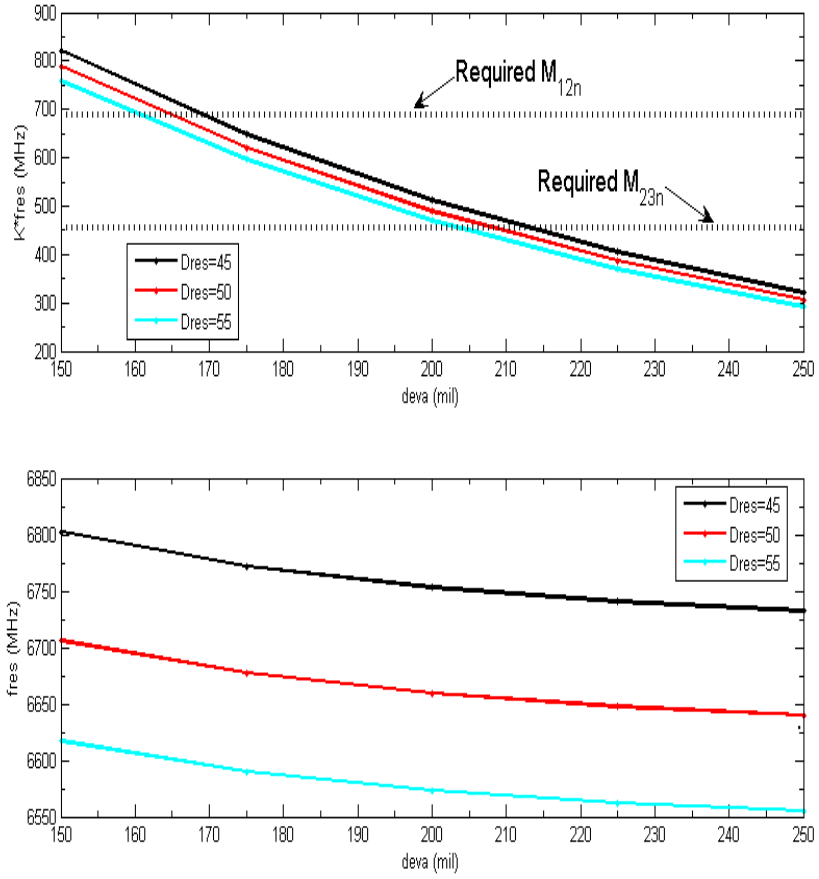

Figure 4.13: Coupling in MHz $=m_{ijn} \times BW$ and resonant frequency according to Fig. 4.12 $arec = 250$ mil, $brec = 115.94$ mil, $wrid = 110$ mil, $hrid = 22.44$ mil and $d1 = 77$ mil

the iris a set of design curves can be obtained. The goal is to achieve the right amount of coupling at the right resonant frequency. A parametric design curve is generated and is shown in Fig. 4.15.

Magnetic Cross-Couplings

Magnetic coupling was previously achieved [70, 98, 99] by side irises adjacent to the lateral walls of the waveguide. This approach proved problematic once the bandwidth of the filter was increased. The reasons for the failure of that approach were investigated. Fig. 4.16 shows the previously proposed coupling structure. Fig. 4.17 shows the coupling in MHz provided by the side iris versus the width of the iris for different iris lengths The most notable observation is that the coupling is not monotonic; it increases, reaches a maximum, then starts decreasing and even becomes negative electric coupling. This can be explained in light of how the electromagnetic fields are distributed in a ridge waveguide cavity. The electric field is mainly concentrated beneath the ridge while the magnetic fields goes to maximum on the periphery of the resonant cavity. Once the width of the iris is increased the iris approaches the ridge waveguide region and the effect of the strong electric fields beneath the ridge waveguide region starts to dominate. Given this limitation it can be seen that the maximum achievable coupling is so much lower than the required coupling. So this approach is not suitable to realize the needed magnetic coupling.

A new scheme that can achieve strong positive magnetic coupling is to use a width-wise iris. This iris extends along the "a" dimension of the waveguide

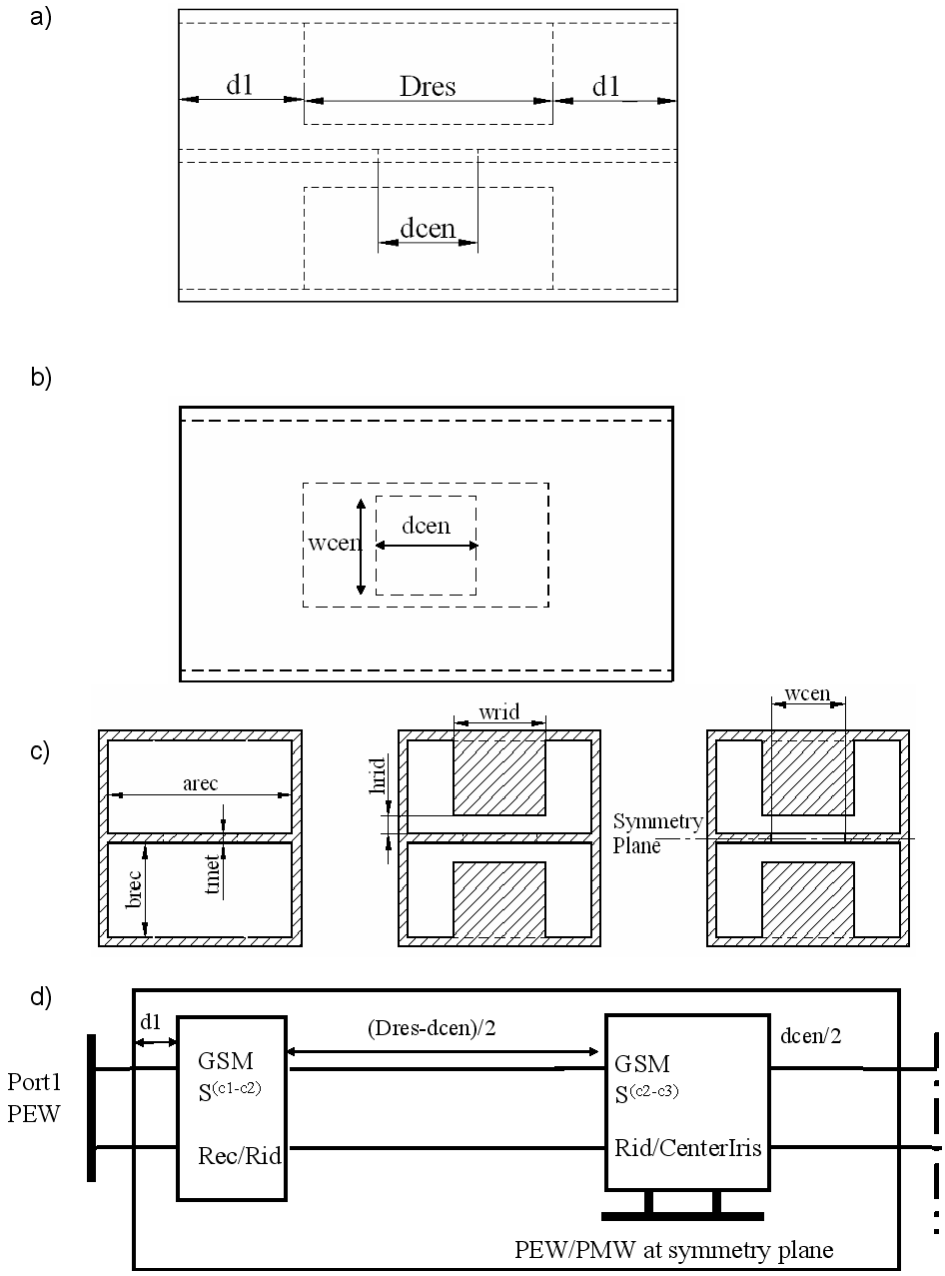

Figure 4.14: a) Side view of the structure used to realize m_{25n} a) Top view of the structure c) Cross sections involved in the mode matching analysis of the structure d) Schematic representation of the calculation of the generalized scattering matrix of the structure Note that the structure is symmetric in the longitudenal and vertical directions

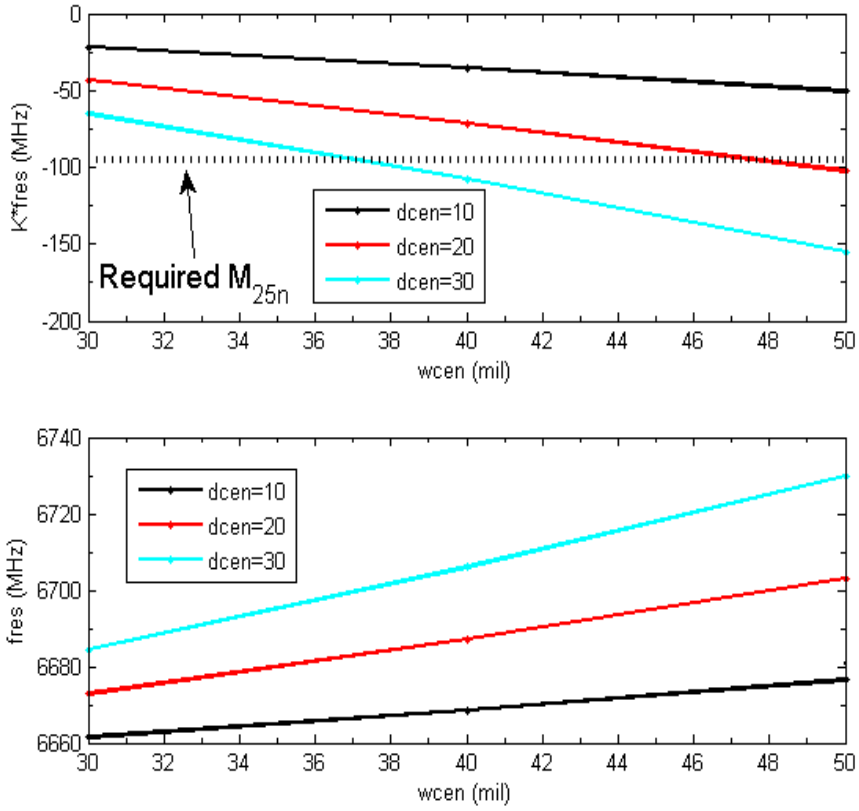

Figure 4.15: Coupling in MHz $=m_{ijn} \times BW$ and resonant frequency according to Fig. 4.14 $arec = 250$ mil, $brec = 115.94$ mil, $wrid = 110$ mil, $hrid = 22.44$ mil,$tmet = 0.5$ mil,$Dres = 100$ mil and $d1 = 275$ mil

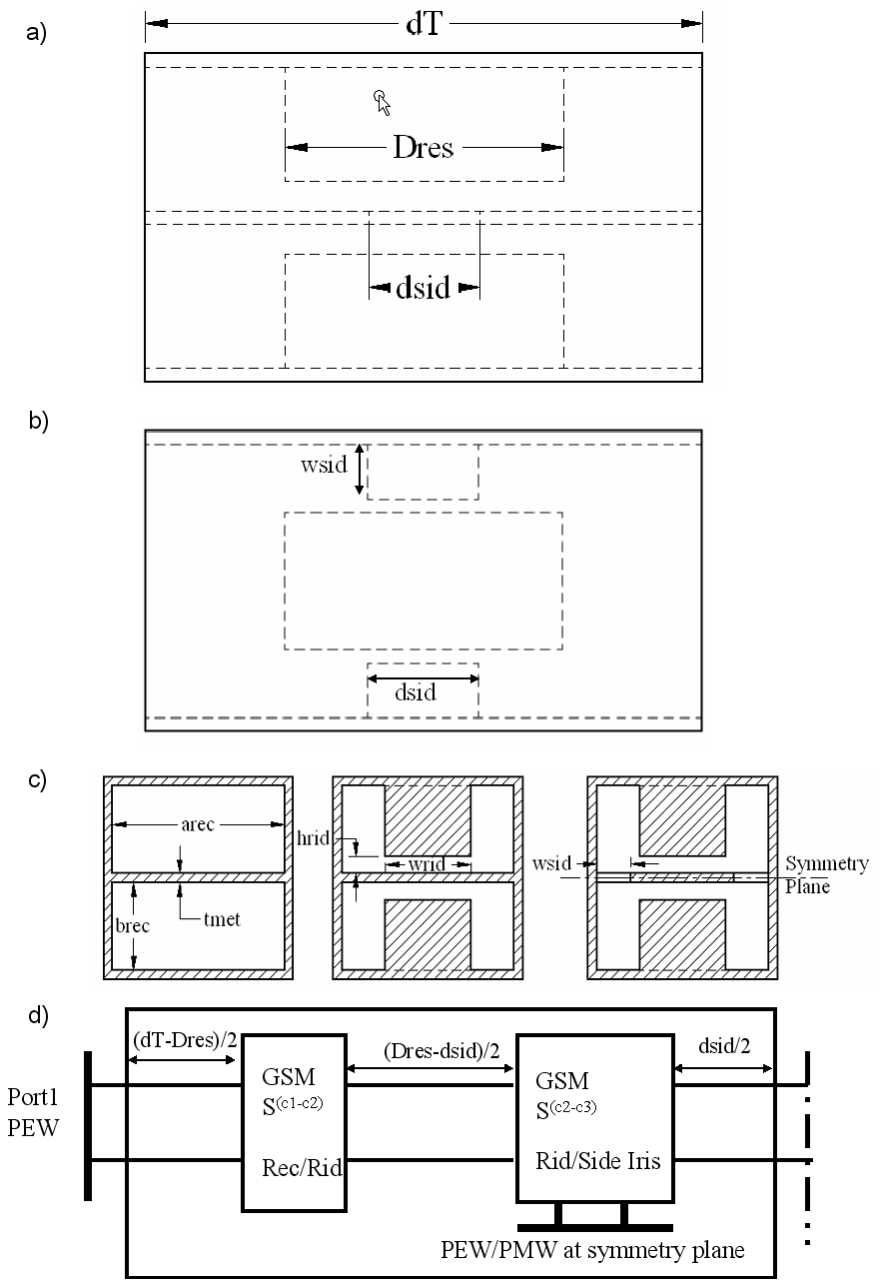

Figure 4.16: a) Side view of the structure used to realize m_{34n} a) Top view of the structure c) Cross sections involved in the mode matching analysis of the structure d) Schematic representation of the calculation of the generalized scattering matrix of the structure Note that the structure is symmetric in the longitudenal and vertical directions

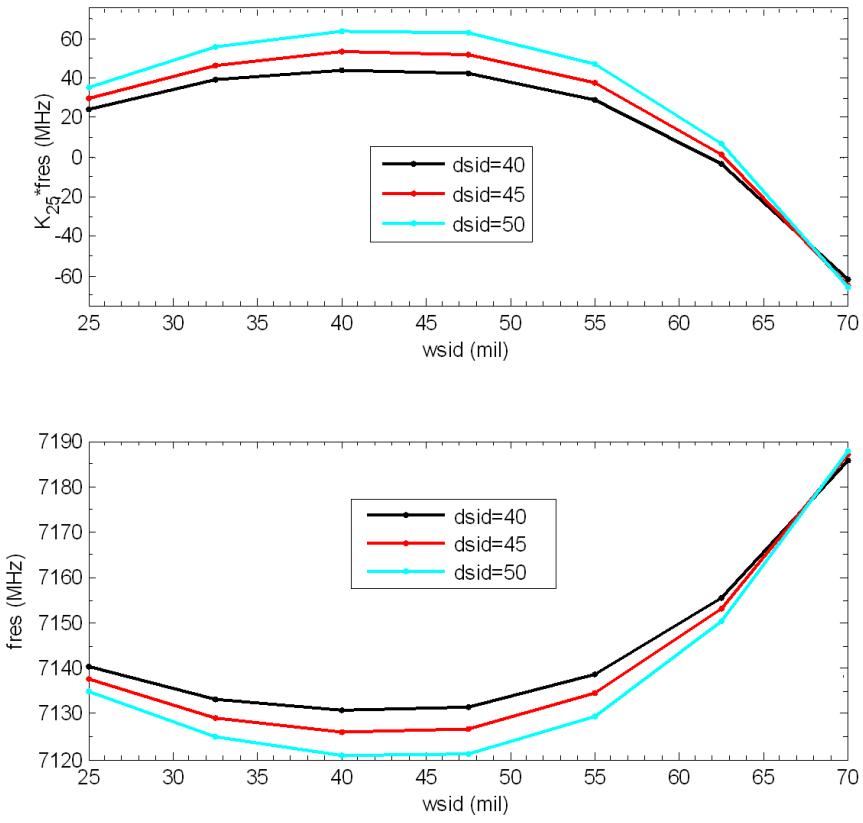

Figure 4.17: Coupling in MHz $=m_{ijn} \times BW$ and resonant frequency according to Fig. 4.16 $arec = 250$ mil, $brec = 115.94$ mil, $wrid = 110$ mil, $hrid = 22.44$ mil,$tmet = 0.5$ mil,$Dres = 52.2$ mil and $dT = 452.5$ mil

and is located right next to the resonator section as shown Fig. 4.18. This scheme will be called magnetic strip iris. Here and on the contrary to the side iris scheme , the iris can be extended in the direction further away from the ridge waveguide region thus harvesting more magnetic field coupling while diminishing the effects of the electric fields. From the coupling curve shown in Fig. 4.19., it is clear that the required coupling, and even higher coupling which translates to even wider fractional bandwidths, is achievable. To show the feasibility of the coupling scheme, two filter designs are presented next, they differ in the way the longitudinal coupling is realized but both share the same realization of the cross coupling.

4.4.3 Filter Design with Rectangular Waveguide Evanescent Sections

In the first design the filter shown schematically in Fig. 4.20 was designed using single ridge waveguide sections to realize the resonators, evanescent rectangular waveguide sections for the adjacent couplings, a centered iris for the negative M_{25n} electric coupling and the proposed magnetic strip iris to realize the positive magnetic coupling M_{34n}. Since the filter is realized in LTCC technology, the vertical dimensions should all be integer multiples of the LTCC layer thickness of 3.74 mils with dielectric constant $\epsilon_r = 5.9$, and all metallization layers thicknesses are 0.5 mil. All dimensions are given in Table 4.2. The full wave response shown in Fig. 4.21 shows asymmetry and tilting of the stop band rejection levels.

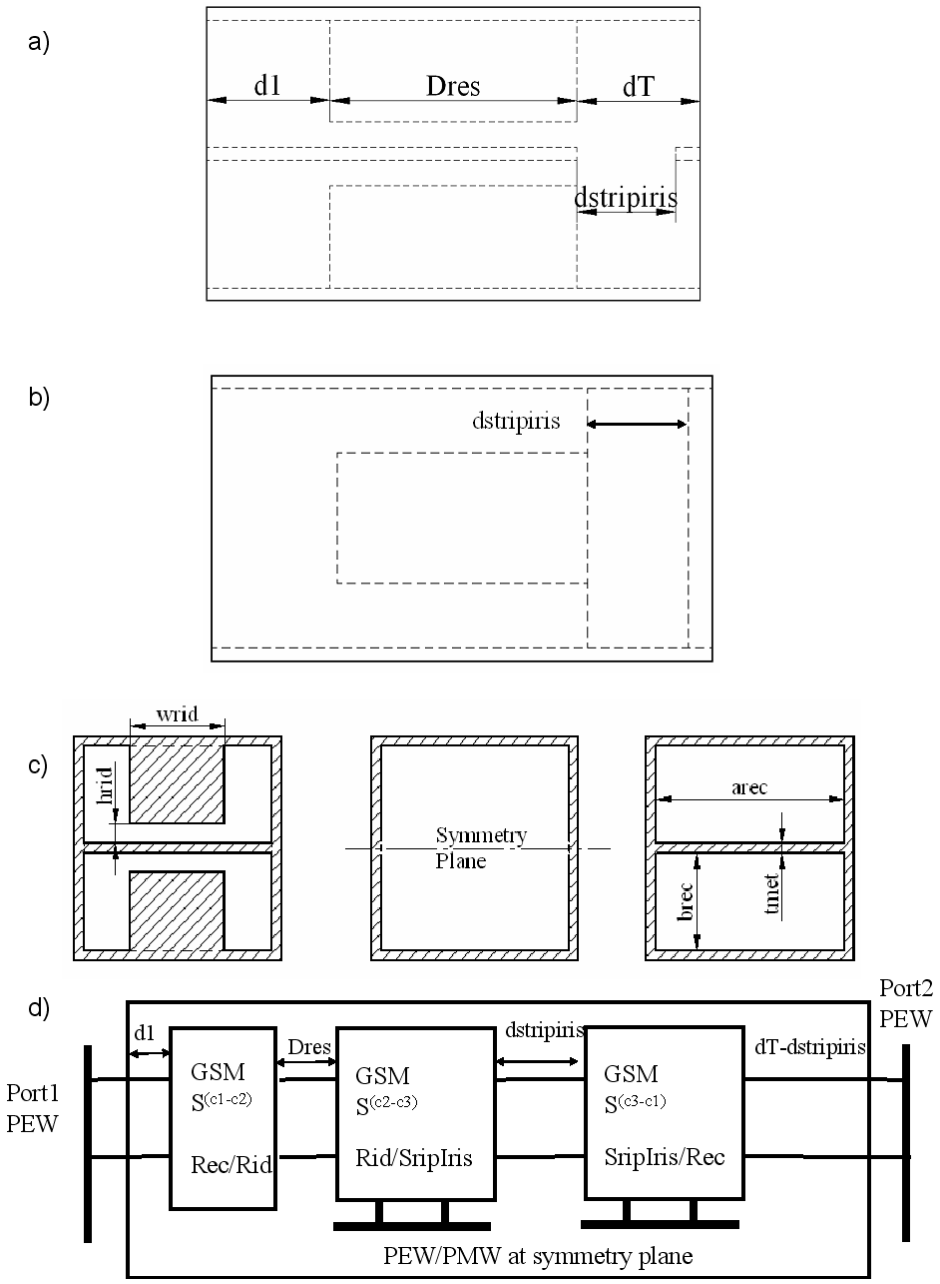

Figure 4.18: a) Side view of the structure used to realize m_{34n} a) Top view of the structure c) Cross sections involved in the mode matching analysis of the structure d) Schematic representation of the calculation of the generalized scattering matrix of the structure.

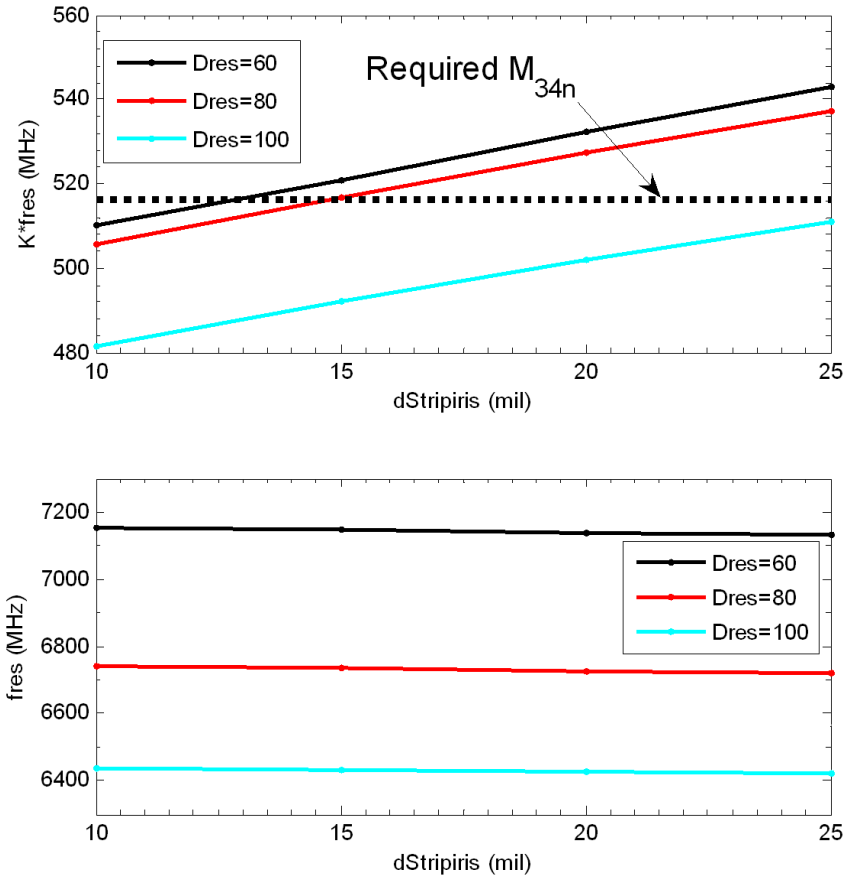

Figure 4.19: Coupling in MHz $=m_{ijn} \times BW$ and resonant frequency according to Fig. 4.18 $arec = 250$ mil, $brec = 115.94$ mil, $wrid = 110$ mil, $hrid = 22.44$ mil, $Dres = 40$ mil, $dT = 50$ mil and $d1 = 228$ mil

Table 4.2: Dimensions of the first Filter to Fig. 4.20 .

Cross-sectional Dimensions in mils					
Dimension	*arec*	*brec*	*wrid*	*hrid*	*wcen*
value	250	115.94	110	22.44	50
Resonators' Dimensions in mils					
*Dres*1		*Dres*2		*Dres*3	
62.1		30.6		43.4	
Coupling sections' Dimensions in mils					
*deva*0	*deva*1	*dcen*	*deva*2	*dstripiris*	*deva*3
53.9	176.3	30.3	228.1	45.3	20

This tilting results in worse rejection in the high frequency band. The origins of the tilting were investigated following well-established ideal circuit parameter extraction techniques [105]

4.4.4 Diagnosis of Filter Response Using Parameter Extraction

Parameter extraction is an important tool that enables successful diagnosis of already designed filters. the aim of parameter extraction is to find a coupling matrix M whose ideal circuit response produces an already obtained electromagnetic response either simulated or measured. It's based on calculation of closed

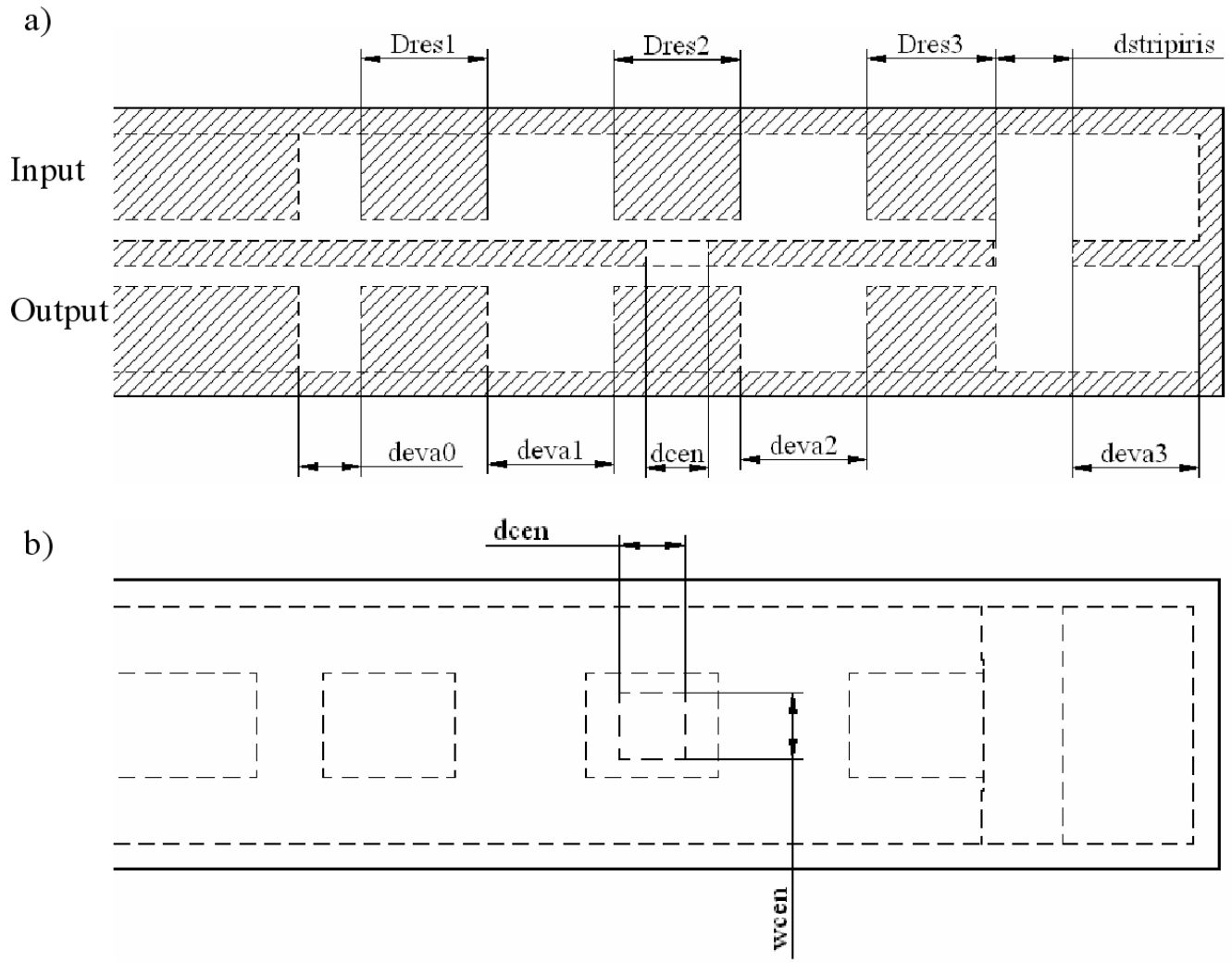

Figure 4.20: a) Side view of the first filter b) Top view of the first filter

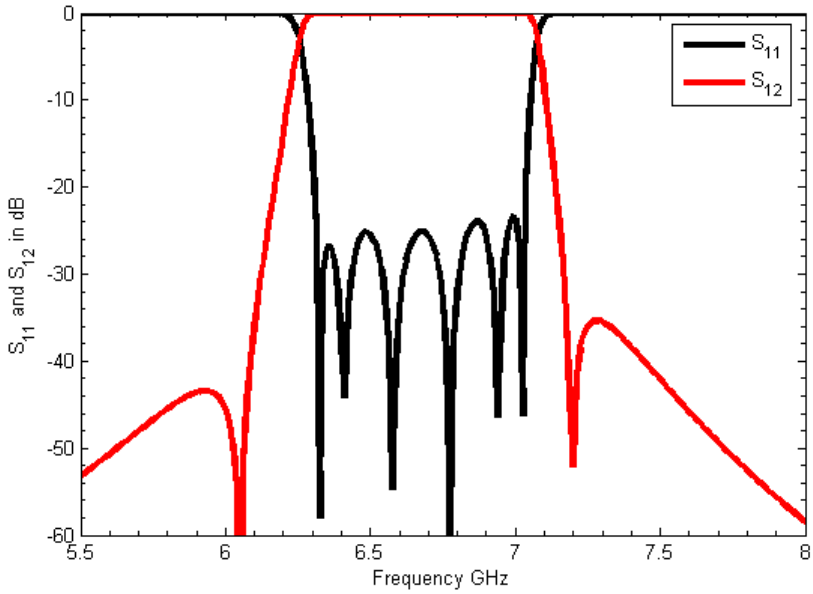

Figure 4.21: Full wave response of the first filter

form recursive formulas derived from the simulated or measured responses. These formulas are based entirely on the precise locations of the zeros and poles of the input impedance functions of the filter. the powerfulness of this approach is that it predicts spurious couplings between nearby resonators. Next we will go through the extraction procedure in details.

The first step in the extraction procedure is the adjustment of the reference plane,since the ideal circuit model assumes that the first resonator is directly connected to the input resistance of the port as can be seen in Fig. 4.3-a In the electromagnetic model the exact location of connection between the resonator and the port is not exactly known, a needed correction of the reference plane is sought. Considering the input section of the filter shown in Fig. 4.10 one can calculate the input reflection coefficient S_{11}. Since ideally the structure is lossless

we have $|S_{11}| = 1$ looking at the phase angle of S_{11} we can note a discontinuity or jump from $-180°$ to $180°$ in the ideal case this jump coincides with the minimum of the derivative of the phase. By determining the frequency of the minimum of the derivative of the phase of S_{11} and adjusting the phase such that the jump from $-180°$ to $180°$ coincides with the minimum of the phase derivative a precise calculation of the required transmission line length to be added to the circuit is achieved. Fig. 4.22 shows the original and adjusted phase response of the input section of the filter. It was calculated that a piece of transmission line of electrical length of $9.3°$ needs to be added to the filter to correctly adjust the reference plane.

The second step in the extraction procedure is to precisely determine the locations of poles and zeros of the odd "electric wall termination" and even "magnetic wall termination" bisected filter network. The odd and even phase response can be obtained either by simulating half the structure twice with the appropriate boundary condition imposed at the plane of symmetry or directly from the response of the whole structure according to the following relations:

$$S_{11m} = (S11 + S12) \tag{4.22}$$

$$S_{11e} = (S11 - S12) \tag{4.23}$$

Fig. 4.23 shows the phase response of both electric and magnetic subcircuits along with the detected locations of the poles and zeros of each response. Once the poles and zeros of the odd and even input reflection coefficient are known

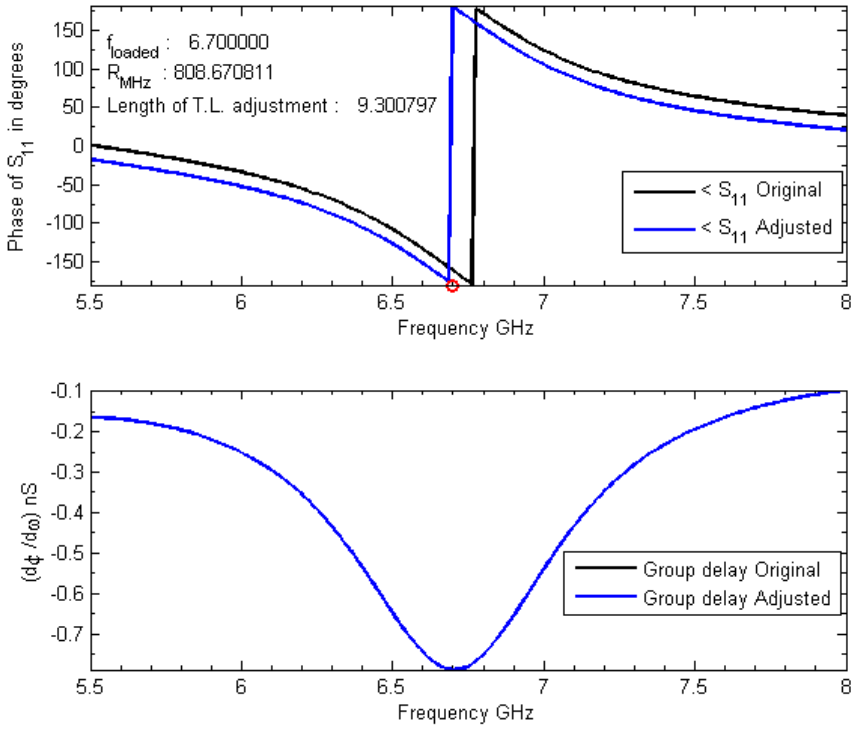

Figure 4.22: Original phase response of S_{11} with the adjustment of the reference plane and the derivative of the phase with respect to frequency

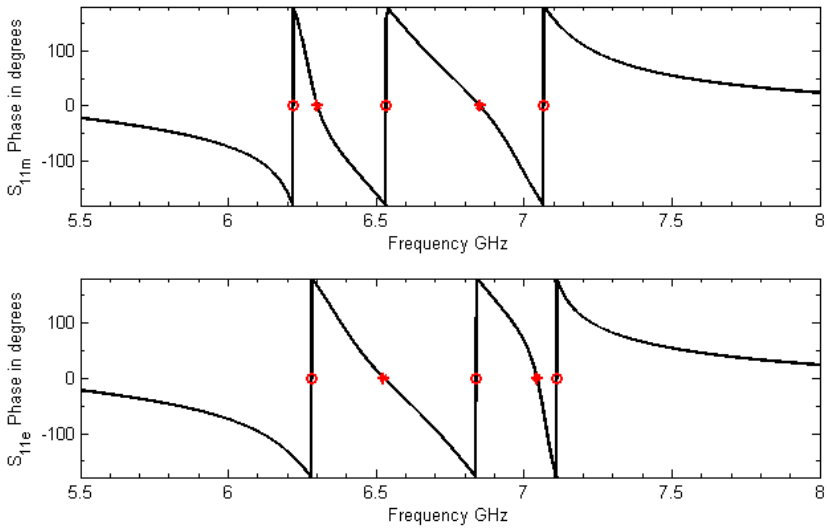

Figure 4.23: Phase response of odd and even subcircuits of the filter

appropriate polynomials can be constructed in the following fashion [105]:

$$Zin^{(i)}_{<e,m>}(\lambda) = j\frac{P_{i<e,m>}(\lambda)}{Q_{i<e,m>}(\lambda)}, i = 1, 2, .., n \tag{4.24}$$

$$P_{i<e,m>}(\lambda) = \sum_{t=0}^{n-i+1} c^i_{<e,m>t}\lambda^t = \prod_{t=1}^{n-i+1}(\lambda - \lambda_{z<e,m>t}) \tag{4.25}$$

$$Q_{i<e,m>}(\lambda) = \sum_{q=0}^{n-i} d^i_{<e,m>q}\lambda^q = \prod_{q=1}^{n-i}(\lambda - \lambda_{p<e,m>q}) \tag{4.26}$$

$$\lambda = \frac{f_o}{BW}(\frac{f}{f_o} - \frac{f_o}{f}) \tag{4.27}$$

The subscripts e or m denote the odd or even subcircuits, while the subscripts z or p denote zeros or poles of the input impedance functions such that $\lambda_{p<e,m>q}$ is the q^{th}normalized pole of the input impedance function while $\lambda_{z<e,m>t}$ is the t^{th}normalized zero of the input impedance function. the input impedance function is related to the input reflection coefficient $S_{11}by$ the following relation:

$$S_{11<e,m>} = \frac{Z^{(1)}_{in<e,m>} - R}{Z^{(1)}_{in<e,m>} + R} \tag{4.28}$$

Once the P and Q polynomials are constructed the following procedure is used to extract all parameters of the filter:

1. Solve the following equation to calculate the center frequency of the filter

$$f_o \frac{\left[\prod_{t=1}^{n-i+1}(f_{zt}^{m}-f_o)\right]\left[\prod_{q=1}^{n-i}(f_{pq}^{e}-f_o)\right]}{\left[\prod_{t=1}^{n-i+1}(f_{zt}^{e}-f_o)\right]\left[\prod_{q=1}^{n-i}(f_{pq}^{m}-f_o)\right]} = \frac{\tan(\frac{\Theta_m(f_o)}{2})}{\tan(\frac{\Theta_e(f_o)}{2})} \tag{4.29}$$

   where Θ_m is the phase of S_{11m}

2. Solve the following equation to calculate R_{in}/R_{out}

$$R_{in} = \left| \frac{\prod_{t=1}^{n}(\lambda_{90}-\lambda_{zmt}^{(1)})}{\prod_{q=1}^{n-1}(\lambda_{90}-\lambda_{pmq}^{(1)})} \right| \tag{4.30}$$

   where λ_{90} is the normalized frequency corresponding to $\pm 90°phase$ of the even mode subcircuit

3. Extract the normalized coupling matrix elements according to the following recursive formulas:

$$m_{ii} = -\frac{1}{2}[c_{m(n-i)}^{(i)} - d_{m(n-i-1)}^{(i)} + c_{e(n-i)}^{(i)} - d_{e(n-i-1)}^{(i)}] \tag{4.31}$$

$$m_{i,(2n+1-i)} = -\frac{1}{2}[c_{m(n-i)}^{(i)} - d_{m(n-i-1)}^{(i)} - c_{e(n-i)}^{(i)} + d_{e(n-i-1)}^{(i)}] \tag{4.32}$$

$$m_{i,i+1} = -\frac{1}{2}[A_m^{(i)} + A_e^{(i)}] \tag{4.33}$$

$$m_{i,2n-i} = -\frac{1}{2}[A_m^{(i)} - A_e^{(i)}] \tag{4.34}$$

   where :

$$A_{<e,m>}^{(i)} = \sqrt{B_{<e,m>}^{(i)} - c_{<e,m>(n-i-1)}^{(i)} + d_{<e,m>(n-i-2)}^{(i)}} \tag{4.35}$$

$$B_{<e,m>}^{(i)} = (c_{<e,m>(n-i)}^{(i)} - d_{<e,m>(n-i-1)}^{(i)}) d_{<e,m>(n-i-1)}^{(i)} \tag{4.36}$$

Finally the recursion relations of the polynomials P and Q are given by:

$$P_{i+1<e,m>}(\lambda) = Q_{i<e,m>}(\lambda) \tag{4.37}$$

$$P_{i<e,m>}(\lambda) = P_{i+1<e,m>}(\lambda)[\lambda + m_{i,i} \pm m_{i,2n+1-i}] - Q_{i+1<e,m>}(\lambda)[m_{i,i+1} \pm m_{i,2n-i}]^2 \tag{4.38}$$

Following the steps outlined in the previous section the following filter parameters were extracted from response of the filter

$$f_o = 6.838745GHz \tag{4.39}$$

$$R_{in} = 1.190891 \tag{4.40}$$

$$M_n = \begin{bmatrix} -0.537 & 0.931 & 0 & 0 & -0.008 & 0.006 \\ 0.931 & -0.525 & 0.631 & 0.081 & -0.114 & -0.008 \\ 0 & 0.631 & -0.401 & 0.709 & 0.081 & 0 \\ 0 & 0.081 & 0.709 & -0.401 & 0.631 & 0 \\ -0.008 & -0.114 & 0.0813 & 0.631 & -0.525 & 0.931 \\ 0.006 & -0.008 & 0 & 0 & 0.931 & -0.537 \end{bmatrix} \tag{4.41}$$

It's worth noting that the resonant frequencies of the cavities are given by

$$f_{oi} = f_o + (\frac{BW \times M_n(i,i)}{2}) \tag{4.42}$$

Using the previous equation the resonant frequencies of the cavities are given by

$$\begin{aligned} f_{o1} &= f_{o6} = 6.645297GHz \\ f_{o2} &= f_{o5} = 6.649576GHz \\ f_{o3} &= f_{o4} = 6.694302GHz \end{aligned} \tag{4.43}$$

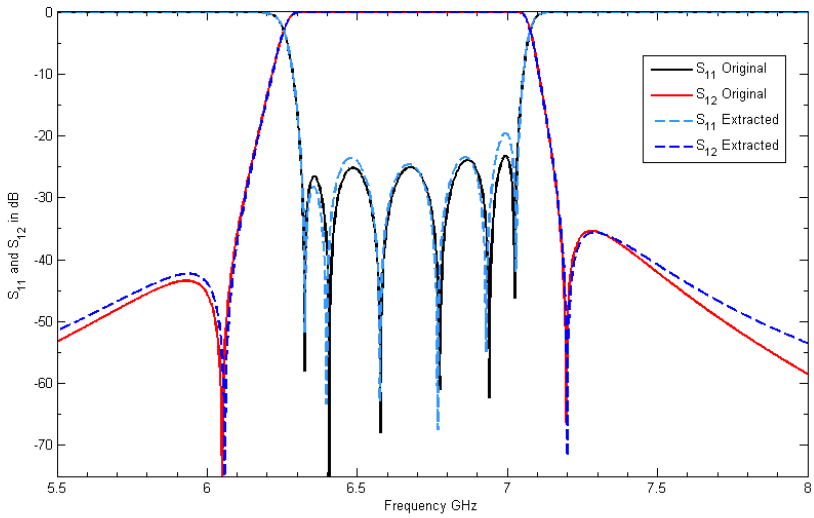

Figure 4.24: Extracted and original reponse of the first filter

Fig.4.24 shows the ideal circuit response obtained using the extracted parameters along with the original response good agreement is observed.

The extraction revealed the existence of spurious undesired cross couplings that cause the asymmetry and tilting of the filter response. Such spurious couplings stem from stray couplings between the electromagnetic fields in the nearby resonant cavities. Minimizing such spurious couplings is sure to enhance the performance of the filter. Namely $M_{15n}, M_{16n}, M_{26n}, M_{24n}$, and M_{35n} have major detrimental effects. If they are suppressed the asymmetry and tilting will be avoided.

4.4.5 Filter Design with Ridge Waveguide Evanescent Sections

Alternative Realization of Longitudinal Coupling

The utilization of narrow ridges to realize adjacent strong coupling was first proposed in [106], and used in [104] to increase the physical lengths of the coupling sections to realizable dimensions. The same approach is used here but for a different purpose. By increasing the physical separation between resonators $1, 5$ and $2, 4$ the spurious undesired cross couplings can be minimized. Fig. 4.26 shows the coupling curves for two ridge waveguide resonators coupled by a section of a narrow ridge waveguide which is under cutoff within the pass band of the filter. The physical length of the coupling section that achieves the required coupling using narrow ridges shown in Fig. 4.26 is longer than that the corresponding physical dimension in the case of rectangular waveguide coupling section shown in Fig. 4.13. The increase of the physical length in this case is desirable as it will help separate the the resonators by a larger physical length while electrically it's achieving the same coupling values. Such larger separation will result in minimizing the spurious undesired couplings.

Filter Realization by successive Realization of subcircuits

In order to reduce the complexity of the optimization procedure used to obtain the final dimensions of the structure that exhibit the required filter function performance a gradual stepped realization of the whole structure is used. In this

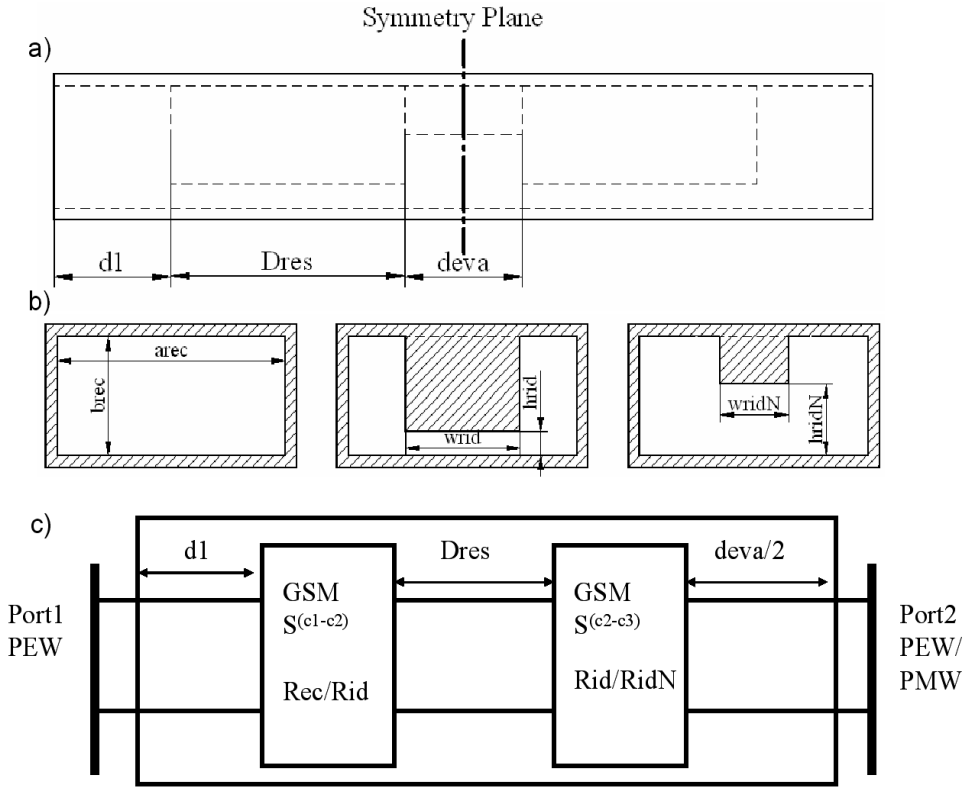

Figure 4.25: a) Side view of the structure used to realize m_{12n} and m_{23n} with narrow ridges b) Cross sections involved in the mode matching analysis of the structure c) Schematic representation of the calculation of the generalized scattering matrix of the structure

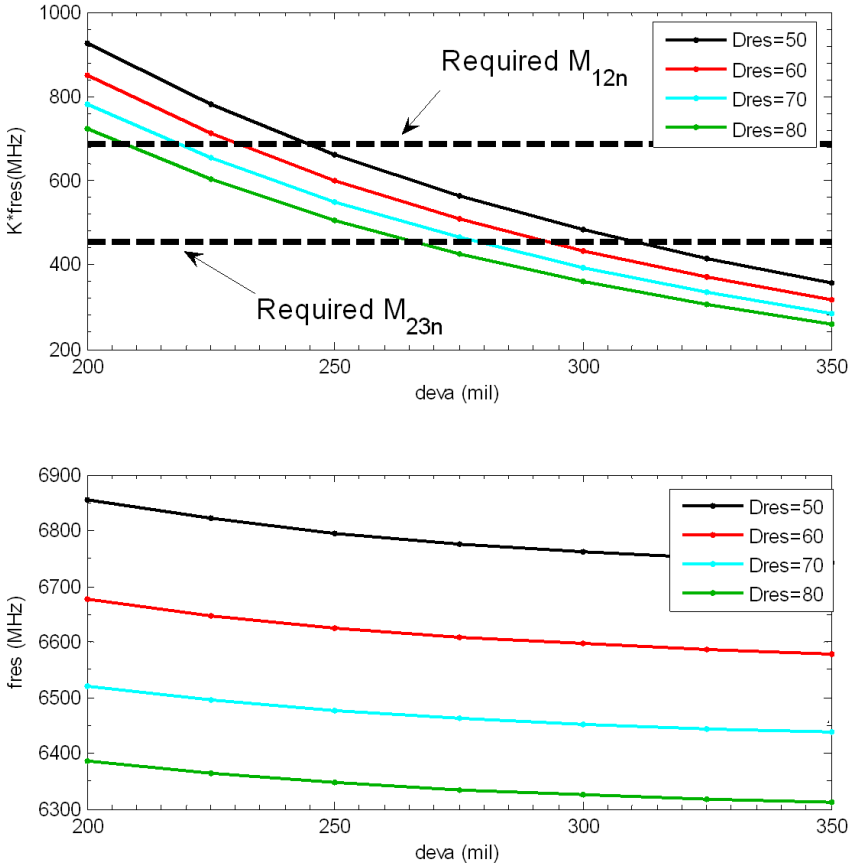

Figure 4.26: Coupling in MHz $=m_{ijn} \times BW$ and resonant frequency according to Fig. 4.25 $arec = 250$ mil, $brec = 115.94$ mil, $wrid = 110$ mil, $hrid = 22.44$ mil, $widN = 42$ mil, $hridN = 71.06$ mil and $d1 = 75$ mil

approach rather than simply plugging in initial dimensions for the whole structure and using brute force optimization routines to obtain the final dimensions a more gradual approach is used. In this approach simple subsections of the filter are realized first starting with dimensions obtained from conventional coupling curves, the advantage being that the optimization variables for the subcircuits are few and the convergence is obtained much faster than if the whole filter is obtained using optimization. The procedure for the 6 pole filter requires 4 steps detailed as follows:

Step-1 : In this step a second order network comprised of an input section, two identical resonators and a coupling section is designed. Fig. 4.27 shows the ideal circuit, the structure used to realize it as well as a comparison of the mode matching response and the ideal circuit response.

Step-2 : In this step a fourth order network comprised of an input section, four resonators and two coupling sections is designed. Fig. 4.28 shows the ideal circuit, the structure used to realize it as well as a comparison of the mode matching response and the ideal circuit response.

Step-3 : In this step a sixth order network comprised of an input section, six resonators and five coupling sections is designed. In essence this is the whole filter without introducing the electric coupling iris that realizes M_{25n}. Fig. 4.29 shows the ideal circuit, the structure used to realize it as well as a comparison of the mode matching response and the ideal circuit response.

Step-4 : In this step the electric coupling iris realizing $M25n$ is introduced resulting in the whole filter structure Fig. 4.30 shows the mode matching response

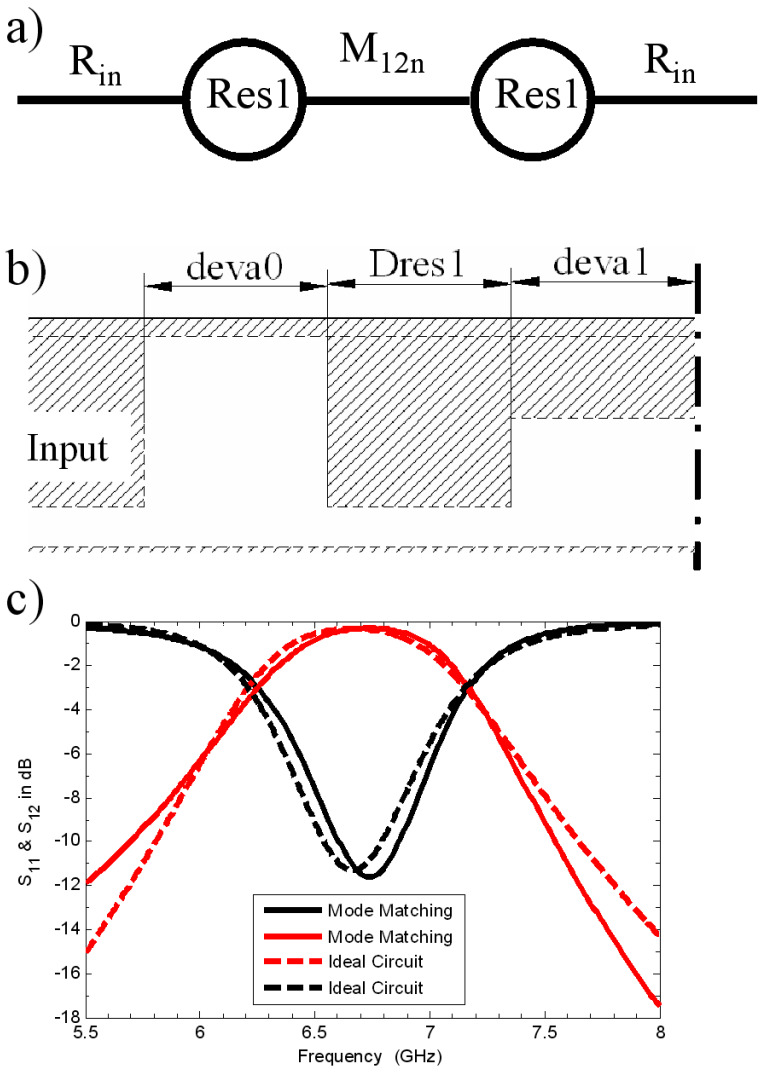

Figure 4.27: a) Schematic diagram of the two port network to be realized b) Side view of half the structure used to realize the network in (a) c) Mode Matching response of the structure in (b) versus the ideal circuit response according to (a)

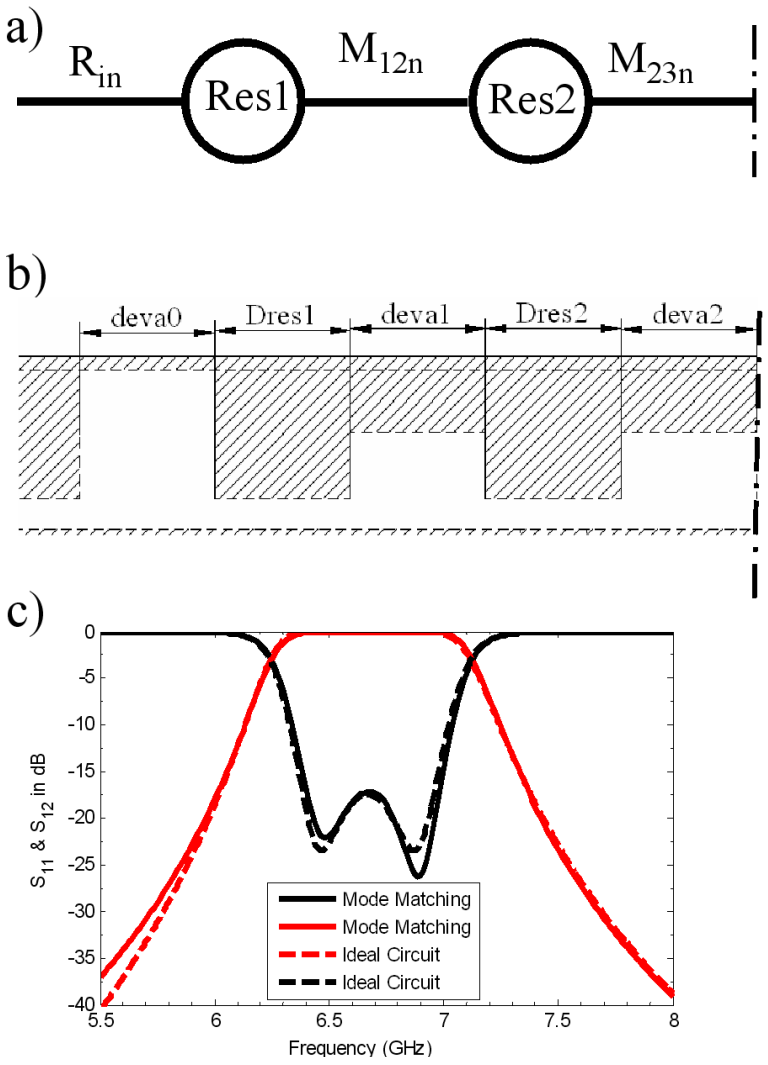

Figure 4.28: a) Schematic diagram of the half the two port network to be realized b) Side view of half the structure used to realize the network in (a) c) Mode Matching response of the structure in (b) versus the ideal circuit response according to (a)

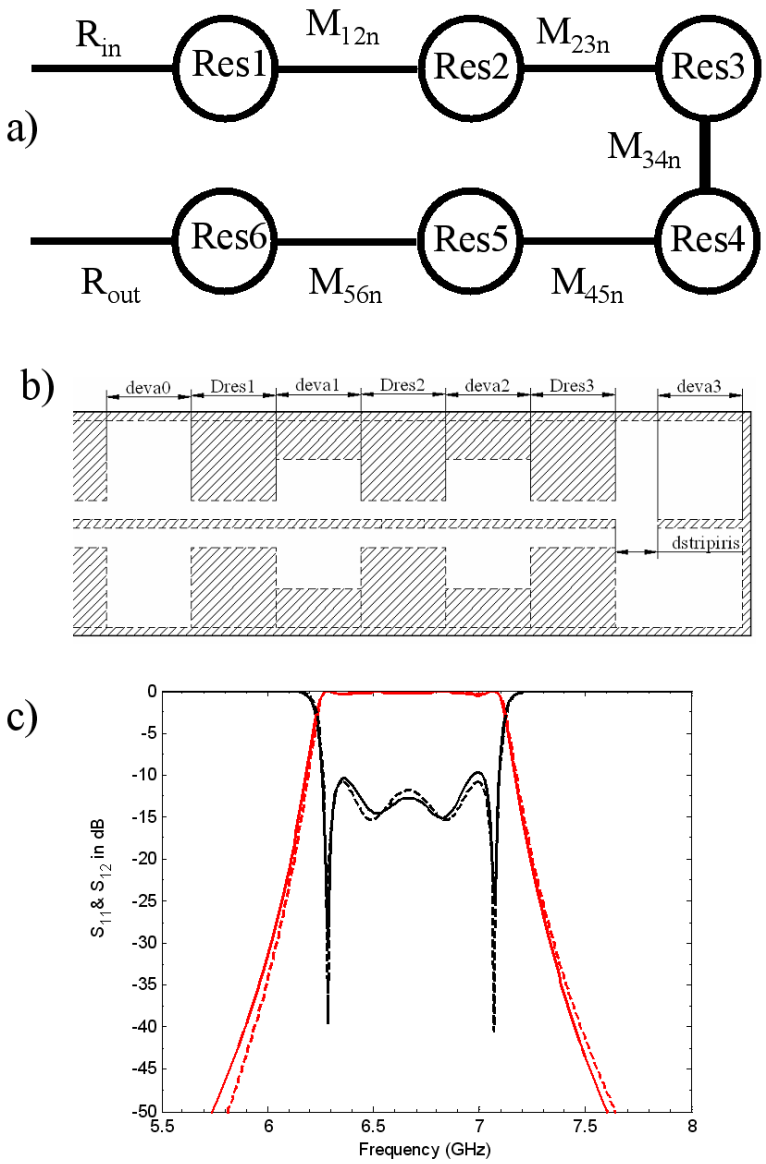

Figure 4.29: a) Schematic diagram of the two port network to be realized b) Side view of the structure used to realize the network in (a) c) Mode Matching response of the structure in (b) versus the ideal circuit response according to (a)

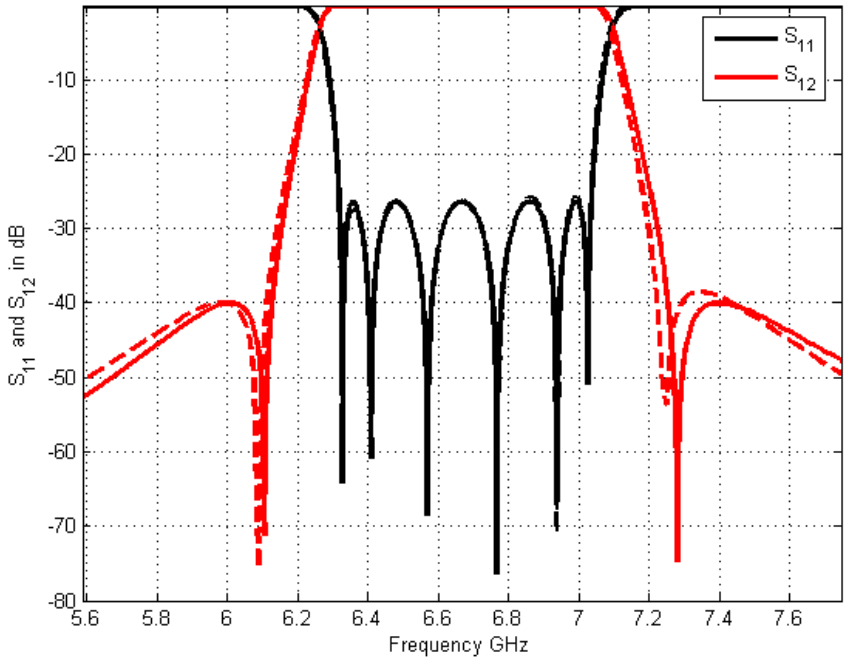

Figure 4.30: Full wave response of the second filter vs. the ideal circuit response

of the whole filter compared to the required ideal circuit response. Good agreement is observed. The response is much better compared to the response obtained before with rectangular waveguide coupling sections although the price paid was an increase of the total length of the filter from 0.66" in the first design to 0.828" in the second design.

To show the effectiveness of the proposed multi-stage realization the dimensions obtained in each step are compared in table 4.3 It can be noticed that the dimensions realized in each step is very slightly changed from one step to the next thus securing a smooth convergence to the optimum values in the final filter while using only a few set of longitudinal dimensions as optimization parameters in each step.

Table 4.3: Dimensions of the four steps of realization of the second Filter According to to Fig. 4.27, 4.28 4.29 .

Dimension	step1	step2	step3	step4
$deva0$	50	48.5	46.3	48
$Dres1$	68.5	72.7	75.8	73.9
$deva1$	241.3	239	236.1	236
$Dres2$	–	39	40	43.4
$deva2$	–	314	315.4	314
$Dres3$	–	–	50.9	51.3
$dstripiris$	–	–	40.9	42.2
$deva3$	–	–	19.2	17.6
$dcen$	–	–	–	32

4.4.6 Design of a Ridge to Stripline Transition.

A transition from the input ridge waveguide to a standard 50Ω stripline is needed to enable the interconnection of the filter with other components in any communication system. The transition takes advantage of similarities of the field distribution of the single ridge section and the single strip section aligned at the same height from the bottom of the housing. The design of the transition is based on the quarter wave transmission line transformer. The design of such transitions was discussed in details in the previous chapter. A four section transition was designed. The thickness of the strip is that of a metallization layer =0.5 mil. The "a" dimension of the housing waveguide of the stripline sections was gradually decreased to increase the cutoff frequency of the first higher order mode of the stripline thus widening the mono-mode range of the transition. The transition and its response are shown in Fig. 4.31 The dimensions are given in Table 4.4.

4.4.7 Final Optimization.

The filter and the transition were connected together. Fig. 4.32 shows schematically the whole structure comprised of the transition and the filter. Final full wave optimization was used again to optimize the whole structure to get the response that resembles the ideal circuit response. To have an efficient optimization given the complexity of the structure an optimization goal function is carefully constructed [107], the filter response is optimized to match the ideal circuit response at critical frequencies only. Specifically S_{11} is optimized at the poles of the

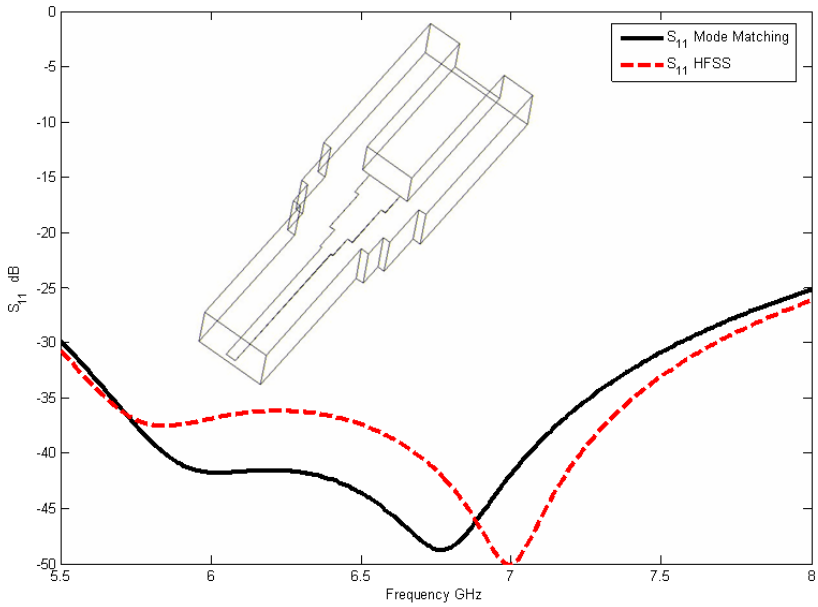

Figure 4.31: Full-wave response of a single ridge to 50Ω strip line transition

return loss as well as at the points where $\frac{dS_{11}}{df} = 0$ (reflection points) while S_{12} is optimized at the zeros of transmission and at the points where $\frac{dS_{12}}{df} = 0$ (side lobes of transmission)

$$\begin{aligned} F(X) &= W_{11} \sum_{i=N1}^{N2} \Delta(S_{11}(X, f_i), Goal_{S11}) + \\ &\quad W_{12} \sum_{j=M1}^{M2} \Delta(S_{12}(X, f_j), Goal_{S12}) \end{aligned} \tag{4.44}$$

$$\text{with } \Delta(x, y, z) = \begin{cases} (x-y)^2 & if(x \neq y,) \\ 0 & if(x = y,) \end{cases} \tag{4.45}$$

To speed up the optimization only longitudinal dimensions were used as the optimization variable set X according to equation4.44, this way the modes of different cross sections of the structure is calculated once and the optimization starts with an inherently good starting point resulting from the last step of the successive re-

alization. The dimensions obtained after optimization are listed in Table 4.4.The optimized full wave response compared to the response obtained by Ansoft HFSS [6] is shown in Fig.4.33 Broad band response of the structure is sown in Fig. 4.34 showing out of band spurious resonances as well as higher order harmonics of the filter.

4.5 Conclusions

In this chapter a detailed design procedure of canonical LTCC ridge waveguide filters for wideband application was presented. Challenges met in designing the filters due limitation posed by the realization of the cross coupling were overcome by a new coupling scheme. That coupling scheme was employed to eliminate the limitations over the bandwidth. In addition, the use of narrow ridge waveguide for the realization of the coupling sections eliminated the undesired cross coupling. Rigorous mode matching method was used for full wave analysis and optimization of the structure. Finally the optimized response of the filter with its transition is compared with HFSS showing good agreement. Limitations on even larger bandwidths for this type of filters stem from the limited validity of the coupling matrix model. The model is valid for fractional bandwidths of up to 20%.

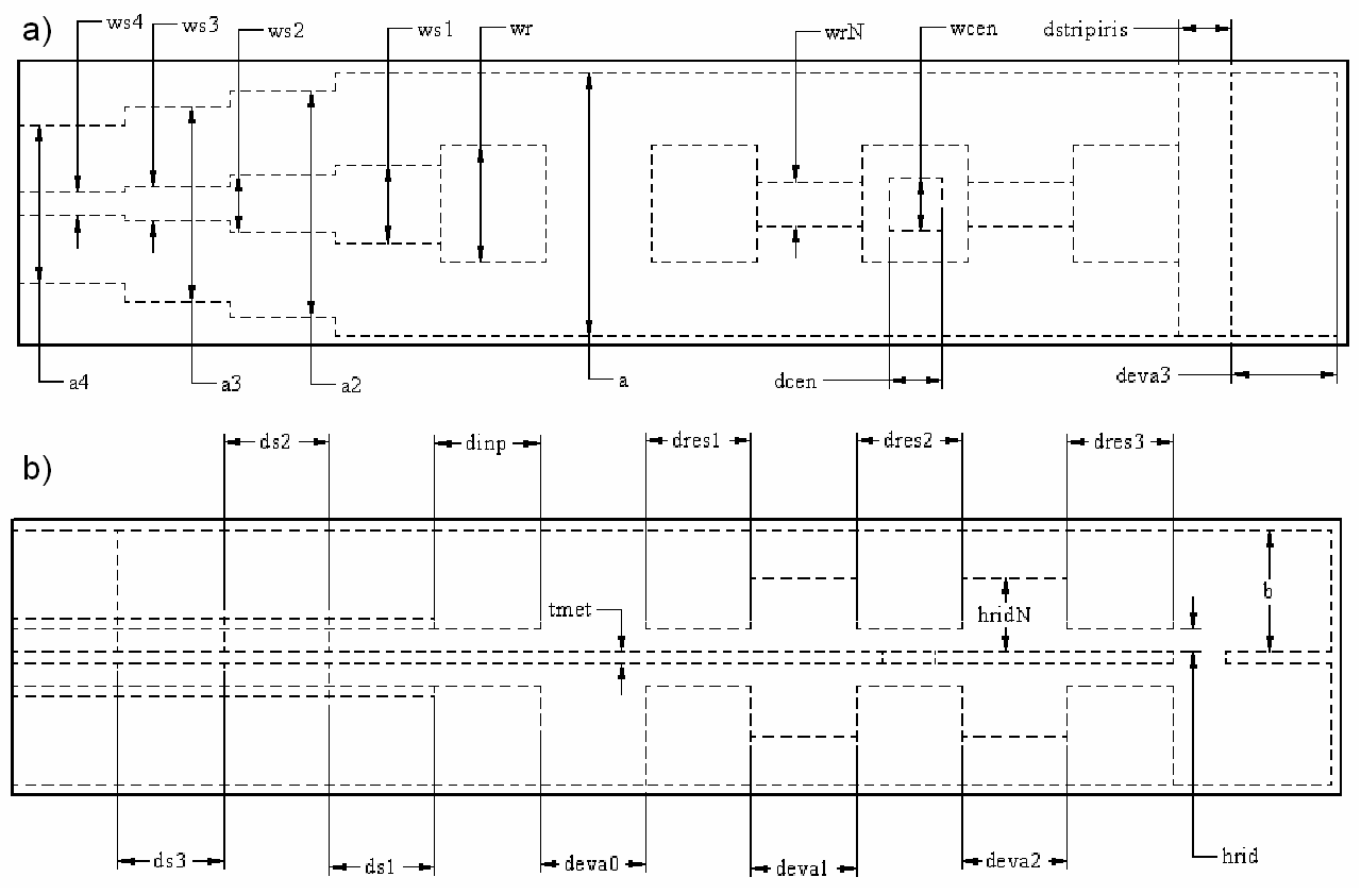

Figure 4.32: a) Side view of the whole structure composed of the second filter and the transition 50 ohm strip line b) Top view of the whole structure

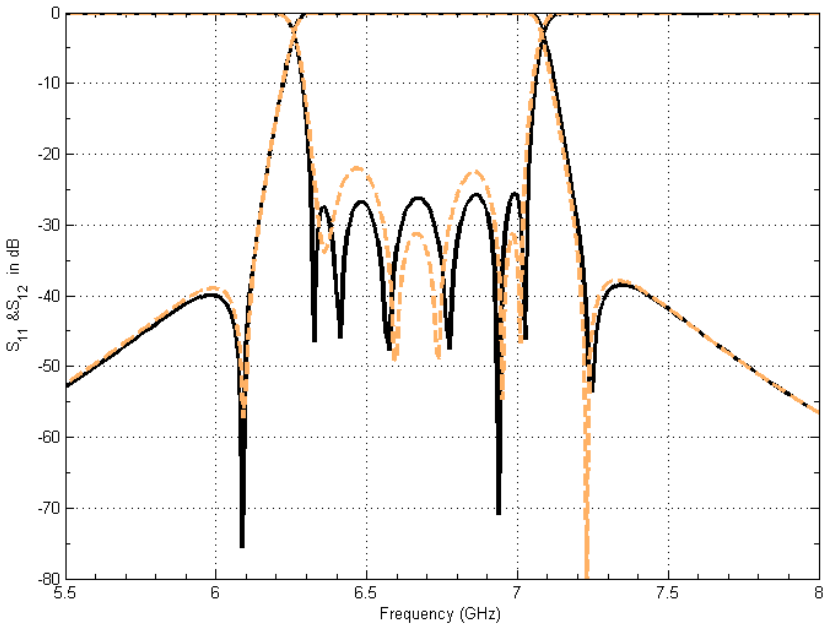

Figure 4.33: Full wave response of the whole structure obtained by mode matching (solid lines) vs.response obtained by HFSS (dotted lines)

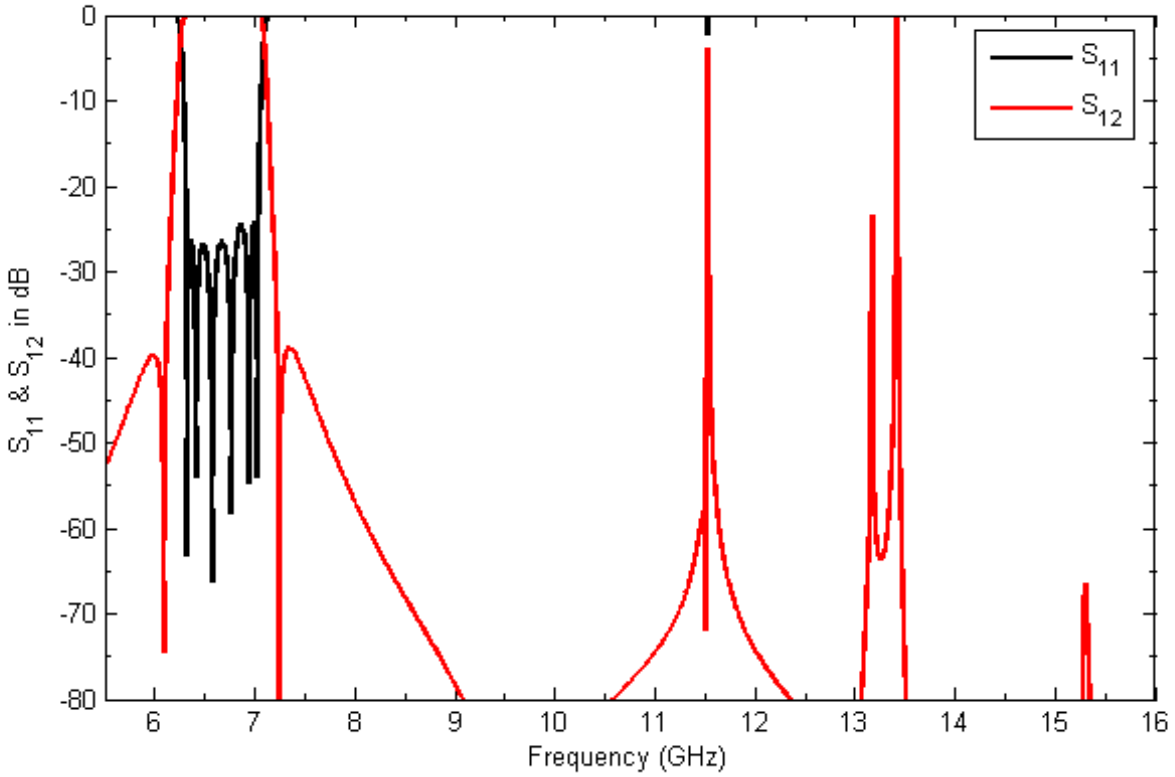

Figure 4.34: Broad band response of the whole structure

Table 4.4: Dimensions of the Optimized Filter and Ridge to Stripline Transition according to Fig. 4.32 .

Cross-sectional Dimensions in mils						
a	b	wr	$hrid$	wrN	$hridN$	$wcen$
250	115.94	110	22.44	42	71.06	50

Resonators' Dimensions in mils		
$dres1$	$dres2$	$dres3$
73.9	43.4	51.3

Coupling Sections' Dimensions in mils						
$dinp$	$deva0$	$deva1$	$dcen$	$deva2$	$dstripiris$	$deva3$
43.7	50	236.7	32	315	42.2	17.6

Transition Dimensions in mils			
$a2$	$a3$	$a4$	
215	185	150	
$ds1$	$ds2$	$ds3$	
49.3	82.4	57.7	
$ws1$	$ws2$	$ws3$	$ws4$
74	55	32	22.5

Chapter 5

Broad-band LTCC Stripline Directional Couplers

5.1 Introduction

Coupled TEM line directional couplers are key components in modern microwave systems. They are often utilized in Microwave Integrated Circuits MIC and large microwave networks. They also find applications in power monitoring, division and combining [108, 109]. In addition they are increasingly employed in sophisticated antenna beam forming networks, such as multi-port Butler matrices consisting of multiple 3-dB couplers [110–112]. They can also be utilized to construct directional filters and multiplexers [47].

Compared to non-TEM couplers realized in waveguide technologies,TEM coupled-lines couplers [113] offer a good alternative for achieving much wider bandwidths where the coupling is almost constant . S. B. Cohn ad R. Levy [114]

provide an exclusive summary on the early stages of the development of directional couplers and summarized the issues faced by the pioneers and what solutions were conceived for the problems encountered

The integration of low loss microwave structures, high speed digital circuits and DC power supplies in modules is an attractive design approach for compact microwave systems. Low Temperature Co-fired Ceramics (LTCC) couplers both in stripline [109, 115] and microstrip lines [116, 117] were reported; however the reported couplers were limited to a single section topology which limits the achievable bandwidth.

In this chapter the design process of a broad-band LTCC multi-section multi-layer LTCC stripline couplers that increase the achievable bandwidth and take advantage of the integration capabilities of LTCC technologies will be presented

5.2 Ideal Circuit Representation

The ideal circuit representation of the TEM coupled-line coupler consists of a four port network with unity impedance terminations on all four ports $Z_o = 1$. The coupled line is completely defined by an electric length ϕ and a coupling factor K. The coupling factor K can be alternatively defined by a pair of normalized impedances Z_{oo} and Z_{oe} such that

$$K = \frac{Z_{oe} - Z_{oo}}{Z_{oe} + Z_{oo}}; with \sqrt{Z_{oe} Z_{oo}} = Z_o \tag{5.1}$$

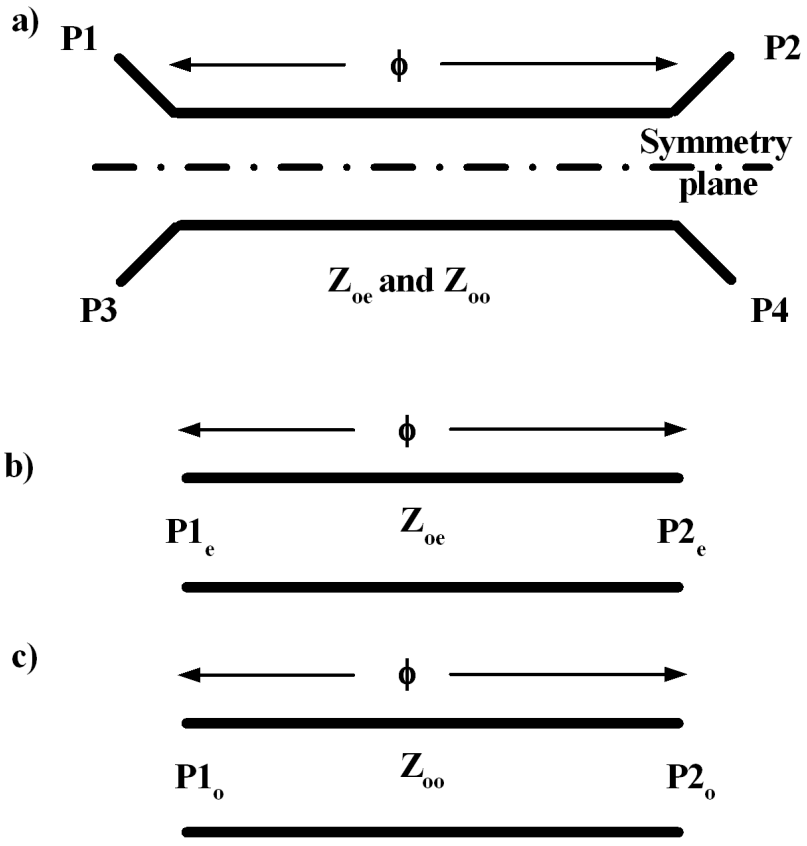

Figure 5.1: a) Ideal circuit of a single section coupled-line directional coupler b) Ideal circuit of the even-mode sub-circuit c) Ideal circuit of the odd-mode sub-circuit

The response of the circuit can be obtained by analyzing two decoupled transmission line circuits corresponding to two boundary conditions imposed at the symmetry plane. If an odd boundary condition which is equivalent to a short circuit is placed at the symmetry plane this would result in a transmission line of an electric length ϕ and its characteristic impedance is given by Z_{oo} while an even boundary condition would result in an open circuit condition imposed at the symmetry plane which would yield a transmission line of an electric length ϕ and its characteristic impedance is given by Z_{oe} The four port behavior of the circuit with port numbering as depicted in Fig. 5.1 is completely described by the two decoupled responses of the two odd and even sub-circuits as follows:

$$\begin{aligned} S_{11} &= \frac{1}{2}(S_{11e} + S_{11o}) \\ S_{12} &= \frac{1}{2}(S_{12e} + S_{12o}) \\ S_{13} &= \frac{1}{2}(S_{12e} - S_{12o}) \\ S_{14} &= \frac{1}{2}(S_{11e} - S_{11o}) \end{aligned} \tag{5.2}$$

Ideal circuit synthesis of single section couplers is quite straight forward [47] given the required coupling factor in dB $C = 10\log\|S13\|^2$ one can calculate the absolute coupling factor $K = 10^{\frac{-C}{20}}$ .Then one can get the required even and odd impedances readily using the following equation:

$$\begin{aligned} Z_{oe} &= Z_o\sqrt{\frac{1+k}{1-k}} \\ Z_{oo} &= Z_o\sqrt{\frac{1-k}{1+k}} \end{aligned} \tag{5.3}$$

The section electric length ϕ is $\lambda/4$ at the center frequency of the coupler.

Ideal circuit synthesis for multi-section couplers is not as straight forward as the single section case Tables for symmetric [113] and asymmetric [118, 119] are readily available.

5.3 Realization of Coupled-line Directional couplers

The feasibility of any coupled-line coupler depends on the possibility of achieving the correct amount of coupling K or ;alternatively expressed; depends on achieving the right Z_{oo} and Z_{oe} and the right Z_o. The coupling in these type of couplers depends mainly on the cross section used to realize the coupler. and as a rule of thumb the tighter the required coupling the more difficult it is to physically achieve the required cross-section. Figure 5.2 shows some of the common cross-sections used to realize the coupled-line couplers

Edge-coupled cross section are common in the loose coupling cases whereas broad-side-coupled cross sections are usually used for tighter couplings For extremely tight coupling in TEM couplers reentrant techniques were introduced for couplers realized in coaxial lines [120], in microstrip lines [121] and in striplines both in side coupled configurations [122] and in broadside configuration [123].Such couplers offer an extremely wide bandwidth for the coupling and also have a very compact size.

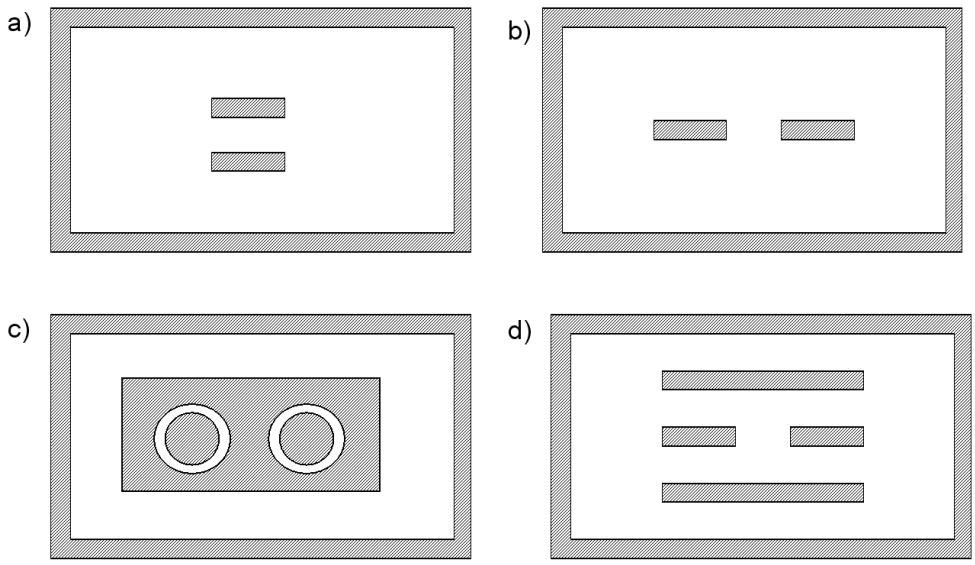

Figure 5.2: Cross sections used to realize coupled-line directional couplers a) Broad-side coupled striplines b) Edge-coupled striplines c) Re-entrant coaxial cross-section d)Re-entrant stripline cross section

5.3.1 LTCC Realization of Coupled-line Directional Couplers

LTCC technology employs multi-layer substrate manufactured by deposition, layer by layer, of dielectric and metallic patterns. In the context of LTCC technology some challenges arise when it is required to realize cross-sections for very tight coupling In the case of broad-side coupled striplines because of the way LTCC technology works the separation between any two conducting lines can not be less than the thickness of one dielectric layer, thus putting a limit on how much coupling can be achieved. Another dilemma is that the separation between the conducting lines is a multiple integer of the dielectric layer thickness. To tackle these limitations a re-entrant type cross-section is introduced,it can be seen in

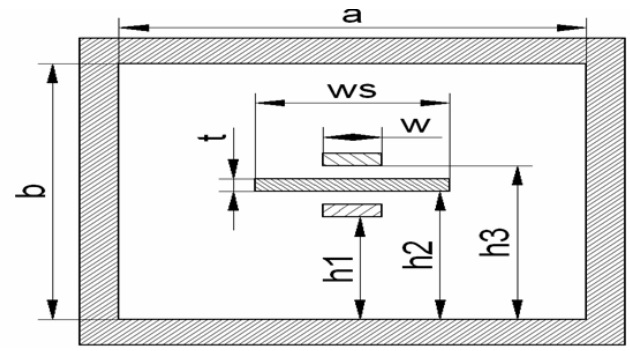

Figure 5.3: Re-entrant type cross section used to realize the proposed coupler

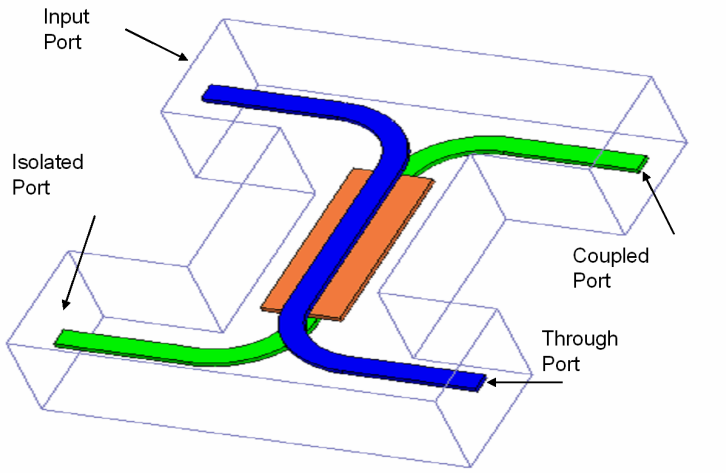

Figure 5.4: 3-D view of a single section multi-layer coupler with port designations

Fig. 5.3

By introducing the floating septum between the two conducting lines an additional degree of freedom is achieved which enables precise design of the coupler cross-section and overcomes some of the limitation posed by the available LTCC technology. A 3D view of a single section coupler using the proposed cross-section is shown in Fig. 5.4.

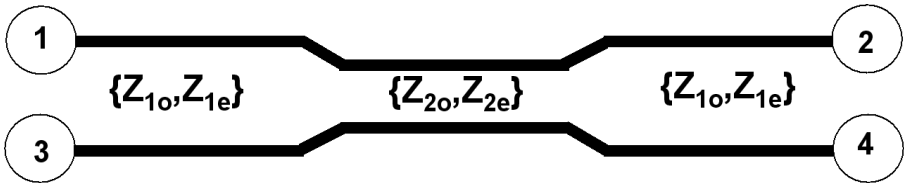

Figure 5.5: Ideal circuit describing a 3-section symmetric coupler

5.4 Design Example

To show the feasibility of the proposed design a three section TEM contra directional coupler will be designed. The coupler has a center frequency of 5.25 GHz, a prescribed coupling of 3 ± 0.5 dB over a 135% fractional bandwidth and it is terminated in 50Ω ports. The coupler will designed assuming an LTCC technology with layer thickness of 3.74 mils and dielectric constant $\epsilon_r = 5.9$

5.4.1 Ideal circuit Design

Ideal transmission line circuit element values are obtained from design tables [113]. A three section coupler was shown to satisfy all the requirement the parameters for the coupler is given below and the response is shown in Fig. 5.6 , Ideally the coupler is fully matched $S_{11} = -\infty$ and fully isolated $S_{14} = -\infty$.

$$\begin{aligned} Z_{oe} &= \begin{bmatrix} 63.5180 & 183.280 & 63.5180 \end{bmatrix} \Omega \\ Z_{oe} &= \begin{bmatrix} 39.3589 & 13.6403 & 39.3589 \end{bmatrix} \Omega \\ K &= \begin{bmatrix} \begin{pmatrix} 0.2348 & 0.8615 & 0.2348 \end{pmatrix} \end{bmatrix} \end{aligned} \tag{5.4}$$

Investigating the coupling required by each section of the coupler it can be readily shown that the middle section requires a very tight coupling of -1.29 dB which

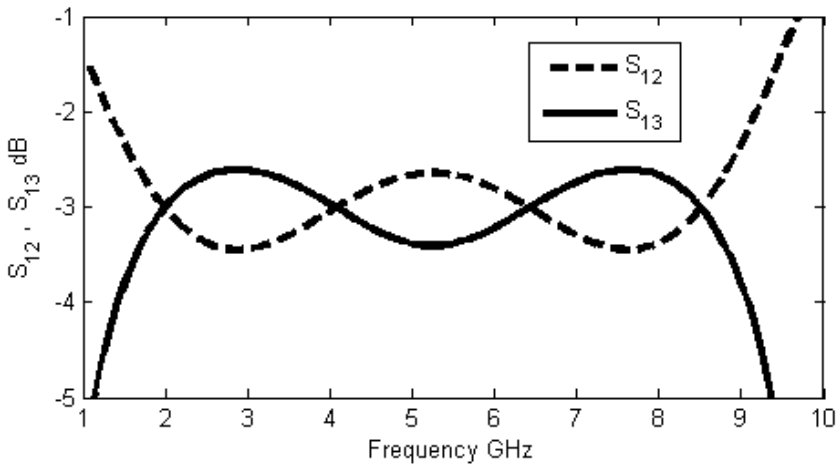

Figure 5.6: Response of a 3-dB coupler

is not achievable given current LTCC technology. To have reasonable impedance values; a tandem connection of two 8.33 dB couplers is used instead The required impedances and coupling factors for the 8.33 dB coupler are given in 5.5. The way the two couplers are connected is shown in Fig. 5.7

$$\begin{aligned} Z_{oe} &= \begin{bmatrix} 55.3030 & 89.7305 & 55.3030 \end{bmatrix} \Omega \\ Z_{oe} &= \begin{bmatrix} 45.2055 & 27.8612 & 45.2055 \end{bmatrix} \Omega \\ K &= \begin{bmatrix} 0.1005 & 0.5261 & 0.1005 \end{bmatrix} \end{aligned} \tag{5.5}$$

5.4.2 Realization of Individual Sections

In this design the reentrant section shown in Fig. 5.3 will be used to offer an extra degree of freedom to offset the restrictions mandated by the LTCC technology. Similar multi-conductor transmission line systems have been heav-

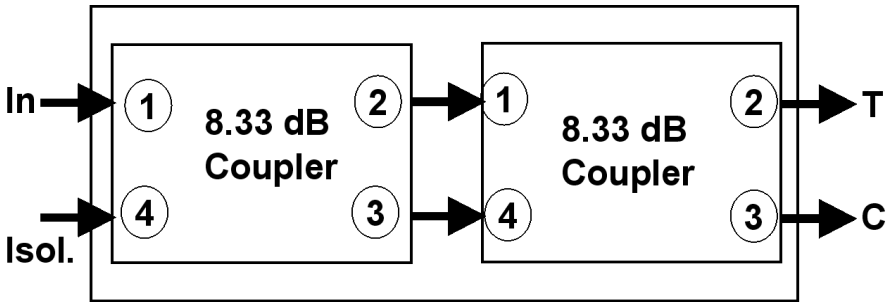

Figure 5.7: Tandem connection of two 8.33 dB couplers

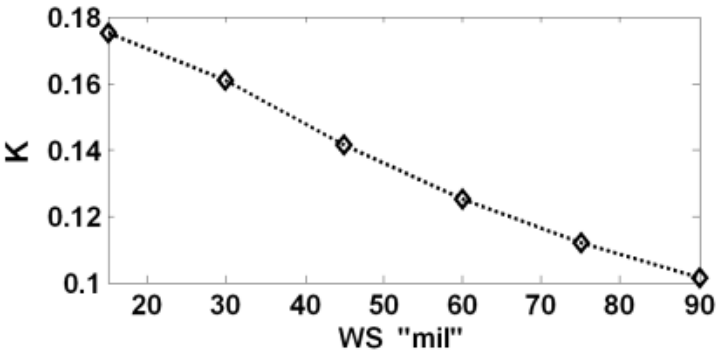

Figure 5.8: Variation of coupling with ws, $a = 200$ mil, $w = 11$ mil $t = 0.5$ mil, $b = 12$ LTCC layers $h1 = 3$ layers $h2 = 6$ layers, $h3 = 9$ layers. LTCC $\epsilon_r = 5.9$ and layer thickness $= 3.74$ mils. The lines are $\lambda g/4$ at $f_o = 5.25$ GHz

ily investigated[124–127] By varying the width of the floating conductor septum while keeping the width of the main lines fixed the coupling of the section can be precisely controlled. Using full-wave simulation of a single section coupler shown in Fig. 5.3 and observing the achieved coupling; the effect of the septum can be quantified. Figure 5.8. shows the variation of the achieved coupling of a single section versus the width of the floating septum.

This cross section will be used to realize the first and third sections while broad side coupled striplines will be used to realize the middle section. Each

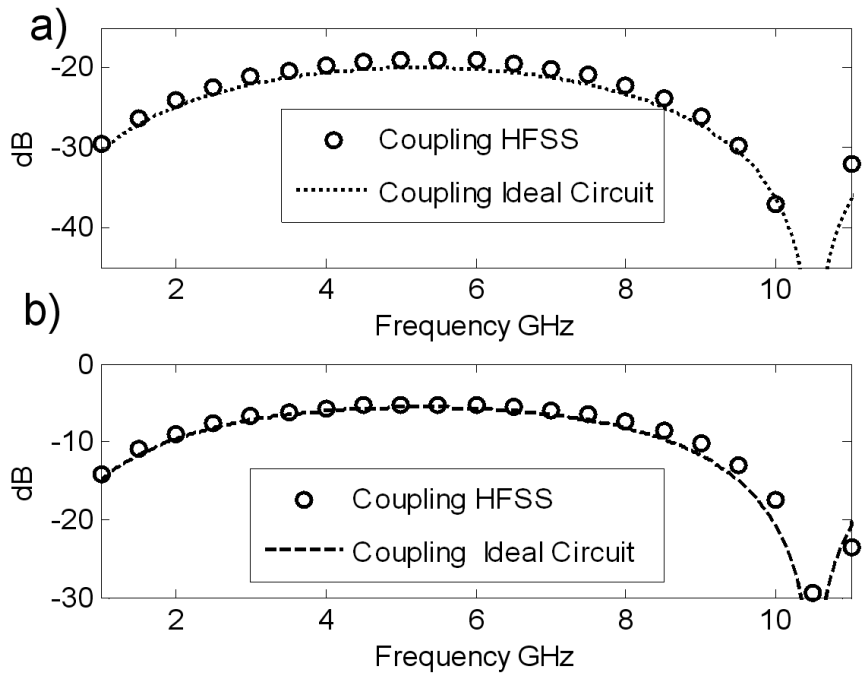

Figure 5.9: a) Coupling Response of a single section coupler using the cross section shown in Figure 5.3 $k \approx 0.1$ b) Coupling Response of a single section coupler using the cross section shown in Figure 5.3 without the middle septum $w = 15$ mil $h1 = 5$ LTCC layers, $h3 = 7$ LTCC layers $k \approx 0.52$ all other dimensions are the same as those given in Figure 5.81. The lines are $\lambda g/4$ at $f_o = 5.25$ GHz

section is designed separately to follow the ideal circuit response of a single section coupler with couplings k of 0.1005 and 0.5261 respectively. Fig. 5.9 shows the full-wave response "coupling only shown" of each section versus its ideal circuit response.

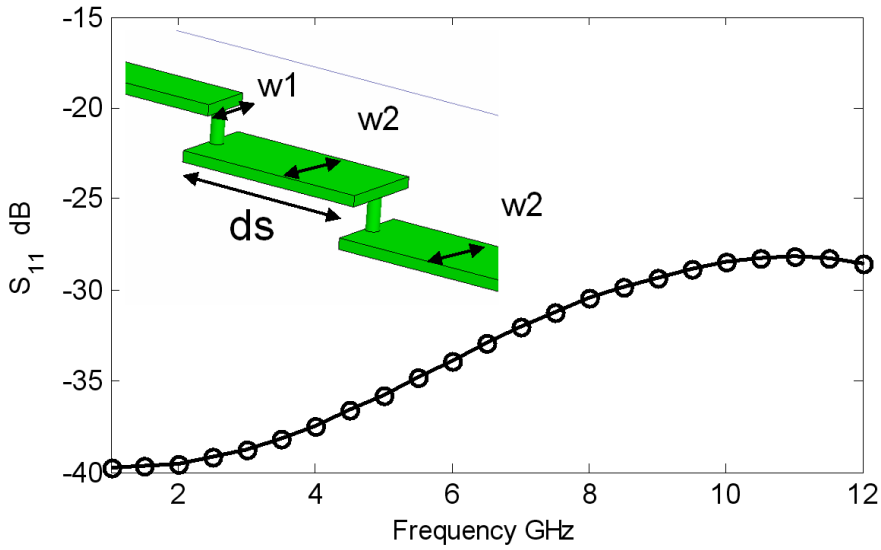

Figure 5.10: Response of the stepped transition. Widths $w1 = 11$ mils, $w2 = 15$ mils, $ds = 25$ mils. Via diameter= 6 mils. Vertical dimensions are provided in TABLE 5.1

5.4.3 Interconnection of Sections

Since each section has different spacing between the coupled lines; a connection mechanism to interconnect the two lines of consecutive sections ought to be found. A direct connection of the lines which utilizes one via going down from the upper line directly to the lower line was shown to severely deteriorate the return loss. A stepped connection between the lines was employed, where an intermediate step is introduced between the lines to be connected. This step is connected by means of vias to the two lines. This arrangement helps secure a smooth transition between the lines The interconnection between the lines is shown in Fig. 5.10 along with its return loss.

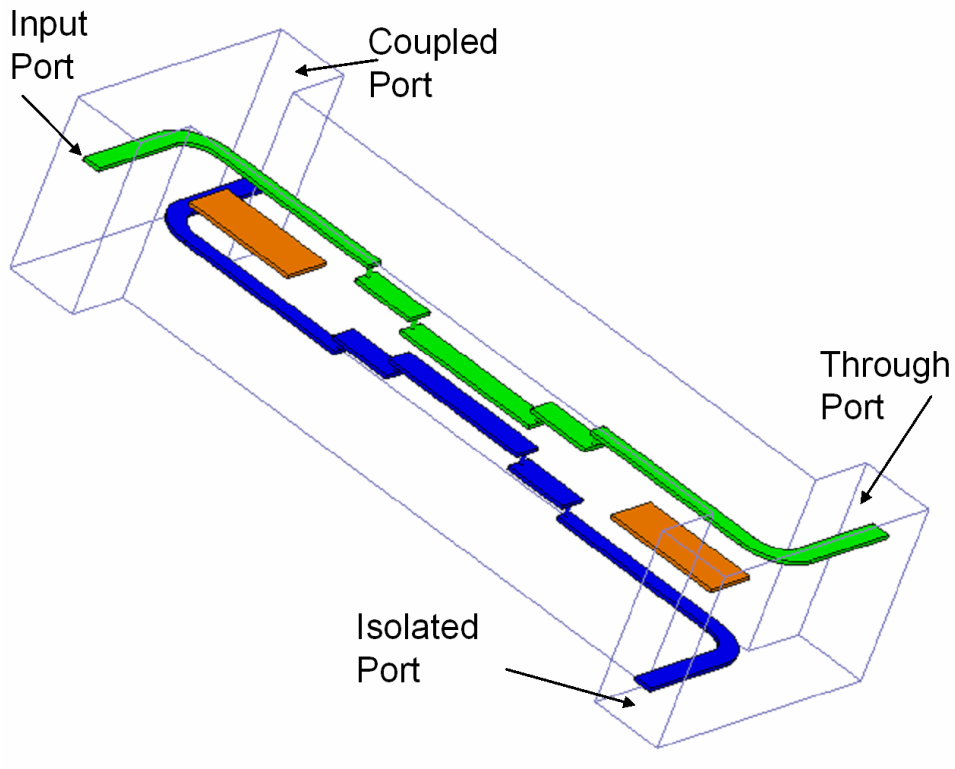

Figure 5.11: 3-D view of the three section coupler with port designations

5.4.4 Realization of Cascaded Coupler

Using the outlined method to design the 8.33 dB coupler a single unit was designed. Fig. 5.11. shows a 3-D view of the 8.3 dB unit while Fig. 5.12. shows a side-view of the coupler. Fig. 5.13. shows its response compared to the ideal circuit response. Good agreement is observed.

One of the benefits of multi-layer LTCC couplers is that it is possible to cascade coupled line couplers, a feature otherwise not feasible in edge coupled stripline or micro strip line couplers where the input and the coupled port both lie on the same side. In the multi-layer structure by bending the ports appropriately cascading is feasible. Fig. 5.14 shows the 3-D view of the cascaded unit while

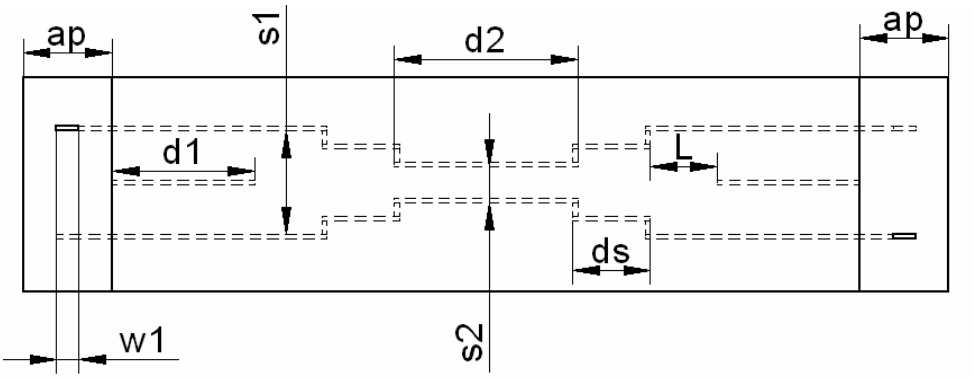

Figure 5.12: Side-View of the proposed coupler, dimensions in TABLE I

Fig.5.15 shows its top view. The full-wave response is shown in Fig. 5.16. All dimensions are given in TABLE 5.1

5.4.5 Practical Considerations

The design process up to this point assumed ideal lossless models which is not the case in any practical context. In LTCC technology common concerns stem from the losses associated with the dielectric materials used in the technology.. Another practical aspect is that the design assumes a perfect knowledge of the dielectric constant ϵ_r of the layers used in the LTCC while in reality the dielectric constant may vary slightly from batch to batch. One other concern is that the alignment of the metallic patterns especially the coupled lines may not be as precise as prescribed by the design. In order to address these consideration additional modelling and simulation was performed on the final design.

To account for the dielectric losses as well as the ohmic losses encountered in the design the model was simulated assuming that the LTCC material has a

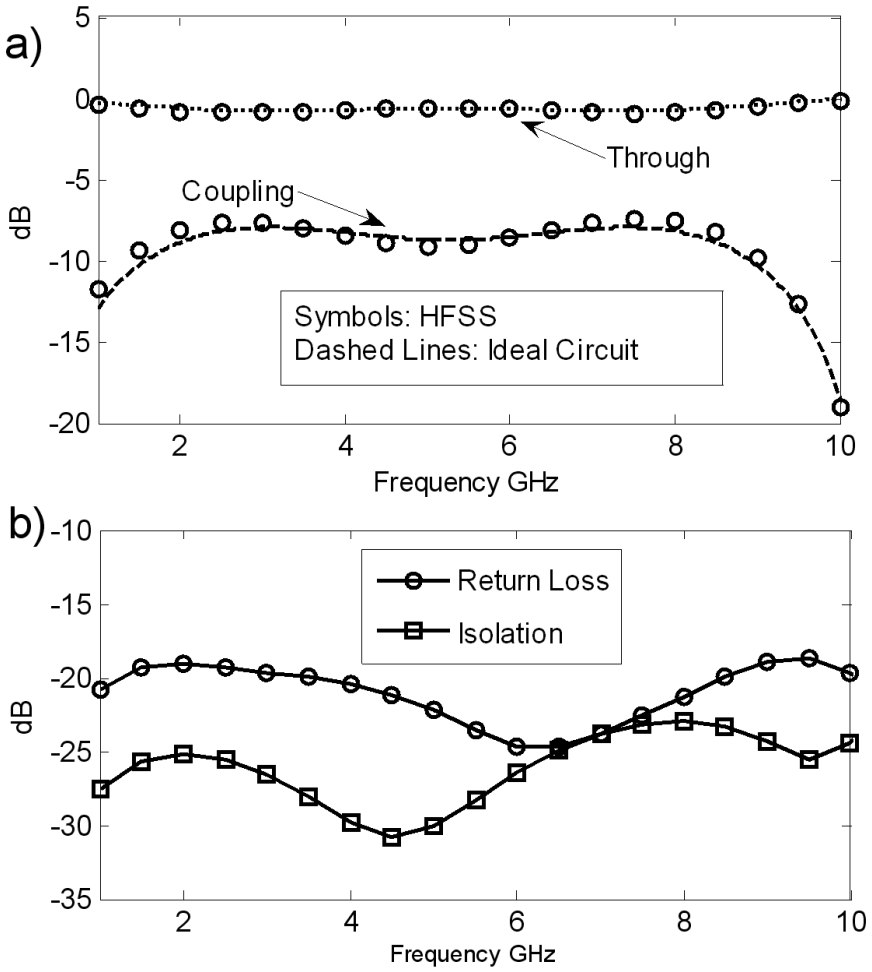

Figure 5.13: a) Coupling and Through response of the 8.33 dB coupler. b) Return Loss and Isolation.

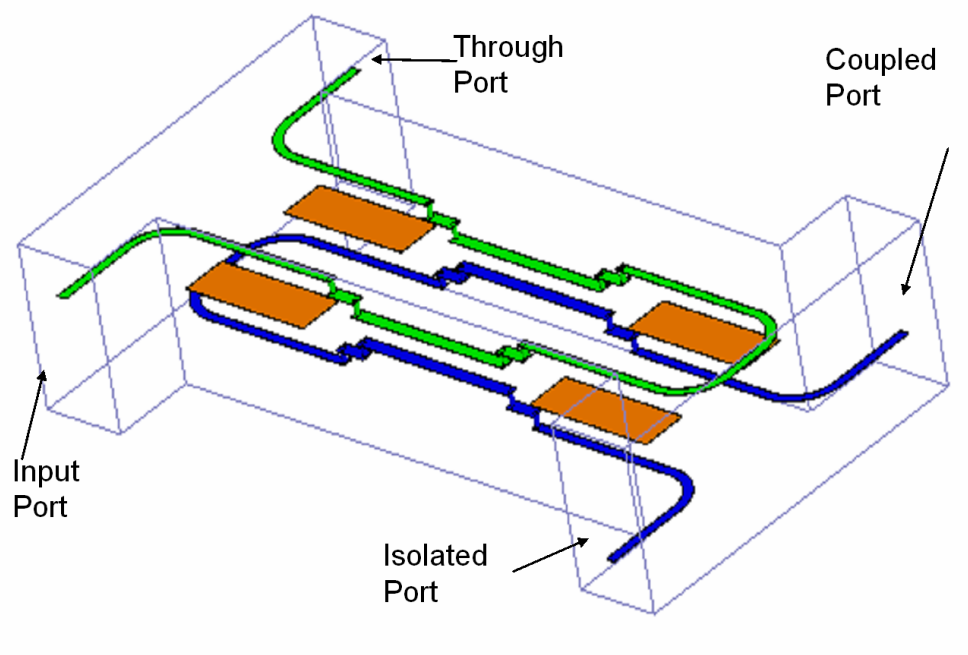

Figure 5.14: 3-D view of the proposed cascaded component.

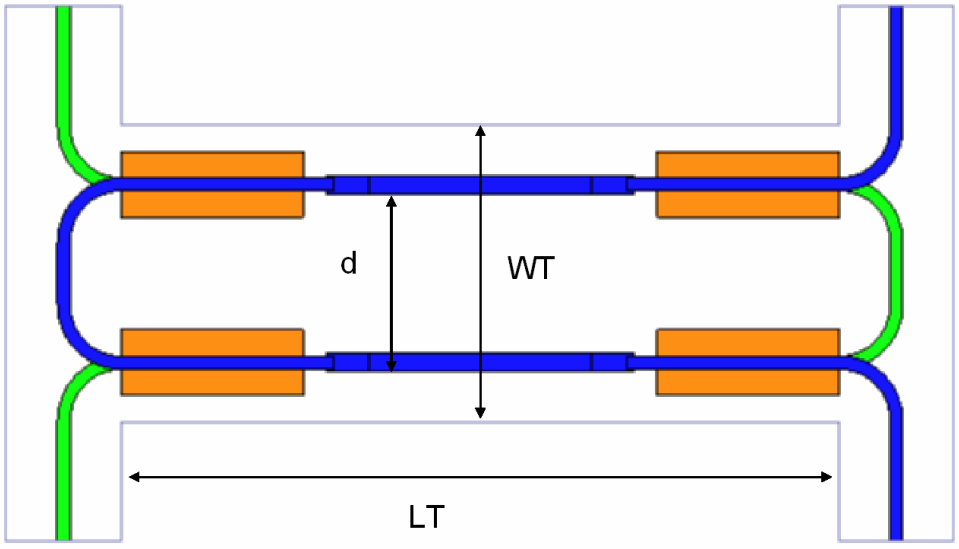

Figure 5.15: Top-View of the proposed cascaded component

Table 5.1: Dimensions of the Coupler according to Fig. 5.3 and Fig. 5.10,5.12 ,and 5.15 .

Dimension	mil	Dimension	mil
ap	100	$w2$	15
b	44.88	$d2$	175
t	0.5	ds	25
$w1$	11	L	20
ws	55	$h1(Section2)$	18.7
$h1(Section1,3)$	11.22	$h2(Section2)$	26.18
$h2(Section1,3)$	22.66	$s2$	7.48
$h3(Section1,3)$	33.66	d	45
$d1$	160	$LTCClayerthickness$	3.74
$s1$	22.44	LT	639
wt	350		

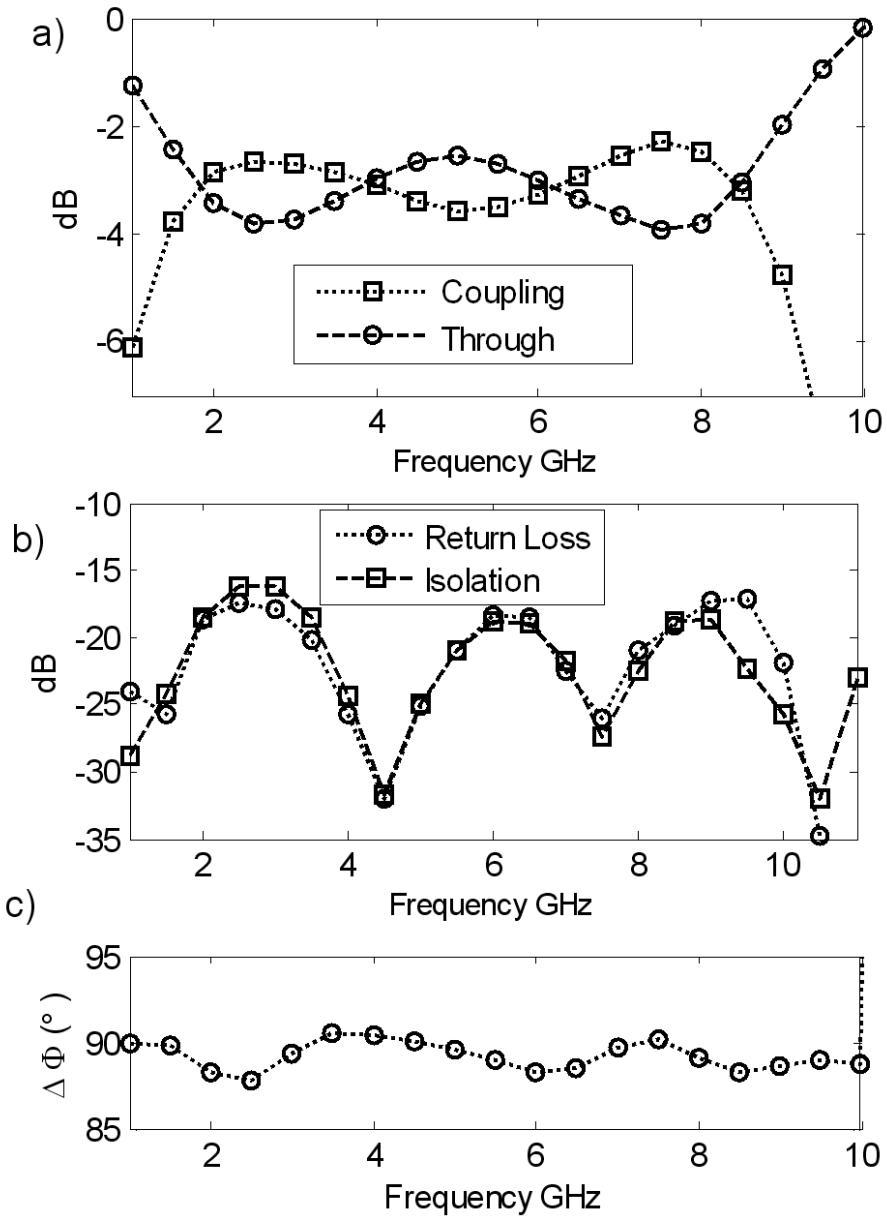

Figure 5.16: a) Coupling and Through response of the 3 dB coupler. b) Return Loss and Isolation. c) Phase difference between coupled and through ports

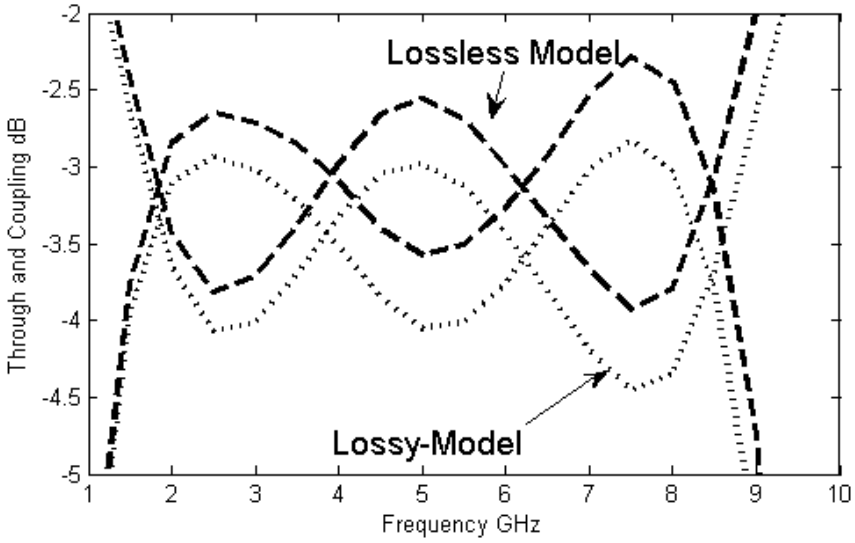

Figure 5.17: Comparison of Coupling and Through responses of the ideal vs. the lossy coupler

dielectric loss tangent $\tan\delta = 0.002$ which is a typical value for such technology, and all the conducting lines and surfaces was assumed to be made of gold with its finite conductivity. Fig. 5.18 and Fig. 5.17 show the comparison between the ideal and the lossy models. A loss of around 0.4 dB at the lower frequency band and around 0.75 dB at the high frequency band is observed.

To account for the uncertainty of the dielectric constant the simulation was run assuming a dielectric constant of 4.9 and 6.5 instead of 5.5 and the results were compared to the ideal case of 5.9. Figure 5.19 shows the comparison of the coupling and through response and show that the effect of the shift of the dielectric constant would result in a shift in the center frequency of the coupler

Lastly to account for any misalignment of the coupled lines an intentional misalignment was assumed in the model, two cases with 2 mil offset and 5 mil

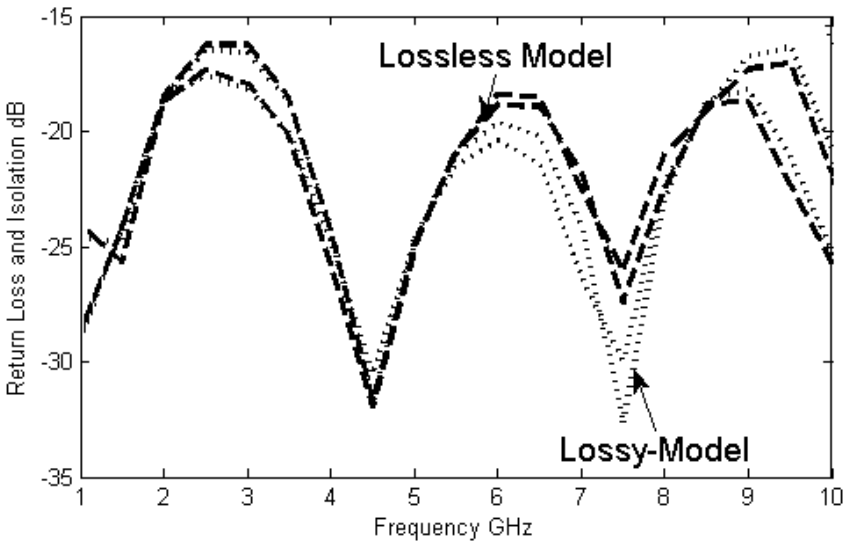

Figure 5.18: Comparison of return loss and isolation responses of the ideal vs. the lossy coupler

offset were investigated Fig. 5.20 shows the results of the coupling and through. While an offset of 2 mils did not have much effect on the response the severe 5 mil offset caused the response to deteriorate considerably. Fig. 5.21 reveals that the return loss and isolation responses did not change much with the offset . possible explanation is that the return loss and isolation are caused and controlled by reactances caused at the discontinuity between the port lines and the coupled lines.[128, 129] .

5.5 Conclusions

In this chapter the design methodology of Multi-section multi-layer LTCC stripline couplers was discussed The use of reentrant cross section enables the designer to achieve precise design values of coupling otherwise restricted by limitations posed

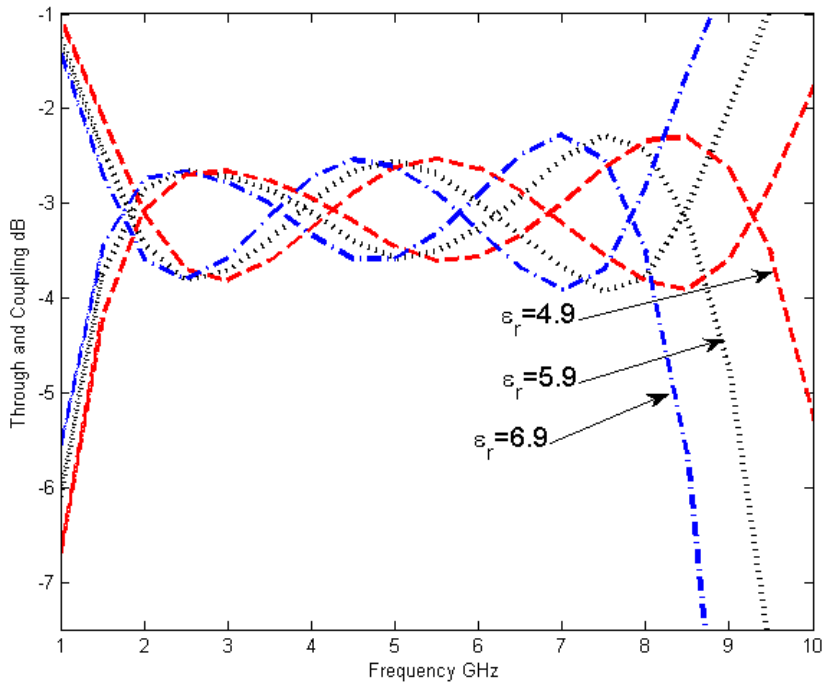

Figure 5.19: Comparison of Coupling and Through responses coupler with different ϵ_r

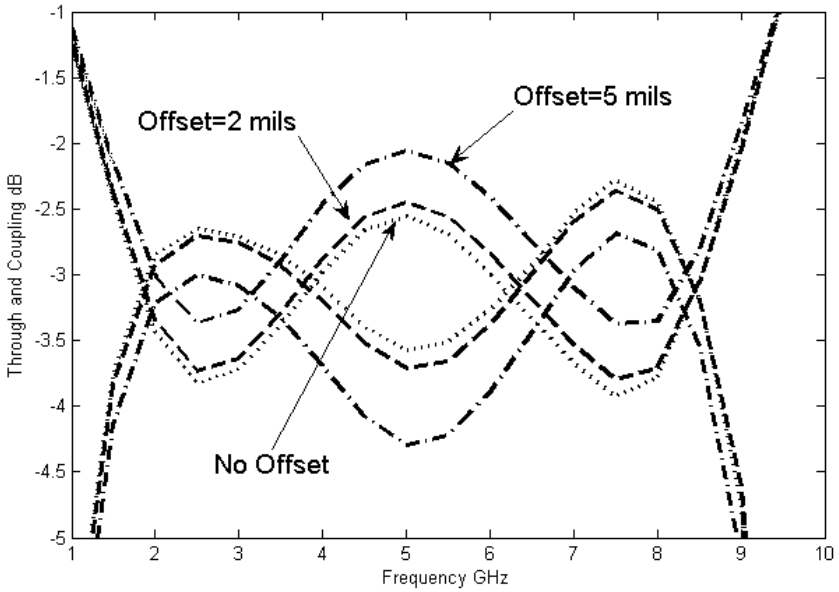

Figure 5.20: Comparison of Coupling and Through responses coupler with different misalignments

by the LTCC technology. Interconnection of different sections of the coupler by a stepped stripline transition between different layers of the structure is shown to enable the realization of broad band coupling performance. The cascading of wideband 8.33 dB couplers enables the realization of tight coupling over a very wide fractional bandwidth.. The design was shown to be insensitive to minor offsets and was shown to incur reasonable losses.

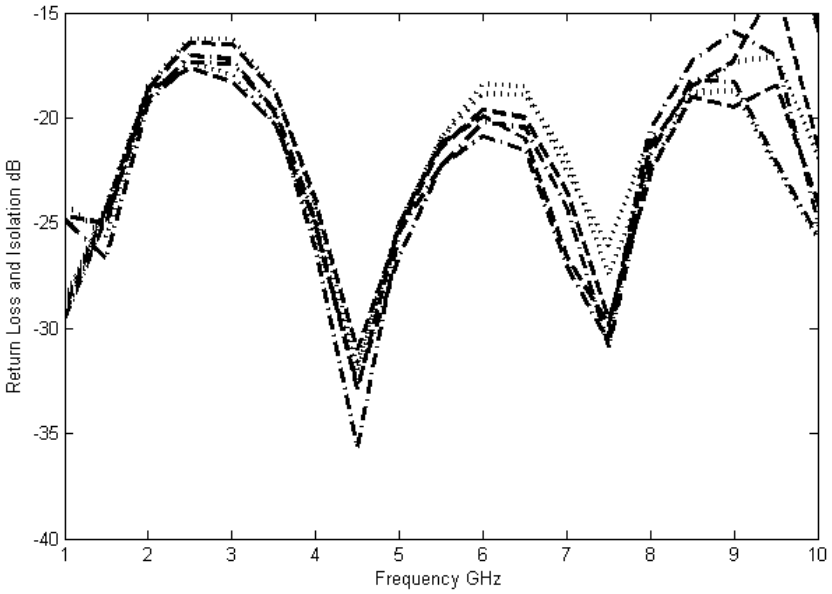

Figure 5.21: Comparison of return loss and isolation responses coupler with different offsets

Chapter 6

Conclusions and Future Work

6.1 Conclusions

The main goal of the dissertation was to demonstrate the challenges and present solutions that enable the successful design and realization of very wide band microwave components, namely microwave filters and directional couplers. Such components are essential for the development of modern communication systems operating at microwave frequencies.

In chapter two a review of the state of the art of numerical techniques used in the computer aided design (CAD) of microwave passive components was presented. A summarization of the various numerical techniques and their different applicability criteria was presented. A special emphasis was awarded to the mode matching techniques as it was the main technique used for most of the designs presented in the dissertation.

Chapter three presents a comprehensive discussion of the subject of wide-

band ridge waveguide directional couplers. Analysis and design of different configurations and arrangements of couplers realized in ridge waveguides was discussed. A new detailed systematic design procedure for ridge waveguide couplers in the two most used configurations "E-plane and H-plane" was presented. This part combined ideal circuit and electromagnetic modeling to obtain very satisfactory initial results. The presented systematic design utilized the numerical efficiency of the mode matching technique to reduce the overall numerical simulation time and resources.

Chapter four was dedicated to the discussion of wide-band ridge waveguide elliptic function filters realized in Low Temperature Co-fired Ceramics (LTCC). This included ideal circuit modeling,as well as electromagnetic modeling of the three dimensional structures used to realize the filters. New schemes to achieve stronger couplings, and to suppress unwanted spurious detrimental couplings were presented.

Chapter five presented a new design for multi-section multi-layer LTCC stripline couplers. The proposed design enables the achievement of precise performance otherwise restricted by limitations posed by available technologies. The realization of ultra wideband performance of the coupler was discussed.

6.2 Future Work

The dissertation tackled design challenges and offered innovative solutions for some of the most important components in modern microwave communication

systems. Interesting points for future research include:

1. Interconnection of wideband ridge waveguide elliptic function filters in compact miniature LTCC based multiplexers

2. Design of mixed mode filters in ridge waveguides to improve out of band rejection and spurious suppression

3. Design of ridge waveguide filters with embedded low pass filters to suppress unwanted harmonics in the rejection band of the filters

4. Design of extracted pole filters in ridge waveguides and LTCC technology. This type of filter offers sharper selectivity and convenience of in-line structures which are easier to manufacture. Miniaturization is accomplished by realization of the filters in LTCC technology.

5. Design of multi-band filters in ridge waveguides and LTCC technology

6. Incorporation of ridge waveguide filters and couplers to construct directional filters and multiplexer

7. The use of advanced compensating techniques to improve the return loss and isolation performance of broadband LTCC stripline couplers.

8. Utilization of broadband LTCC stripline couplers in realizing sophisticated antenna beam forming networks, such as multi-port Butler matrices

Bibliography

[1] T. Itoh (editor), *Numerical Techniques for Microwave and Millimeter-Wave Passive-Structures*. New York: John Wiley, 1989.

[2] J. D. G. Swanson and W. J. R. Hoefer, *Microwave Circuit Modeling Using Electromagnetic Field Simulation*. Boston, London: Artech House, 2003.

[3] J. Webb and S. Parihar, "Finite element analysis of H-plane rectangular waveguide problems," *IEE Proc.*, vol. 133 pt. H, no. 2, pp. 91–94, Apr. 1986.

[4] P. P. Silvester and R. L. Ferrari, *Finite Elements for Electrical Engineers*. New York: Cambridge University Press, 1996.

[5] M. Koshiba and M. Suzuki, "Application of the Boundary-Element method to waveguide discontinuities," *IEEE Trans. Microw. Theory Tech.*, vol. 34, pp. 301–307, Feb. 1986.

[6] *Ansoft High Frequency Structure Simulator (HFSS)*. Ansoft Corporation.

[7] G. Mur, "Finite difference method for the solution of electromagnetic waveguide discontinuity problem," *IEEE Trans. Microw. Theory Tech.*, vol. 22, pp. 54–57, Jan. 1974.

[8] W. K. Gwarek, "Analysis of arbitrarily shaped two-dimensional microwave circuits by Finite-Difference Time-Domain method," *IEEE Trans. Microw. Theory Tech.*, vol. 36, pp. 738–744, Apr. 1988.

[9] A. Taflove and S. Hagness, *Computational Electromagnetics: The Finite-Difference Time-Domain Method*. Norwood, MA: Artech House, 2000.

[10] S. Haffa, D. Hollmann, , and W. Wiesbeck, "The finite difference method for S-parameter calculation of arbitrary three-dimensional structures," *IEEE Trans. Microw. Theory Tech.*, vol. 40, pp. 1602–1610, Aug. 1992.

[11] *EMPIRE: A full 3-D field solver*. Institut fuer Mobil und Satellitenfunktechnik GMbH (IMST).

[12] R. F. Harrington, *Field Computation by Moment Methods*. New York: Macmillan, 1968.

[13] *SONNET: 3D Planar High-Frequency Electromagnetic Software.* Sonnet Software Inc.

[14] *IE3D: A full-wave, method-of-moments based simulator.* Zeland Software, Inc.

[15] P. B. Johns, "A symmetrical condensed node for the TLM method," *IEEE Trans. Microw. Theory Tech.*, vol. 35, no. 4, pp. 370–377, 1987.

[16] C. Christopoulos, *The Transmission-Line Modeling Method TLM.* New York: IEEE Press, 1995.

[17] *Multi-Purpose Electromagnetic Field Simulation Tool (MEFiSTo).* Faustus Scientific Corporation.

[18] T. Itoh, "Analysis of microstrip resonators," *IEEE Trans. Microw. Theory Tech.*, vol. 22, pp. 946–952, 1974.

[19] G. Conciauro, M. Guglielmi, and R. Sorrentino, *Advanced modal analysis: CAD techniques for waveguide components and filters.* John Wiley, 1999.

[20] J. Uher, J. Bornemann, and U. Rosenberg, *Waveguide Components for Antenna Feed Systems.* Boston: Artech House, 1993.

[21] G. Conciauro, P. Arcioni, M. Bressan, and L. Perregrini, "Wideband modeling of arbitrarily shaped H plane waveguide components by the 'Boundary Integral-Resonant Mode Expansion method'," *IEEE Trans. Microw. Theory Tech.*, vol. 44, pp. 1057–1066, July 1996.

[22] P. Arcioni, M. Bressan, G. Conciauro, and L. Perregrini, "Wideband modeling of arbitrarily shaped E plane waveguide components by the 'Boundary Integral-Resonant Mode Expansion method'," *IEEE Trans. Microw. Theory Tech.*, vol. 44, no. 11, pp. 2083–2092, Nov. 1996.

[23] J. M. Reiter and F. Arndt, "A Boundary Contour Mode-Matching method for the rigorous analysis of cascaded arbitrarily shaped H-plane discontinuities in rectangular waveguides," *IEEE Microwave Guided Wave Lett.*, vol. 2, pp. 403–405, Oct. 1992.

[24] ——, "Rigorous analysis of arbitrarily shaped H- and E-plane discontinuities in rectangular waveguides by a full-wave Boundary Contour Mode-Matching method," *IEEE Trans. Microw. Theory Tech.*, vol. 43, pp. 796–801, Apr. 1995.

[25] R. H. MacPhie and K. L. Wu, "A full-wave modal analysis of arbitrarily shaped waveguide discontinuities using the finite plane-wave series expansion," *IEEE Trans. Microw. Theory Tech.*, vol. 47, no. 2, pp. 232–237, Feb. 1999.

[26] ——, "A full-wave modal analysis of inhomogeneous waveguide discontinuities with both planar and circular cylindrical boundaries," *IEEE Trans. Microw. Theory Tech.*, vol. 49, pp. 1132–1136, June 2001.

[27] F. Arndt, J. Brandt, V. Catina, J. Ritter, I. Rullhusen, J. Dauelsberg, U. Hilgefort, and W. Wessel, "Fast CAD and optimization of waveguide components and aperture antennas by hybrid MM/FE/MoM/FD methods-state-of-the-art and recent advances," *IEEE Trans. Microw. Theory Tech.*, vol. 52, no. 1, pp. 292–305, Jan. 2004.

[28] F. Arndt, R. Beyer, J. M. Reiter, T. Sieverding, and T. Wolf, "Automated design of waveguide components using hybrid mode-matching/numerical EM building-blocks in optimization-oriented CAD frameworks-state of the art and recent advances," *IEEE Trans. Microw. Theory Tech.*, vol. 45, no. 5, pp. 747–760, May 1997.

[29] *Wasp-Net*. Bremen, Germany: Microwave Innovation Group.

[30] *Microwave Wizard*. Bremen, Germany: Mician GbR.

[31] A. Wexler, "Solution of waveguides discontinuities by modal analysis," *IEEE Transactions on Microwave Theory and Techniques*, vol. 15, pp. 508–517, 1967.

[32] J. Bornemann and F. Arndt, "Modal-S-matrix design of optimum stepped ridged and finned waveguide transformers," *IEEE Trans. Microw. Theory Tech.*, vol. 35, no. 6, pp. 561–567, June 1987.

[33] H. Patzelt and F. Arndt, "Double-plane steps in rectangular waveguides and their application for transformers, irises, and filters," *IEEE Trans. Microw. Theory Tech.*, vol. 82, no. 5, pp. 771–776, May 1982.

[34] J. Dittloff and F. Arndt, "Computer-aided design of slit-coupled H-plane T-junction diplexers with E-plane metal-insert filters," *IEEE Trans. Microw. Theory Tech.*, vol. 36, no. 12, pp. 1833–1840, Dec. 1988.

[35] ——, "Rigorous field theory design of millimeter-wave E-plane integrated circuit multiplexers," *IEEE Trans. Microw. Theory Tech.*, vol. 37, no. 2, pp. 340–350, Feb. 1989.

[36] W. Menzel and I. Wolff, "A method for calculating the frequency-dependent properties of microstrip discontinuities," *IEEE Trans. Microw. Theory Tech.*, vol. 25, pp. 107–112, Feb. 1977.

[37] S. W. Drabuwitch, "Multimode antennas," *Microwave Journal*, vol. 9, pp. 41–51, 1966.

[38] P. J. B. Clarricoats and K. R. Slinn, "Numerical method for the solution of waveguide discontinuity problems," *Electronic Letters*, pp. 226–227, 1966.

[39] J. A. R. Cruz, "Contribution to the cad of microwave-millimeterwave passive devices by mode-matching techniques," Ph.D. dissertation, Univ. Politécnica de Madrid, Madrid, Spain, 2005.

[40] C. Wang, "Modeling of conductor, dielectric loaded resonators, filters and double ridge waveguide t-junctions," Ph.D. dissertation, University of Maryland, College Park, MD, USA, 1997.

[41] Y. Rong, "Modeling of combline coaxial, ridge waveguide filters and multiplexers," Ph.D. dissertation, University of Maryland, College Park, MD, USA, 1999.

[42] Y. Rong and K. A. Zaki, "Characteristics of generalized rectangular and circular ridge waveguides," *IEEE Trans. Microw. Theory Tech.*, vol. 48, pp. 258–265, Feb. 2000.

[43] R. Sorrentino and T. Itoh, "Transverse resonance analysis of finline discontinuities," *IEEE Trans. Microw. Theory Tech.*, vol. 32, no. 12, pp. 1633–1638, Dec. 1984.

[44] H. Y. Yee, "Transverse modal analysis of printed circuit transmission lines," *IEEE Trans. Microw. Theory Tech.*, vol. 33, no. 9, pp. 808–816, Sept. 1985.

[45] H. Riblet, "The short-slot hybrid junction," *Proc. IRE*, vol. 40, pp. 180–184, Feb. 1952.

[46] R. Levy, "Analysis and synthesis of waveguide multiaperture directional couplers," *IEEE Trans. Microw. Theory Tech.*, vol. 16, pp. 995–1006, Dec. 1968.

[47] G. L. Matthaei, L. Young, and E. M. T. Jones, *Microwave Filters, Impedance-Matching Networks and Coupling Structures.* Boston: Artech House, 1980.

[48] K. G. Patterson, "A method for accurate design of a broad-band multibranch waveguide coupler," *IRE Trans. Microw. Theory Tech.*, vol. 7, pp. 466–473, Oct. 1959.

[49] A. A. Oliner, "Equivalent circuits for small symmetrical longitudenal apertures and obstacles," *IRE Trans. Microw. Theory Tech.*, vol. 8, pp. 72–80, Jan. 1960.

[50] H. Schmiedel and F. Arndt, "Field theory design of rectangular waveguide multiple-slot narrow-wall couplers," *IEEE Trans. Microw. Theory Tech.*, vol. 34, pp. 791–798, July 1986.

[51] T. Sieverding, U. Papziner, and F. Arndt, "Mode-matching cad of rectangular or circular multi-aperture narrow-wall couplers," *IEEE Trans. Microw. Theory Tech.*, vol. 45, pp. 1034–1040, July 1997.

[52] L. Young, "Synchronous branch-guide directional couplers for low and high power applications," *IEEE Trans. Microw. Theory Tech.*, vol. 10, pp. 459–475, Nov. 1962.

[53] R. Levy and L. F. Lind, "Synthesis of symmetrical branch-guide directional couplers," *IEEE Trans. Microw. Theory Tech.*, vol. 16, pp. 80–89, Feb. 1968.

[54] R. Levy, "Analysis of practical branch-guide couplers," *IEEE Trans. Microw. Theory Tech.*, vol. 17, pp. 289–290, May 1969.

[55] ——, "Zolotarev branch-guide couplers," *IEEE Trans. Microw. Theory Tech.*, vol. 21, pp. 95–99, Feb. 1973.

[56] F. Alessandri, G. Bartolucci, and R. Sorrentino, "Admittance matrix formulation of waveguide discontinuity problems: Computer aided design of branch guide directional couplers," *IEEE Trans. Microw. Theory Tech.*, vol. 36, pp. 394–403, Feb. 1988.

[57] T. Shen and K. A. Zaki, "Waveguide branch couplers for tight couplings," *IEEE Trans. Microw. Theory Tech.*, vol. 48, pp. 2432–2438, Dec. 2000.

[58] T. Shen, Y. Rong, and K. A. Zaki, "Full-wave optimum design of millimeter-wave rectangular waveguide narrow-wall branch couplers," *Proc. 1999 IEEE MTT-S Int. Microwave Symp. Dig.*, pp. 1729–1732, June 1999.

[59] F. Arndt, B. Koch, H. J. Orlok, and N. Schroder, "Field theory design of rectangular waveguide broad-wall metal-insert slot couplers for millimeter-wave applications," *IEEE Trans. Microw. Theory Tech.*, vol. 33, pp. 95–104, Feb. 1985.

[60] H. A. Bethe, "Theory of diffraction by small holes," *Phys.Rev.*, vol. 66, pp. 163–182, May 1944.

[61] N. A. McDonald, "Electric and magnetic coupling through small apertures in shielded walls of any thickness," *IEEE Trans. Microw. Theory Tech.*, vol. 20, pp. 689–695, Oct. 1972.

[62] R. Levy, "Improved single and multiaperture waveguide coupling theory, including explanation of mutual interactions," *IEEE Trans. Microw. Theory Tech.*, vol. 28, pp. 331–338, Apr. 1980.

[63] S. B. Cohn, "Optimum design of stepped transmission-line transformers," *IRE Trans. Microw. Theory Tech.*, vol. 11, pp. 16–21, Apr. 1955.

[64] L. Young, "The quarter wave transformer prototype circuit," *IEEE Trans. Microw. Theory Tech.*, vol. 8, pp. 483–489, Sept. 1960.

[65] W. J. Getsinger, "Ridge waveguide field description and application to directional couplers," *IRE Trans. Microw. Theory Tech.*, vol. 40, pp. 41–50, Jan. 1962.

[66] J. A. Ruiz-Cruz, Y. Zhang, K. A. Zaki, A. J. Piloto, and J. M. Rebollar, "Ridge waveguide branch-line directional couplers for wideband applications and LTCC technology," *Proc. 2005 IEEE MTT-S Int. Microwave Symp. Dig.*, pp. 1219–1222, June 2005.

[67] P. Lomer and J. W. Crompton, "A new form of hybrid junctions for microwave frequencies," *Proc. Inst. Elec. Eng.*, vol. 104B, pp. 261–264, May 1957.

[68] R. Levy, "A guide to the practical application of chebyshev functions to the design of microwave components," *Proc. Inst. Elec. Eng.*, vol. 106C, pp. 193–199, Sept. 1959.

[69] T. Shen, "Full-wave modeling and design of waveguide passive components," Ph.D. dissertation, University of Maryland, College Park, MD, USA, 2001.

[70] J. A. Ruiz-Cruz, M. E. Sabbagh, K. A. Zaki, J. M. Rebollar, and Y. Zhang, "Canonical ridge waveguide filters in LTCC or metallic cavities," *IEEE Trans. Microw. Theory Tech.*, vol. 53, no. 1, pp. 174–182, Jan. 2005.

[71] J. Helszajn, *Ridge Waveguides and Passive Microwave Components*. London: The Institute of Electrical Engineers, 2000.

[72] W. J. Hoefer and M. N. Burton, "Closed-form expressions for the parameteres of finned and ridged waveguides," *IEEE Trans. Microw. Theory Tech.*, vol. 82, pp. 2190–2194, Dec. 1982.

[73] M. M. Fahmi, J. A. Ruiz-Cruz, K. A. Zaki, and A. J. Piloto, "LTCC wideband canonical ridge waveguide filters," *Proc. 2005 IEEE MTT-S Int. Microwave Symp. Dig.*, pp. 249–252, June 2005.

[74] Z. M. Liu, J. A. Ruiz-Cruz, C. Wang, and K. A. Zaki, "An extremely wideband ridge waveguide filter," *Proc. 2004 IEEE MTT-S Int. Microwave Symp. Dig.*, pp. 615–618, June 2004.

[75] R. Levy and S. Cohn, "A history of microwave filter research, design, and development," *IEEE Trans. Microw. Theory Tech.*, vol. 32, no. 9, pp. 1055–1067, Sept. 1984.

[76] R. Levy, R. V. Snyder, and G. Matthaei, "Design of microwave filters," *IEEE Trans. Microw. Theory Tech.*, vol. 50, no. 3, pp. 783–793, March 2002.

[77] A. A. Oliner, "Historical perspectives on microwave field theory," *IEEE Trans. Microw. Theory Tech.*, vol. 32, no. 9, pp. 1022–1045, Sept. 1984.

[78] I. C. Hunter, L. Billonet, B. Jarry, and P. Guillon, "Microwave filters - applications and technology," *IEEE Trans. Microw. Theory Tech.*, vol. 50, no. 3, pp. 794–805, March 2002.

[79] R. R. Mansour, "Filter technologies for wireless base stations," *IEEE microwave magazine*, pp. 68–74, March 2004.

[80] S. B. Cohn, "Properties of ridge waveguide," *Proc. IRE*, vol. 35, pp. 783–788, Aug. 1947.

[81] S. Hopfer, "The design of ridged waveguide," *IRE Trans . Microwave Theory Tech.*, vol. 5, pp. 20–29, Oct. 1955.

[82] A. M. K. Saad, J. D. Miller, A. Mitha, and R. Brown, "Analysis of antipodal ridge waveguide structure and application on extremely wide stopband lowpass filter," *Proc. 1986 IEEE MTT-S Int. Microwave Symp. Dig.*, pp. 361–363, June 1986.

[83] C. Wang and K. Zaki, "Full-wave modeling of generalized double ridge waveguide T-junctions," *IEEE Trans. Microw. Theory Tech.*, vol. 44, no. 12, pp. 2536–2542, Dec. 1996.

[84] M. A. E. Sabbagh, H.-T. Hsu, K. A. Zaki, P. Pramanick, and T. Dolan, "Full wave optimization of stripline tapped-in ridge waveguide bandpass filters," *Proc. 2002 IEEE MTT-S Int. Microwave Symp. Dig.*, June 2002.

[85] C. Wang and K. A. Zaki, "Modeling of couplings between double-ridge waveguide and dielectric-loaded resonator," *IEEE Trans. Microw. Theory Tech.*, vol. 46, no. 12, pp. 2404–2411, Dec. 1998.

[86] H. Yao, X. Liang, K. A. Zaki, and A. Martin, "Wide-band waveguide and ridge waveguide T-junctions for diplexer applications," *IEEE Trans. Microw. Theory Tech.*, vol. 41, no. 12, pp. 2166–2173, Dec. 1993.

[87] T. Shen and K.Zaki, "Length reduction of evanescent-mode ridge waveguide bandpass filters," *Proc. 2001 IEEE MTT-S Int. Microwave Symp. Dig.*, pp. 1491–1494, June 2001.

[88] J. A. Ruiz-Cruz, M. E. Sabbagh, K. A. Zaki, and J. M. Rebollar, "Full-wave design of canonical ridge waveguide filters," *Proc. 2004 IEEE MTT-S Int. Microwave Symp. Dig.*, pp. 603–606, June 2004.

[89] A. Bailey, W.Foley, M. Hageman, C. Murray, A. Piloto, K. Sparks, and K. Zaki, "Miniature ltcc filters for digital receivers," *Proc. 1997 IEEE MTT-S Int. Microwave Symp. Dig.*, pp. 999–1002, June 1997.

[90] D. stevens and J. Gipprich, "Microwave characterization and modelling of multilayered cofired ceramic waveguides," *Proc. 1998 IEEE MTT-S Int. Microwave Symp. Dig.*, pp. 195–200, June 1998.

[91] A. Piloto, K. Leahy, B. Flanick, and K. A. Zaki, "Waveguide filters having a layered dielectric structure," U.S. Patent 5 382 931, Jan. 17, 1995.

[92] Y. Rong, K. Zaki, M. Hageman, D. Stevens, and J. Gipprich, "Low-temperature cofired ceramic (LTCC) ridge waveguide bandpass chip filters," *IEEE Trans. Microw. Theory Tech.*, vol. 47, pp. 2317–2324, Feb. 1999.

[93] ——, "Low-temperature cofired ceramic (LTCC) ridge waveguide multiplexers," *Proc. 2000 Int. Microwave Symp. Dig.*, vol. 2, pp. 1169–1172, June 2000.

[94] A. E. Williams, "Four-cavity elliptic waveguide filter," *IEEE Trans. Microw. Theory Tech.*, vol. 18, pp. 1109–1113, Dec. 1970.

[95] A. E. Williams and A. E. Atia, "Dual-mode canonical waveguide filters," *IEEE Trans. Microw. Theory Tech.*, vol. 25, pp. 1021–1026, Dec. 1977.

[96] A. E. Atia and A. E. Williams, "Nonminimum-phase optimum-amplitude bandpass waveguide filters," *IEEE Trans. Microw. Theory Tech.*, vol. 22, pp. 425–431, Apr. 1974.

[97] L. Accatino, G. Bertin, and M. Mongiardo, "Elliptical cavity resonators for dual-mode narrow-band filters," *IEEE Trans. Microw. Theory Tech.*, vol. 45, pp. 2393–2401, Dec. 1997.

[98] T. Shen, H.-T. Hsu, K. Zaki, and A. E. Dolan, "Full-wave design of canonical waveguide filters by optimization," *IEEE Trans. Microw. Theory Tech.*, vol. 51, pp. 504–511, Feb. 2003.

[99] J. A. Ruiz-Cruz, K. A. Zaki, J. R. Montejo-Garai, and J. M. Rebollar, "Design of elliptic filters in rectangular waveguide with capacitive and inductive irises and integrated coaxial excitation," *Proc. 2005 IEEE MTT-S Int. Microwave Symp. Dig.*, June 2005.

[100] I. Hunter, *Theory and Design of Microwave Filters.* London: IEE Electromagnetic waves series 4, 2001.

[101] M. E. Sabbagh, K. A. Zaki, H.-W. Yao, and M. Yu, "Full-wave analysis of coupling between combline resonators and its application to combline filters with canonical configurations," *IEEE Trans. Microw. Theory Tech.*, vol. 49, pp. 2384–2393, Dec. 2001.

[102] A. E. Atia, A. E. Williams, and R. W. Newcomb, "Narrow-band multiple-coupled cavity synthesis," *IEEE Trans. Circuit Syst.*, vol. CAS-21, pp. 649–655, Sept. 1974.

[103] A. E. Atia and A. E. Williams, "New types of bandpass filters for satellite transponders," *COMSAT Tech. Rev.*, vol. 1, pp. 21–43, FAll 1971.

[104] Z. M. Liu, J. A. Ruiz-Cruz, C. Wang, and K. A. Zaki, "An extremely wideband ridge waveguide filter," *Proc. 2004 IEEE MTT-S Int. Microwave Symp. Dig.*, pp. 615–618, June 2004.

[105] H.-T. Hsu, Z. Zhang, K. A. Zaki, and A. E. Atia, "Parameter extraction for symmetric coupled-resonator filters," *IEEE Trans. Microw. Theory Tech.*, vol. 50, pp. 2971–2978, Dec. 2002.

[106] Y. Rong, K. Zaki, J. Gipprich, M. Hageman, and D. Stevens, "Low-temperature cofired ceramic (LTCC) wide-band ridge-waveguide bandpass filters," *IEEE Trans. Microw. Theory Tech.*, vol. 47, pp. 1836–1840, Sept. 1999.

[107] W. A. Atia, K. A. Zaki, and A. E. Atia, "Synthesis of general topology multiple coupled resonator filters by optimization," *Proc. 1998 IEEE MTT-S Int. Microwave Symp.Dig.*, pp. 821–824, June 1998.

[108] J. Gipprich, L. Dickens, B. Hayes, and F. Sacks, "A compact 8-14 GHz LTCC stripline coupler network for high efficiency power combining with better than 82% combining efficiency," *Proc. 1995 IEEE MTT-S Int. Microwave Symp. Dig.*, pp. 1583–1586, June 1995.

[109] G. Ferrel, L. Dickens, J. Gipprich, B. Hayes, and F. Sacks, "A high efficiency 10 watt poer amplifierassembly using combining techniques," *Proc. 1995 IEEE MTT-S Int. Microwave Symp. Dig.*, pp. 327–330, June 1995.

[110] M. Bona, L. Manholm, and J. P. Starski, "Low-loss compact butler matrix for a microstrip antenna," *IEEE Trans. Microw. Theory Tech.*, vol. 50, pp. 2069–2075, Sept. 2002.

[111] K. Wincza and S. Gruszczynski, "A broadband 4x4 butler matrix for modern day antennas," *Proc. 35th Eur. Microw. Conf. Paris, France*, pp. 1331–1334, Oct. 2005.

[112] W. R. Li, C. Y. Chu, K. H. Lin, and S. F. Chang, "Awitched-beam antenna based on modified butler matrix with low sidelobe level," *Electronic Letters*, pp. 290–292, March 2004.

[113] E. G. Cristal and L. Young, "Theory and tables of optimum symmetrical tem-mode coupled transmission-line directional couplers," *IEEE Trans. Microw. Theory Tech.*, vol. 13, pp. 544–558, Sept. 1965.

[114] S. B. Cohn and R. Levy, "History of microwave passive components with particular attention to directional couplers," *IEEE Trans. Microw. Theory Tech.*, vol. 32, pp. 1046–1054, Sept. 1984.

[115] Y. Dai, Y. Lu, Q. Luo, B. Zhan, X. Wang, and Y. Liang, "A microminiature 3db multilayer double-octave coupler using ltcc," *Proc. 2005 Asia Pacific Microwave Conference*, vol. 1, pp. 573–576, Dec. 2005.

[116] W. Chang, D. Jung, and C. Park, "A k-band ltcc smd type balun using a multilayer coupler insensitive to misalignment," *Proc. 2006 IEEE Radio and Wireless Symp.*, pp. 595–597, Jan. 2006.

[117] A. Sawicki and K. Sachse, "Novel coupled-line conductor-backed coplanar and microstrip directional couplers for pcb and ltcc applications," *IEEE Trans. Microw. Theory Tech.*, vol. 51, pp. 1743–1751, June 2003.

[118] R. Levy, "General synthesis of asymmtric multi-element coupled-transmission-line directional couplers," *IEEE Trans. Microw. Theory Tech.*, vol. 11, pp. 226–237, July 1963.

[119] ——, "Tables for asymmtric multi-element coupled-transmission-line directional couplers," *IEEE Trans. Microw. Theory Tech.*, vol. 12, pp. 275–279, May 1964.

[120] S. B. Cohn, "The re-entrant cross-section and wide-band 3-db hybrid couplers," *IEEE Trans. Microw. Theory Tech.*, vol. 11, pp. 254–258, July 1963.

[121] A. Pavio and S. Sutton, "A microstrip re-entrant mode quadrature coupler for hybrid and monolithic circuit applications," *Proc. 1990 IEEE MTT-S Int. Microwave Symp. Dig.*, pp. 573–576, May 1990.

[122] L.Lavendol and J. taub, "Re-entrant directional couplers using strip transmission line," *IEEE Trans. Microw. Theory Tech.*, vol. 13, pp. 700–701, Sept. 1965.

[123] R. Hayes, J. Gipprich, and M. Hershfeld, "Stripline re-entrant coupler network for cofired multilayer microwave circuits," *Proc. 1996 IEEE MTT-S Int. Microwave Symp. Dig.*, pp. 801–804, June 1996.

[124] S. Yamamoto, T. Azakami, and K. Ikataru, "Coupled strip transmission line with three center conductors," *IEEE Trans. Microw. Theory Tech.*, vol. 14, pp. 446–461, Oct. 1966.

[125] V. Tripathi, "On the analysis of symmetrical three-line microstrip circuits," *IEEE Trans. Microw. Theory Tech.*, vol. 25, pp. 726–729, Sept. 1977.

[126] P.Pieters, S. Brebels, E. Byene, and R. Mertens, "Generalized analysis of coupled lines in multilayer microwave mcm-d technology - application coplanar lange couplers," *IEEE Trans. Microw. Theory Tech.*, vol. 47, pp. 1863–1872, Sept. 1999.

[127] C. Tsai and K. Gupta, "Cad procedure for planar re-entrant type couplers and three line baluns," *Proc. 1993 IEEE MTT-S Int. Microwave Symp. Dig.*, pp. 1013–1016, June 1993.

[128] S. Gruszczynski, K. Wincza, and K. Sachse, "Design of compensated coupled-stripline 3-db directional couplers, phase shifters,and magic-t's - part i: single-section coupled-line circuits," *IEEE Trans. Microw. Theory Tech.*, vol. 54, pp. 3986–3994, Nov. 2006.

[129] ——, "Design of compensated coupled-stripline 3-db directional couplers, phase shifters,and magic-t's -part ii: broadband coupled-line circuits," *IEEE Trans. Microw. Theory Tech.*, vol. 54, pp. 3501–3507, Sept. 2006.